2017

Analysis and Design of High-Frequency Soft-Switching DC-DC Converter for Wireless Power Charging Applications

Abhishek V. Danekar
Wright State University

ANALYSIS AND DESIGN OF HIGH-FREQUENCY SOFT-SWITCHING DC-DC CONVERTER FOR WIRELESS-POWER CHARGING APPLICATIONS

A thesis submitted in partial fulfillment

of the requirements for the degree of

Master of Science in Electrical Engineering

By

ABHISHEK V. DANEKAR

B. E., Dr. Babasaheb Ambedkar Marathwada University, 2013

2017

Wright State University

WRIGHT STATE UNIVERSITY
GRADUATE SCHOOL

April 21, 2017

I HEREBY RECOMMEND THAT THE THESIS PREPARED UNDER MY SUPERVISION BY Abhishek V. Danekar ENTITLED Analysis and Design of High-Frequency Soft-Switching DC-DC Converter for Wireless-Power Charging Applications BE ACCEPTED IN PARTIAL FULFILLMENT OF THE REQUIREMENTS FOR THE DEGREE OF Master of Science in Electrical Engineering.

Marian K. Kazimierczuk, Ph.D.

Thesis Director

Brian Rigling, Ph.D.

Chair
Department of Electrical Engineering
College of Engineering and
Computer Science

Committee on
Final Examination

Marian K. Kazimierczuk, Ph.D.

Yan Zhuang, Ph.D.

Saiyu Ren, Ph.D.

Robert E. W. Fyffe, Ph.D.
Vice President for Research and
Dean of the Graduate School

Abstract

Danekar, Abhishek V., M.S.E.E., Department of Electrical Engineering, Wright State University, 2017. *Analysis and Design of High-Frequency Soft-Switching DC-DC Converter for Wireless Power Charging Applications.*

Wireless power transfer (WPT) technology is becoming attractive in a wide variety of applications such as electric-vehicle charging, induction heating, charging portable applications, industrial robots, and biomedical implants. Recent studies have shown various techniques to implement wireless power transfer and these techniques differ based on the type of applications. For example, for electric vehicle charging, the power levels are in the range 5 kW to 25 kW and the operating frequency is in the range 70 kHz to 110 kHz. On the other hand, for consumer applications, the power levels vary from a few watts to hundreds of watts and operates at frequencies of the order of 5 MHz to 10 MHz. This thesis addresses the analysis, design, implementation, and simulation of a wireless charging system targeted towards a high-frequency, low-power portable application with wide separation between transmitter and receiver.

The WPT system is composed of three important blocks: inverter (or transmitter), transformer (or coil), and rectifier (or receiver). Hard-switching inverters and rectifiers have major drawbacks at high frequencies due to large switching power loss. Therefore, soft-switching Class-E topology is chosen. The Class-E dc-ac inverter with CLL resonant tank, also referred to as $\pi 2a$ impedance matching network is analyzed, designed, and simulated to observe its superior performance over other topologies at varying coupling coefficients and loads. Four soft-switching rectifier topologies are analyzed, designed, and simulated to evaluate their behavior at high frequencies. Their compatibility with Class-E inverters in the presence of loosely-coupled transformers is discussed. The physical and commercial limitations of using transformers with magnetic core is presented. Therefore the preferred solution, an air-core transformer is designed and integrated with the rectifier to evaluate their characteristics at selected coupling coefficient.

The overall system including the inverter, loosely-coupled air-core transformer, and rectifier was designed for the following specifications: operating frequency 6.78 MHz, output power across a single-load 40 W, output voltage 25 V, and target coupling coefficient of 0.5. Simulation results have been provided to validate the theoretical predictions. The major challenges faced during the integration of these building blocks are addressed. Finally, conclusions, contributions, and scope for future work are provided.

Acknowledgment

Firstly, I owe my deepest gratitude to my advisor Dr. Marian K. Kazimierczuk, whose support, encouragement and continuous optimism throughout this journey has helped achieve this milestone. I would also like to thank my thesis committee members Dr. Yan Zhuang and Dr. Saiyu Ren for their suggestions and valuable comments. I am forever thankful to my colleagues Agasthya Ayachit and Dalvir Saini for their guidance, support and, for creating a cordial working environment. Most importantly, it is pleasure to thank all my friends, who supported me all these years and provided me with necessary distractions from the research and made the journey cheerful.

Last but not the least, I would like to express my profound and sincere gratitude towards my family Mr. Vijay Danekar, Mrs. Rohini Danekar and Rishikesh Danekar for their unparalleled love, support and faith in me. They compassionately encouraged me to explore new directions in life. This wonderful journey would not have been possible without them. Thank you.

Contents

List of Figures

List of Tables

1 Wireless Power Transfer System

1.1 History

In 1864, by means of a mathematical model James C. Maxwell predicted the existence of radiowaves. Maxwell's equations are the most significant and successful formulae till date. Later in 1884, John H. Poynting introduced a technique which played a very vital role in quantifying electromagnetic energy. This technique is known as Poynting vector. In 1888, Heinrich Hertz successfully displayed the experimental evidence of existence of radio-waves. Hertz implemented Maxwell's theory while experimenting on radio-waves. Hertz used spark-gap radio transmitter for this experiment. Towards the end of 19th century wireless power transfer (WPT) technology started coming into existence. In 1899, Nicola Tesla came up with the idea of wireless power transfer and performed the first WPT experiment. He said "This energy will be collected all over the globe preferably in small amounts, ranging from a fraction of one to few horse-power. One of its chief uses will be the illumination of isolated houses". Tesla carried out many power transmission experiments comprising magnifying transmitters, the ultimate motive was to develop worldwide wireless power distribution system. From 1899 to 1900, Tesla performed experiments in Colorado Springs, CO, USA involving wireless power transmission via electric field and capacitive coupling along with transmission lines and waveguide-like effects. [1]

Tesla constructed a massive coil that was connected to the 200 ft. high mast with a 3 ft. diameter spherical ball at its top. This huge structure is called as 'Tesla Tower'. The coil was resonating at the frequency of 150 kHz and a power of 300 kW is supplied to it. Unfortunately, since the transmitted power dispersed in all directions using 150 kHz radio-waves the experiment failed. After the failure of first WPT trial, wireless communication and remote sensing dominated the history of radio-waves. Probably operating frequency of the Tesla's tower was not optimum

and so the higher frequency version of this structure was required to overcome the difficulties like transmitted power and transfer efficiency. After the World War II, there were many technological advances like Radio Detection and Ranging (RADAR) system and highly efficient microwave tubes capable of operating at high frequencies were developed. Also, sending a high power beam over a long distance became possible. The transmission of power wirelessly with the help of microwaves is called as Microwave Power Transfer (MPT). In 1960s, William C. Brown performed several experiments and research activities regarding MPT. Brown developed a special type of antenna capable of both receiving and rectifying microwave signals. This antenna is called as Rectenna. In 1964, Brown successfully performed an experiment involving powering the wired helicopter through MPT technology. And four years later in 1968 Brown was successful in powering the free flying helicopter. During the late 20th century MPT experiments mainly focused on Solar Power Satellite (SPS) applications. If we compare the conventional power distribution system with the microwave based power distribution system, there are several parameters need to be addressed. First of all, the high voltage power lines have strong electromagnetic field surrounding them which can cause significant impacts on environment. In case of microwave based systems, if a well collimated beam is considered, the microwave signal has to travel distance of about 200 km, 100 km to leave the atmosphere and another 100 km to reenter resulting less impact on environment. The main advantage of the microwave based system is that the power density of the microwave beam can be controlled and kept under the safety limits. However, for the high power transmission, the cross section of the beam and the size of the antenna required is very large. Far-field transmission is appropriate for variety of uses such as in low power sensor networks where efficiency can be compromised and high power systems such as space, military and industrial applications where capability to receive power is far more important than

the cost of the system. It is not feasible to implement microwave-based systems to wirelessly power majority of devices that people interact with on a daily basis because of the safety issues. For the moderate power requirement, ranging from few watts to hundreds of watts and distances ranging between 0 to few meters, near field wireless power transfer system operating at frequency up to 100 MHz is a way better choice than microwave based systems. The near field wireless transfer delivers higher efficiency and even the RF exposure limit for such systems is less stringent. The near field power transmission can be implemented through an electric field. Even the Tesla's experiment as well as the most recent experiments, both achieved the near field power transmission through an electric field. The near field power transmission is non directional and it allows transmission through variety of obstacles (walls, furniture, people), since there is no interaction between them. Whereas the microwave based systems are highly directional and they require line-of-sight transmission.[1]

1.2 Background

The wireless power transfer system can be categorized based on the mechanism employed to achieve power transfer or on the distance between the source and load of the system. Depending upon the distance between source and load, the wireless power transfer system can be classified in following three categories.

- Near field
- Mid field
- Far field

Near-Field Wireless Power Transfer System

The near field wireless power transfer system can be further classified into two sub

categories i.e. short-range near field wireless power transfer system (less than couple of cm) and mid-range near field wireless power transfer system.

Short-Range Near Field Wireless Power Transfer System

Nowadays, many consumer electronic devices have started implementing wireless power transfer systems to power the devices. These devices require strongly coupled contactless charging systems. Generally, short-range wireless power systems consist of two coils, one in the charging station and another in the device. These systems are constructed including ferrite cores and to achieve the corresponding strong coupling they require precise alignment of the projections or slots in the device. The key motive behind designing strongly coupled contactless systems is safety. Since the name suggests contactless systems, there is no conductive path between charger and the device. The challenges involved while designing the device suitable for portable electronics is maintaining high efficiency, allowing freedom of movement and reducing the use of bulky magnetic materials. The structure comprises of an inverter. The main function of an inverter is to convert the direct current (DC) source to the alternating current (AC) at suitable frequency. The frequency for such systems ranges from hundreds of kilohertz of several megahertz. The overall losses in the systems are curbed by choosing the Class-D or Class-E type amplifiers. These amplifiers are the best candidates for high efficiency applications. Impedance transformation network is included in the near field wireless power transfer system. The impedance transformation operates in accordance with the inverter i.e. the transformation of impedance is carried out in such a way that range of loads are in the best possible efficiency portion of the inverter. The output part of the near field wireless power transfer system consists of another impedance transformation network, rectifier and a regulation circuitry. The impedance transformation network on the output side makes sure that

the load at the output established appropriate impedance. The alternating signal is then rectified through AC to DC rectifier and passes on to regulator which ensures that the device attached at the load is fed with stable supply. The application of various devices at the load according to the requirement introduce varying loads on the switching amplifiers. As a result, this introduces main challenge for the short range wireless power transfer system in achieving high efficiency and also maintaining the stability in power delivery. The solution to this problem is obtained by optimizing the performance of Class-E switching amplifier. In summary, the shorter distance between the transmitter and receiver coil (few millimeters to few centimeters) confirms the safer operation because the relationship between the field strength and the distance declines at a much faster rate. As a result of these merits, short-range near field wireless power transfer systems become the best candidates for powering the consumer electronic devices.

Mid-Range Near Field Wireless Power Transfer System

The similar concepts as in short-range power transfer systems can be implemented for extending the power transfer distance in mid-range wireless power transfer system. The improvement of power transfer efficiency of the far field system is achieved using the large antennas. In case of near field systems, the power transfer efficiency can be improved by using large inductive coils between transmitter and receiver. In any magnetic-field based near field wireless power transfer system, mutual inductance between the transmitting and receiving coil and the parasitic resistance of the coils are the two major factors which restrain the maximum power transfer distance.

One of the important aspect of near-field wireless power transfer system is to maintain the high efficiency of the overall system. As a result, a highly efficient inverter must be employed which will drive the transmitter coil generating a high

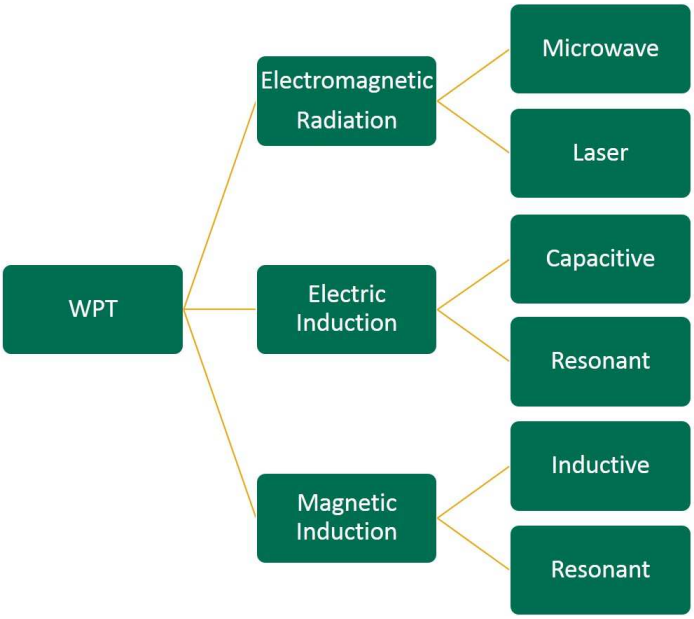

Figure 1.1: Types of wireless power transfer (WPT) technologies [3] [4].

frequency ac signal. In practice, switching power amplifiers must be used to tackle this problem since their maximum theoretical efficiency is 100%. In wireless power transfer systems, there are mainly three types of power switching amplifier which can provide high efficiencies for the overall systems namely Class-E, Class-D and full-bridge Class-D.[2]

Fig. 1.1 represents the classification of the wireless power transfer system based on the mechanism employed. The wireless power transfer system is broadly classified into three types i.e. Electromagnetic radiation, Electric induction and Magnetic induction. The electromagnetic radiation WPT system covers the power transfers involving very large distances. On the contrary, both electric induction WPT and magnetic induction WPT deal with near field power transfers. Firstly, the electromagnetic induction WPT system deals with very long distance applications. The applications such as space and Solar Power Satellite (SPS) fall under the category of the electromagnetic radiation WPT. As we discussed earlier, in order to achieve very long distance power transfer, Microwave Power Transfer (MPT) and Laser Power

transfer (LPT) technologies are necessary. Thus, the electromagnetic radiation WPT systems are classified into Microwave and Laser categories. Secondly, as the name suggests, the electric induction WPT works on the principle of electric field. Alternatively, the electric induction WPT is also known as Capacitive Power Transfer (CPT) since, it makes use of the electric field formed due to the displacement current between two electrodes. The electric induction WPT offers some advantages such as uninterrupted power transfer between the source and load even if there is a metal barrier between them. The construction of the electric induction WPT is simple and compact. However, the electric induction WPT may have harmful impacts on the human body. The electric induction WPT can be further classified as Resonant and Capacitive. Lastly, the magnetic induction WPT operates in the principle of the magnetic field. There are basically two ways to achieve the power transfer by magnetic induction method one by resonant coupling and the other by inductive coupling. The resonant coupling method works on the concept of resonance between the transmitter and receiver coils. The resonant coupling is one of the popular method to achieve the wireless power transfer with high efficiency. In case of the inductive coupling, the transmitter generates a magnetic field and the corresponding magnetic flux links the energy to the receiver side. The applications which demand for power transfer ranging from few microwatts to kilowatts with high efficiency employ inductively coupled magnetic induction WPT system. [4]

1.3 Thesis Outline

The power transfer model developed in this thesis is based on the inductively coupled wireless power transfer (WPT). This thesis is composed of six chapters.

- Chapter 1 explains the history of wireless power transfer system. This chapter presents various experiments performed by Hertz, Maxwell and Tesla that are related to wireless power transfer system. This also includes the advancements

in increasing the range of conventional wireless power transfer system by utilizing the Microwave Power Transfer (MPT) technology. Also, several advantages, disadvantages and applications of the WPT systems are discussed.

- Chapter 2 focuses on design and construction of high frequency resonant rectifiers. The construction, analysis and detailed study of the Class-E rectifiers is included in this chapter. Four configurations of the Class-E rectifier are studied namely 1. current-driven Class-E low dv/dt (ZVS) rectifier, 2. voltage-driven Class-E low dv/dt (ZVS) rectifier, 3. current-driven Class-E low di/dt (ZCS) rectifier and 4. voltage-driven Class-E low di/dt (ZCS) rectifier. The principle of operation, static and transient analysis, zero voltage, and zero current switching profiles and efficiencies of each rectifier configuration are examined in detail.

- Chapter 3 presents the magnetic characteristics and the design of transformer. The magnetic characteristics include study of fundamental magnetic relationships, hysteresis, and the losses incurred due to skin and proximity effect. The transformer design process takes into account study of various core material related properties and their tradeoffs. The method employed to design the transformer i.e. area product method is elaborated. The transformer is designed to be coupled with current-driven Class-E low dv/dt (ZVS) rectifier and voltage-driven Class-E low di/dt (ZCS) rectifier.

- Chapter 4 explains the design and analysis of the high frequency inverter. The highly efficient Class-E resonant ZVS inverter is studied. The Class-E resonant ZVS inverter is designed to be coupled with current-driven Class-E low dv/dt (ZVS) rectifier and voltage-driven Class-E low di/dt (ZCS) rectifier. The principle of operation, overall power losses, and efficiencies are accounted for both

the configurations.

- Chapter 5 provides information about design of the overall high-frequency wireless power transfer system. This system is designed including Class-E resonant ZVS inverter, transformer and a bridge rectifier. The system designed in this chapter aims for achieving power of 40 W at the output voltage of 25 V. The system is designed for ISM band frequency of 6.78 MHz.

- Chapter 6 explains the technical challenges, conclusions, and contributions regarding the thesis. The technical challenges include the roadblocks encountered while designing the individual components, which may prove fruitful for those who choose the similar path.

2 Rectifier

2.1 Introduction

Basically, in almost all electronic devices the power processing technologies emerged from two fundamental schemes. The resonant scheme and the pulse width modulation (PWM) scheme. The PWM scheme is also known as the duty-cycle modulation scheme. The PWM scheme is dependent on interjecting power flow and controlling duty cycle, which generates pulses of current and voltage of specific amplitudes. In resonant topology, power processing is achieved in a simple sinusoidal form. The implementation of these schemes is based on factors like switching frequency, circuit complexity, applications, etc.

The PWM scheme discovers its application mainly in low power devices, where there is very little scope for complexity and better controllability is desired. The PWM converters are designed for the switching frequency between 30-50 kHz. The converters operating efficiently in this frequency range deliver optimal weight, size, reliability and cost.

The resonant topology has potential to drive high power applications. Most of these high power applications require a variable switching frequency to provide control over output voltage and current. The major difficulty with a resonant topology is its circuit complexity. In certain modern applications, it is required to have switching frequencies in the megahertz range. MOSFETs can be developed which operate at tens of megahertz frequency. But with higher switching frequency comes major limitations such as electromagnetic interference (EMI). Moreover, when the switch turns OFF with an inductive load, high voltage spikes occur. On the contrary, when a switch is turning ON, the energy stored in the junction capacitance is trapped and dissipated in the device and hence the device is said to have operated with capacitive turn-ON. Mainly, the parasitic inductances such as leakage inductance in the case of

transformer and junction capacitance in the case of switches are responsible for the inductive turn-OFF and capacitive turn-on of converters. Thus, at high switching levels converters experience hard switching which also introduces electromagnetic noise interference.

The solution to the problem of hard switching is achieved by devices developed on the zero-current switching (ZCS) principle and zero-voltage switching (ZVS) principle. The converters developed on the zero-current switching principle are called quasi-resonant converters. The quasi-resonant converters use LC resonant tank circuits to shape the current waveforms. Also, a condition of zero current is created for the device to switch at a proper instant of time. The quasi-resonant converters can be termed as hybrid converters between PWM and resonant topologies and their operation is based on the principle of inductive or capacitive energy storage and transfer. The objective of coupling LC tank circuit and the power switch together is to shape the current and voltage waveforms and also to store and transfer the energy from input to output. However, the converters based on zero current switching principle are incapable of reducing the high switching losses that occur due to capacitive turn ON so their operation is generally preferred in the lower megahertz range. If duality principle is applied to quasi-resonant converters operating on zero current switching principle, we obtain a new family of quasi-resonant converters operating on zero voltage switching principle. In the case of zero current and zero voltage switching techniques, the LC resonant tank circuit shapes the current and voltage waveform of the device and creates a zero current and zero voltage condition so that the device turns OFF and turns ON at the proper time instant respectively. The zero voltage switching technique has several advantages over zero current switching technique at high frequency levels such as it eliminates switching losses, reduces switch stresses, and both of which eventually lead to enhancement in efficiency. Again, elimination of

noise occurred while switching and reduction in electromagnetic interference (EMI) act as a driving force during the design of devices at high frequency levels. But, all of the above merits can be achieved if the parasitic elements such as leakage inductance in the case of transformer and junction capacitance in the case of a switch are absorbed into circuit itself. [5]

In recent years, there has been a necessity of designing the smaller and lighter power supplies. These power supplies demand resonant power converters operating at higher frequencies. The size of the components used for designing the converters such as inductors, capacitors, and coils can be reduced to a significant ratio by high-frequency operation. A typical high-frequency resonant converter circuit comprises of a DC to AC inverter (preferably Class-E or Class-D) and an AC to DC rectifier (preferably Class-E) since they offer a great degree of power density, faster response and efficient operation even there is variation in input voltage or load resistance. However, there are certain drawbacks associated with these inverters and rectifiers such as losses incurred due to the reverse recovery effect of the p-n junction diodes and also due to the diode junction capacitance. Also, when there is a need to configure rectifier and inverter together then there may be incompatibility issues between them. Sometimes, the rectifier is current-driven or voltage-driven so, the source may introduce harmonic content leading to inefficient operation. The solution to overcoming these problems comprises of using Schottky diodes in place of p-n junction diodes as they offer very low reverse recovery time eliminating the reverse recovery effect. The incompatibility issues can be fought by including the appropriate interface between the inverter and rectifier coupling. The interface circuits are the series or parallel combination of inductor and capacitors. There is flexibility offered to the designer to choose component values of these interface circuits such that the phase difference between the source voltage and current is eliminated. The value of the power factor

comes close to 1 if there is no phase difference between the source voltage and current. Since these interface circuits allow the power factor to come close to 1 they can be also called as passive power-factor correctors. In the next section, Class-E rectifiers are designed working with zero voltage and zero current switching technique and are further categorized into the voltage and current driven rectifiers. [6]

2.2 Current-Driven Class-E Low dv/dt (ZVS) Rectifier

2.2.1 Circuit Description

The Class-E low dv/dt (ZVS) rectifier is driven by an ac current source. The schematic of rectifier is shown in Fig. 2.1 which consists of a rectifying diode D, capacitor C, filter inductor L_f, filter capacitor C_f and load resistor R_L. The filter inductor-filter capacitor duo, $L_f - C_f$ combination form a second order low pass filter. The rectifier is driven by the ac current source i_R and output is measured across the load resistor. The primary function of the rectifier is to convert the sinusoidal ac voltage or current into a DC voltage or current respectively. As a result, we obtain a DC power at the output. The switching of the diode between turn ON and turn OFF is based on the rate of change of diode voltage with respect to time. When the diode voltage goes to zero, it signifies that the diode is in ON condition and on the contrary when there is a non-zero voltage across diode, then we can say that diode is in OFF condition. In this case the rectifier follows the zero voltage switching principle. The resonant action caused by inductor and capacitor duo is initialized by turn OFF of diode in case of zero voltage switching. The main function of the shunt capacitance is to shape the diode voltage in such a way that the switching of the diode commences at a low dv/dt. We know that during transitions, junction capacitance is developed due to irregularity in the charge. But, due to implementation of shunt capacitance the current through diode junction capacitance will be reduced. Since we discussed earlier the zero voltage or zero current switching principle has its merits only when the diode junction capacitance and parasitic capacitances of transformer (coupled) and inductor are absorbed into shunt capacitance. Any ripple in the output voltage of the rectifier is handled by the second order low pass filter. A current sink is formed by second order low pass output filter and load resistor since the current through filter inductor and DC current at load resistor are approximately equal.[7]

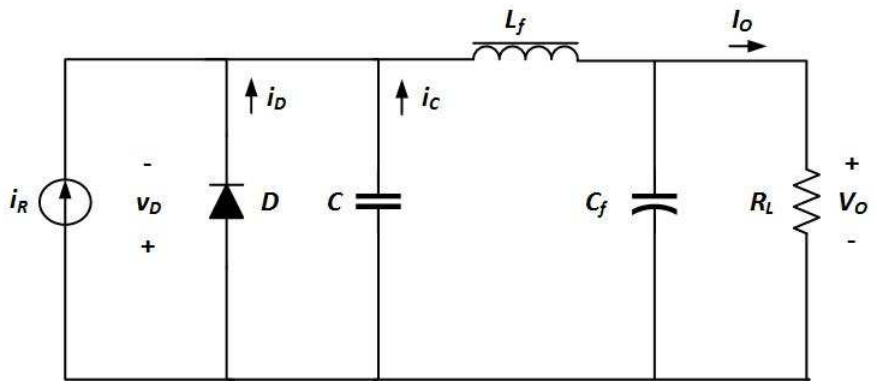

Figure 2.1: current-driven Class-E low dv/dt (ZVS) rectifier [7].

2.2.2 Principle of Operation

The duty cycle is equal to 0.5, in this case, i.e. for the conduction angle to be 180°. The rectifier input current is sinusoidal in nature and at the output rectified DC output current is obtained. The parallel combination of diode and capacitor is driven by the difference between the DC output current and the input current i.e. $I_O - i_R$. For the diode to turn ON, it needs 0.7 V (0.4 V in case of Schottky Diode). When the diode turns ON, the current $I_O - i_R$ starts flowing through the diode. At this instance, the voltage drop across diode and capacitor current are zero. The peak value of the diode current is denoted by I_{DM}. When the forward current of diode decreases to zero, diode turns OFF. At this point, current $I_O - i_R$ starts flowing through the capacitor. The general equation of the capacitor current can be given as $i_C = C\frac{dv_D}{dt}$ which means the capacitor current and the diode voltage are related. As a result, when the capacitor current goes to negative the diode voltage starts decreasing gradually. The minimum diode voltage is achieved at zero capacitor current and again it slowly starts to rise to zero when capacitor current is positive. Thus, the diode switches ON and OFF at low dv/dt reducing the switching losses and switching noise eventually reducing the EMI effect.[7]

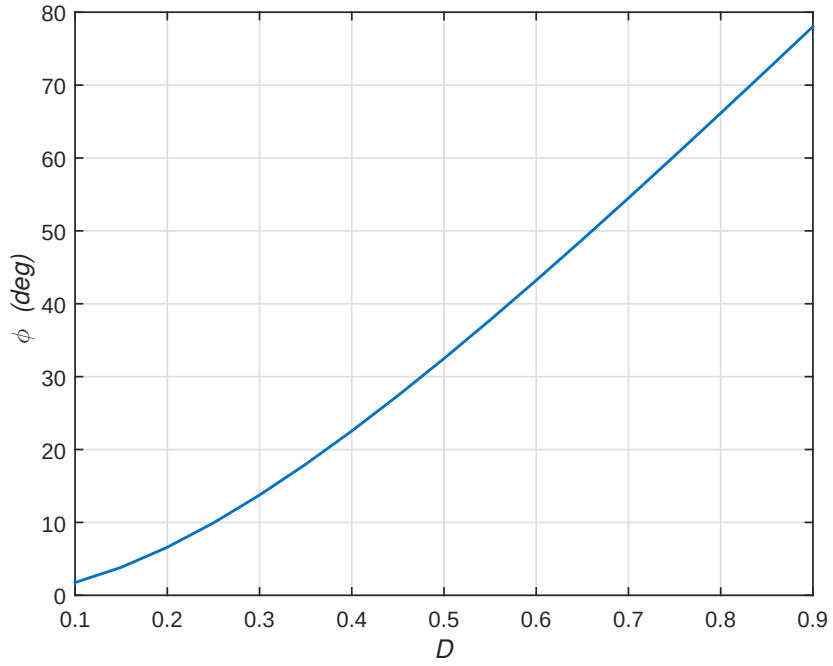

Figure 2.2: Phase angle as a function of duty cycle.

2.2.3 Effect of Variation in Duty Cycle on Phase Angle and AC-to-DC Current and Voltage Transfer Function

The equations for phase angle, AC-to-DC voltage, and current transfer function are followed from "Resonant Power Converters" by Kazimierczuk [7]. Fig. 2.2 shows the relation between duty cycle and the phase of the rectifier. The variations in duty cycle have corresponding changes in turn ON and turn OFF time of the diode and eventually on the AC-to-DC current and voltage transfer functions. The phase angle of the rectifier is given as,

$$\phi = \tan^{-1} \frac{1 - \cos(2\pi D)}{2\pi(1 - D) + \sin(2\pi D)} \tag{2.1}$$

where D is the duty cycle of the rectifier. As we increase the duty ratio from 0 to 1, the phase angle starts increasing linearly from 0° to 90° until $D = 0.95$ and decreases beyond it.

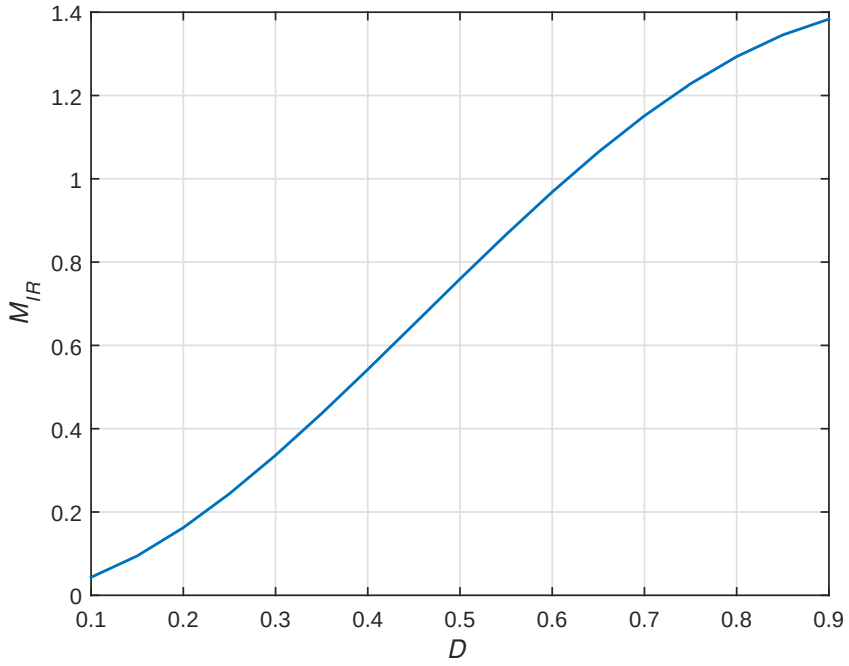

Figure 2.3: AC-to-DC current transfer function as a function of duty cycle.

Fig. 2.3 shows the relation between AC-to-DC current transfer function and the duty cycle of the rectifier. The AC-to-DC current transfer function is defined as the ratio of DC output current I_O to the RMS value of the input current i_R. It can be also represented in phase angle term as,

$$M_{IR} = \frac{I_O}{i_R} = \sqrt{2}\sin(\phi) \tag{2.2}$$

where ϕ is the phase angle of the rectifier. As the duty cycle starts increasing from 0 to 1, the corresponding phase angle increases from 0° to 90° and eventually the AC-to-DC current transfer function increases from 0 to 1.414.

Fig. 2.4 shows the relation between AC-to-DC voltage transfer function and the duty cycle of the rectifier. The AC-to-DC voltage transfer function is defined as the ratio of RMS value of the input current i_R to the DC output current I_O i.e., it is reciprocal of the AC-to-DC current transfer function. It can be also represented in

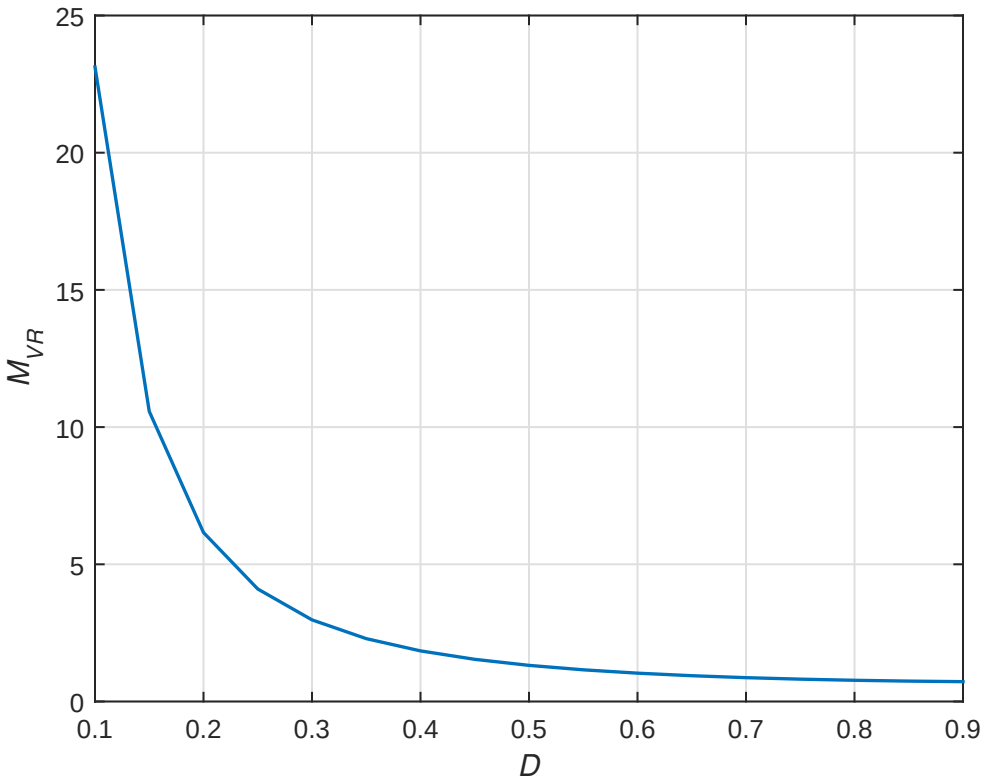

Figure 2.4: AC-to-DC voltage transfer function as a function of duty cycle.

phase angle term as,

$$M_{VR} = \frac{i_R}{I_O} = \frac{1}{\sqrt{2}\sin(\phi)} \tag{2.3}$$

where ϕ is the phase angle of the rectifier. As the duty cycle starts increasing from 0 to 1, the corresponding phase angle starts increasing from 0° to 90°, the AC-to-DC voltage transfer function decreases from 23 to 0.71. However, the AC-to-DC current and voltage transfer function are dependent on phase angle and eventually on the duty cycle of the rectifier.

2.2.4 Effect of Variation in Duty Cycle on Diode Voltage and Current

In this section, we will establish the relation between duty cycle and the diode voltage and current waveforms normalized with respect to dc output voltage V_O and current

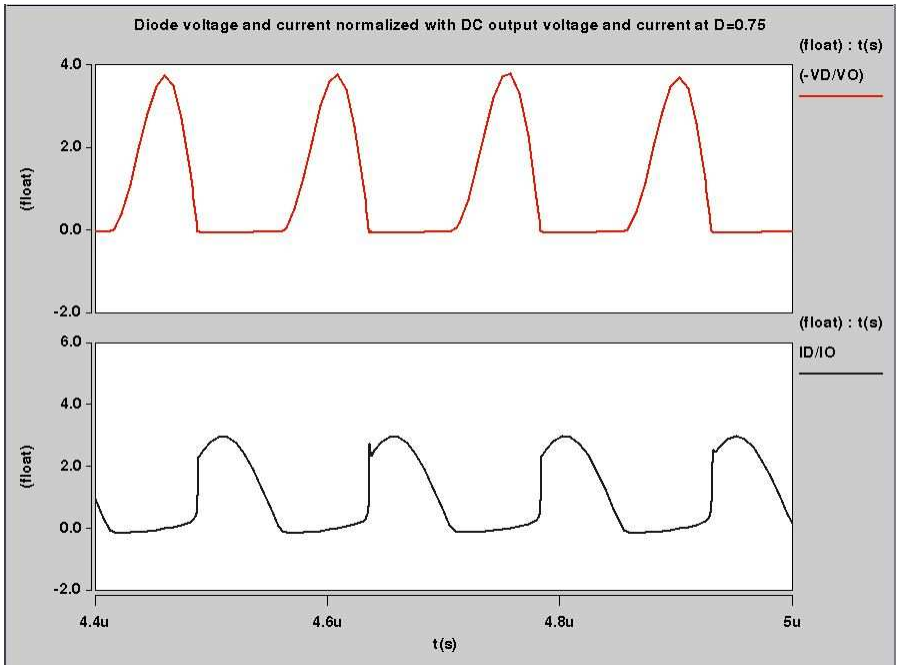

Figure 2.5: Diode voltage and current normalized with DC voltage and current at $D = 0.75$.

I_O. We will vary the duty cycle in steps i.e. $D = 0.75$, 0.5 and 0.25 and observe the corresponding effect on the diode and current waveforms. The following Fig. 2.5 shows the waveforms of diode voltage and current normalized with respect to DC output voltage and current for duty cycle $D = 0.75$. Observing the figure, we can say that at $D = 0.75$, the ratio of diode voltage to DC output voltage reaches to 4. At this instance, the ratio of diode current to DC output current is zero. In other words, the diode is in turn OFF condition till $\omega t = \frac{\pi}{2}$ and it turns ON when the diode current starts to increase. At $D = 0.75$, the phase angle of the rectifier is 60.28°. With the help of phase angle, we obtained the AC-to-DC current transfer function M_{IR} as 1.228.

Fig. 2.6 shows the waveforms of diode voltage and current normalized with respect to DC output voltage and current for duty cycle $D = 0.5$. For $D = 0.5$, the ratio of diode voltage to DC output voltage reaches to 4. At this instance, the ratio of diode current to DC output current is zero. In other words, the diode is in turn OFF

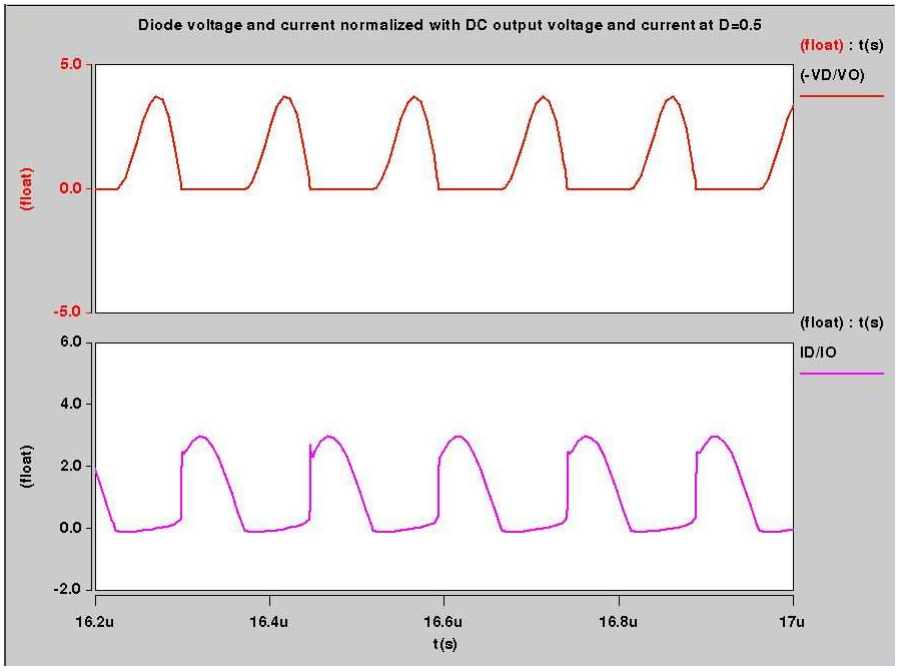

Figure 2.6: Diode voltage and current normalized with DC voltage and current at $D = 0.5$.

condition till $\omega t = \pi$ and it turns ON when the diode current starts to increase. At $D = 0.5$, the phase angle of the rectifier is 32.48°. With the help of phase angle, we obtained the AC-to-DC current transfer function M_{IR} as 0.7595.

Fig. 2.7 shows the waveforms of diode voltage and current normalized with respect to DC output voltage and current for duty cycle $D = 0.25$. For $D = 0.25$, the ratio of diode voltage to DC output voltage reaches to 2. At this instance, the ratio of diode current to DC output current is zero. In other words, the diode is in turn OFF condition till $\omega t = \frac{3\pi}{2}$ and it turns ON when the diode current starts to increase. At $D = 0.25$, the phase angle of the rectifier is 9.93°. With the help of phase angle, we obtained the AC-to-DC current transfer function M_{IR} as 0.2438.

In summary, the duty cycle of the rectifier controls the diode voltage and current normalized with DC output voltage and current. As we decrease the duty cycle, the phase angle along with AC-to-DC current transfer function drops. As a result, the diode takes a longer time to turn ON.

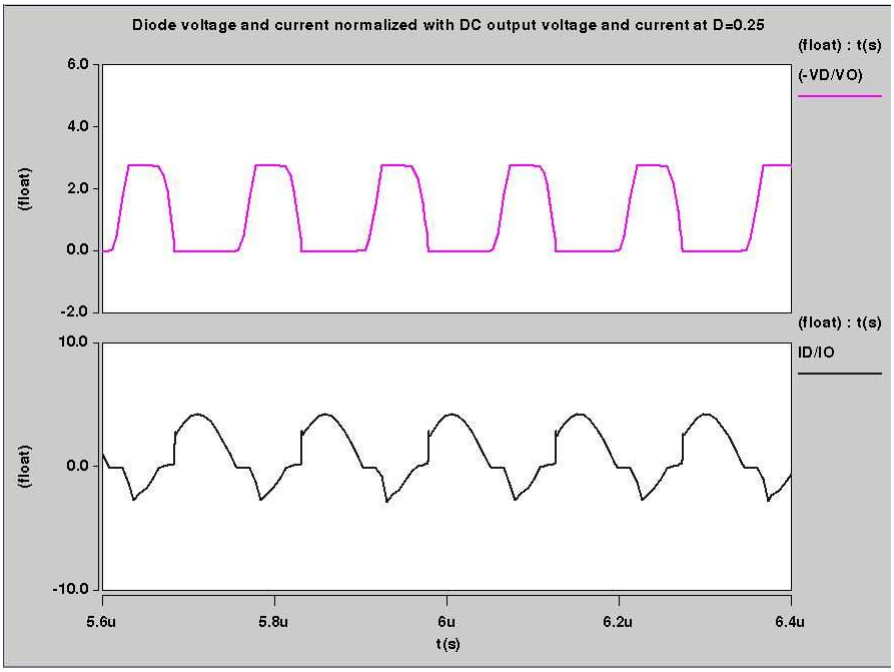

Figure 2.7: Diode voltage and current normalized with DC voltage and current at $D = 0.25$.

2.2.5 Parameters of Current-Driven Class-E Low dv/dt (ZVS) Rectifier

Table 1 comprises of values of parameters of current-driven Class-E low dv/dt (ZVS) rectifier such as duty cycle, phase angle, AC-to-DC current and voltage transfer function.

Table 1: Parameters of Current-Driven Class-E Low dv/dt (ZVS) Rectifier.

Duty Cycle (D)	**Phase** ($^\circ$)	M_{IR}	M_{VR}
0	0	0	∞
0.1	1.7523	0.0432	23.1240
0.15	3.8348	0.0946	10.5728
0.2	6.5939	0.1624	6.1578
0.25	9.9295	0.2489	4.1007
0.3	13.7506	0.3362	2.9748
0.35	17.9780	0.4365	2.2910
0.4	22.5449	0.5422	1.8843
0.45	27.3950	0.6507	1.5368
0.5	32.4816	0.7595	1.3167
0.55	37.7655	0.8661	1.1546
0.6	43.2136	0.9683	1.0327
0.65	48.7980	1.0640	0.9398
0.7	54.4946	1.1513	0.8686
0.75	60.2824	1.2282	0.8142
0.8	66.1431	1.2934	0.7732
0.85	72.0599	1.3455	0.7432
0.9	78.0176	1.3834	0.7229
0.95	84.0022	1.4065	0.7110

2.2.6 Component Values

The current-driven Class-E low dv/dt (ZVS) is designed following the design example from "Resonant Power Converters" by Kazimierczuk [7] to obtain DC output voltage between 12 V to 15 V, output power between 25 W to 40 W for 6.78 MHz frequency.

Initially, the amplitude of the input current I_m is given as,

$$I_m = \frac{\sqrt{2}I_O}{M_{IR}} = \frac{\sqrt{2}V_O}{M_{IR}R_L} = 4.966 \text{ A}. \tag{2.4}$$

where I_O is the DC output current, M_{IR} is the AC-to-DC current transfer function, V_O is the DC output voltage and R_L is the load resistance. Observing the above equation, we can say that the amplitude of the input current is inversely proportional to the AC-to-DC transfer function and eventually to the duty cycle.

The minimum value of the filter inductance can be obtained assuming maximum allowable peak to peak current ripple in filter inductor is 10% of the output current as follows.

$$L_{fmin} = \frac{(1-D)V_O}{0.1fI_O} = 4.147 \ \mu\text{H}. \tag{2.5}$$

where D is the duty cycle, V_O is the DC output voltage, I_O is the DC output current and f is the operating frequency.

The minimum value of the filter capacitance can be obtained as follows.

$$C_{fmin} = \frac{25}{\pi^2 f^2 L_{fmin}} = 13.28 \text{ nF}. \tag{2.6}$$

The value of shunt capacitance can be obtained with the help of load resistance as follows.

$$C = \frac{1}{\pi\omega R_{Lmin}} = 1.328 \text{ nF}. \tag{2.7}$$

Considering the output voltage and output power as 15 V and 40 W respectively, we can obtain parameters of current-driven Class E low dv/dt (ZVS) rectifier as follows.

Maximum output current:

$$I_{Omax} = \frac{P_{Omax}}{V_O} = 2.667 \text{ A}. \tag{2.8}$$

Minimum load resistance:

$$R_{Lmin} = \frac{V_O}{I_{Omax}} = 5.624\ \Omega. \tag{2.9}$$

Maximum diode voltage for $D = 0.5$:

$$V_{DM} = 3.562 V_O = 53.43\ \text{V}. \tag{2.10}$$

Maximum diode current for $D = 0.5$:

$$I_{DM} = 2.862 I_{Omax} = 7.633\ \text{A}. \tag{2.11}$$

2.2.7 Results

The simulation results for current-driven Class-E low dv/dt (ZVS) rectifier are shown as follows. The capacitor current and the capacitor voltage waveforms for the corresponding input current of the current-driven Class-E low dv/dt (ZVS) rectifier are shown in Fig. 2.8. The capacitor current plays a very important role in the switching of the diode because it shapes the voltage across diode and capacitor while the diode is OFF. When capacitor current is negative, then the diode voltage gradually decreases. When capacitor current is zero then the diode voltage reaches its minimum value. Again, when capacitor current is positive, the diode voltage reaches to zero and we know that ideal diode turns ON when its voltage reaches zero. The maximum and average capacitor current is obtained as 2.3632 A and 0.028 A. The maximum and average capacitor voltage is obtained as 62.414 V and 14.356 V.

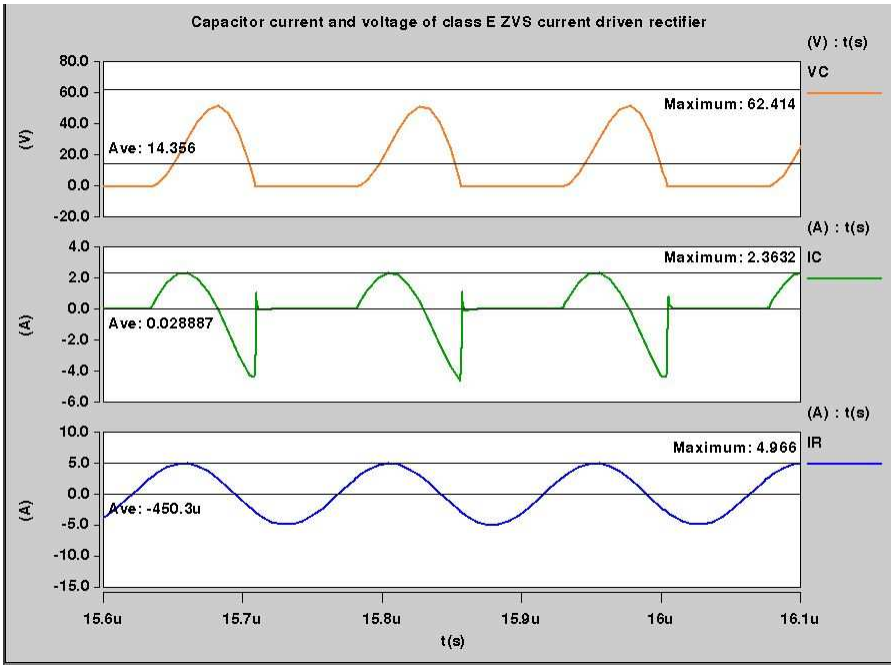

Figure 2.8: Capacitor current, voltage and input current of current-driven Class-E low dv/dt rectifier.

The diode current and the diode voltage waveforms for the corresponding input current of the current-driven Class-E low dv/dt (ZVS) rectifier are shown in Fig. 2.9. When the diode is OFF, the capacitor C will be in parallel combination with the current sink and will be driven by the difference between input current and DC output current. When the forward voltage of the diode reaches its threshold level it turns ON and then the difference between input current and DC output current starts flowing through the diode. Since the capacitor current and the diode voltage are related as per the general equation $i_C = C\frac{dv_D}{dt}$, during the diode turn OFF, capacitor current goes to zero and hence the derivative of diode voltage with respect to time also goes to zero. In summary, we can conclude that the transition of diode takes place at low dv/dt contributing in the reduction of switching losses and switching noise. The waveforms of diode current and voltage complement each other. The maximum and average value of diode current measured is 7.9708 A and 2.5313 A respectively and the maximum and average value of diode voltage measured is 0.5920 V and -14.356

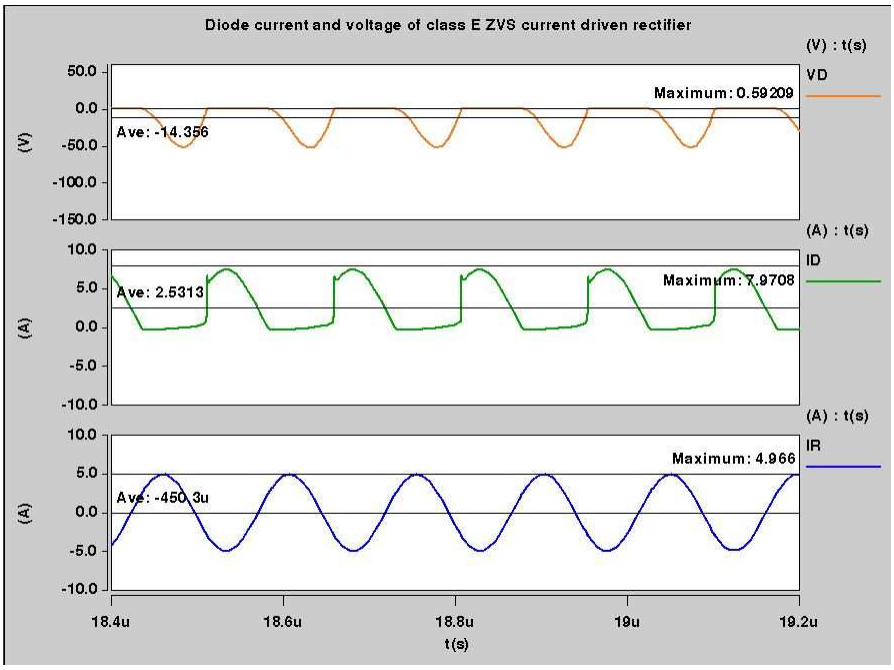

Figure 2.9: Diode current and voltage of Current-Driven Class-E Low dv/dt Rectifier.

V respectively.

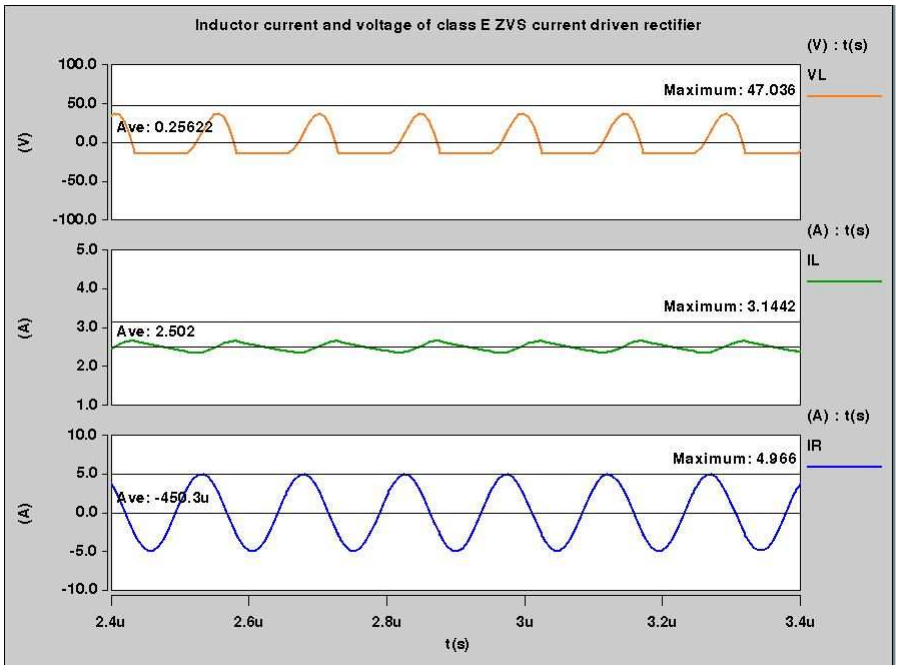

Figure 2.10: Inductor current,voltage and input current of current-driven Class-E low dv/dt rectifier.

The inductor current and voltage waveforms for the corresponding input current of the current-driven Class-E low dv/dt (ZVS) rectifier are shown in Fig. 2.10. We know that the filter formed at the output portion of the rectifier comprises of capacitor C_f, inductor L_f and load resistance R_L. The capacitor C_f and inductor L_f determine the corner frequency of the filter at the output. In order to avoid any ripple at the output, the current across the filter inductor is assumed to be approximately equal to DC output current. However, the voltage across the inductor is partly sinusoid. The maximum and average inductor current measured is 3.1442 A and 2.502 A respectively and the maximum and average inductor voltage measured is 47.036 V and 0.256 V respectively.

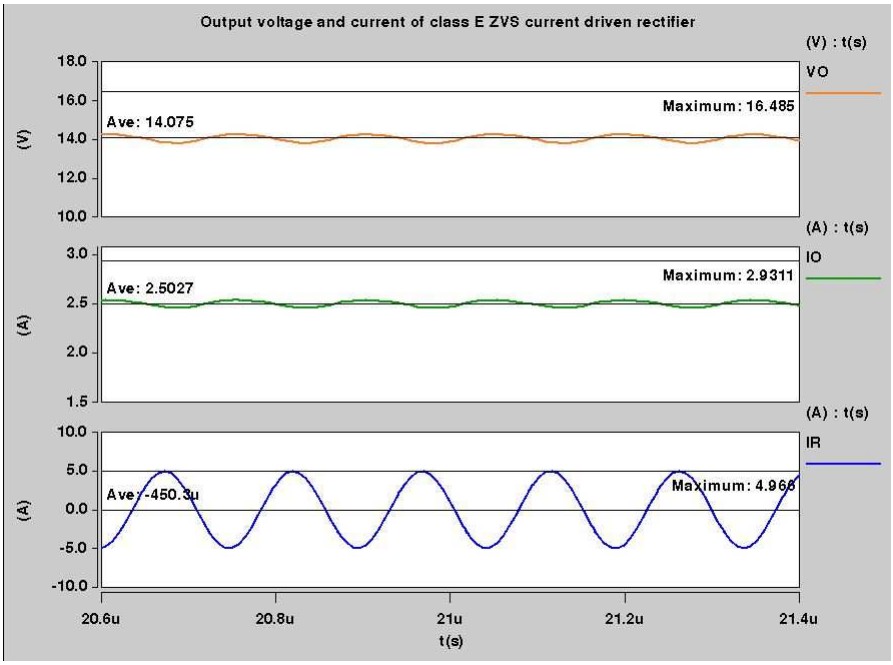

Figure 2.11: Output voltage, current and input current of current-driven Class-E low dv/dt rectifier.

The output voltage waveform for the corresponding input current of the current-driven Class-E low dv/dt (ZVS) rectifier is shown in Fig.2.11. The current-driven Class-E low dv/dt (ZVS) rectifier has sinusoidal current source at the input whereas at the output DC voltage is obtained. The desired DC output voltage for the given specifications is 15 V. We obtained the maximum and average DC output voltage of the rectifier as 16.485 V and 14.075 V respectively and maximum and average DC output current of the rectifier as 2.9311 A and 2.5027 A respectively.

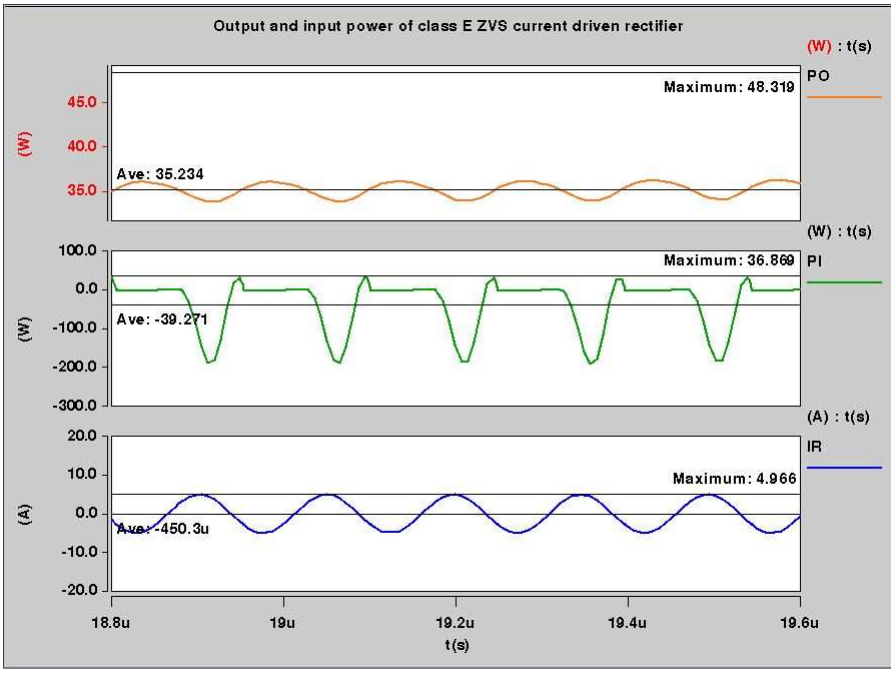

Figure 2.12: Input, output power and input current of current-driven Class-E low dv/dt rectifier.

The input power and output power waveform for the corresponding input current of the current-driven Class-E low dv/dt (ZVS) rectifier are shown in Fig. 2.12. The current-driven Class-E low dv/dt (ZVS) rectifier has sinusoidal current source at the input whereas at the output DC power is delivered to the load. The desired DC output power for the given specifications is 40 W. We know that power is nothing but the product of voltage and current. The maximum and average value of the input power is obtained as 36.869 W and -39.271 W respectively. Whereas, the maximum and average value of the output power is obtained as 48.319 W and 35.234 W respectively. The efficiency of the rectifier is defined as ratio of the average output power to the input power which can be given as,

$$\eta = \frac{P_o}{P_I} = \frac{35.234}{|39.271|} = 89.72\ \% \tag{2.12}$$

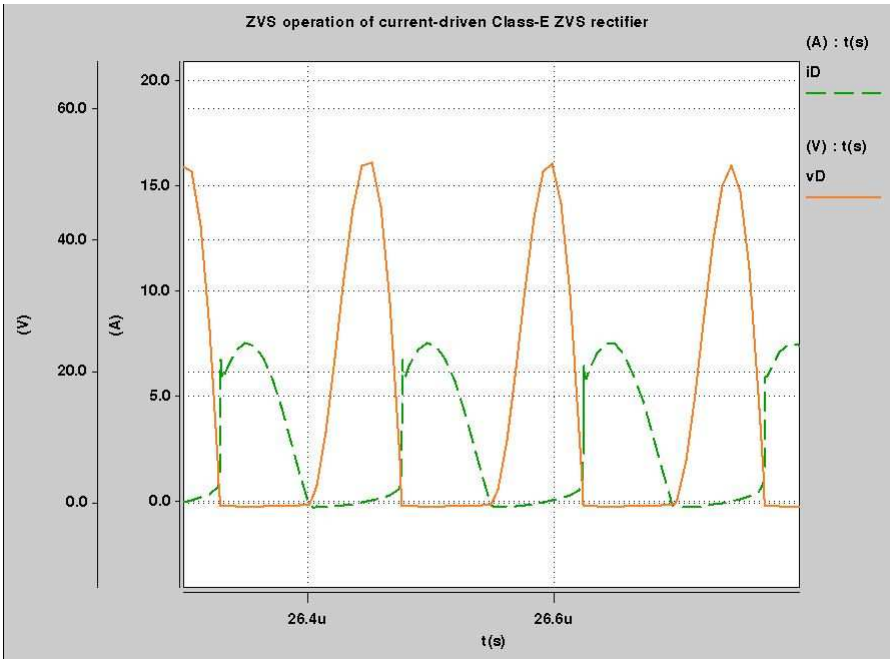

Figure 2.13: ZVS operation of current-driven Class-E low dv/dt (ZVS) rectifier.

The ZVS operation of the current-driven Class-E low dv/dt rectifier is shown in Fig. 2.13. The diode voltage waveform of the rectifier is reversed and superimposed on the diode current waveform. The condition for the zero voltage switching is that the switch voltage should be equal to zero at the turn ON instance of the diode. When the switch voltage goes to zero, the diode current starts increasing and the diode turns ON. If the diode voltage is non-zero at the turn ON instance, the diode voltage and diode current waveform overlap on each other causing switching losses. The switching losses lead to power loss. Therefore, the switching losses have an adverse effect on the efficient operation of the rectifier.

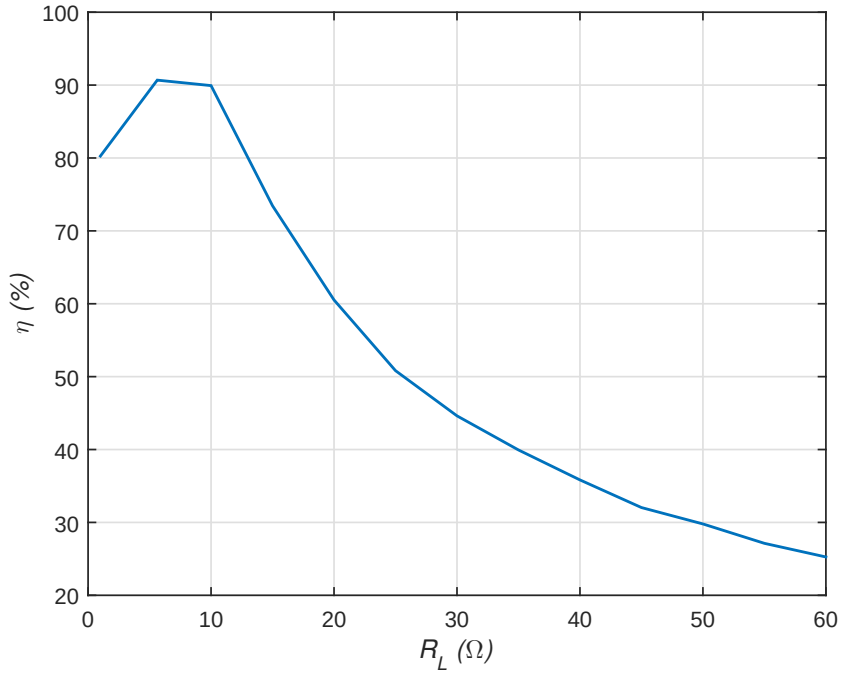

Figure 2.14: Efficiency as a function of the load resistance of the rectifier.

2.2.8 Effect of Change in Load Resistance on the Efficiency of the Current-Driven Class-E Low dv/dt Rectifier

We know that the load at the output of the rectifier can vary depending on the applications. The following Fig. 2.14 shows change in efficiency of the current-driven Class-E low dv/dt (ZVS) rectifier when there is variation in load resistance from 1 Ω to 60 Ω in the intervals of 5 Ω. The rectifier satisfies the ZVS condition from $R_L = 1$ Ω to $R_L = 10$ Ω and beyond that, it operates in non-ZVS mode. As we increase the load resistance, the output power and the efficiency of the rectifier starts decreasing. The highest efficiency is obtained at $R_L = 5.624$ Ω. Therefore, $R_L = 5.624$ Ω can be called as the optimum load resistance for the given specifications.

2.3 Voltage-Driven Class-E Low dv/dt (ZVS) Rectifier

2.3.1 Circuit Description

The Class-E low dv/dt (ZVS) rectifier driven by a voltage source V_R. This rectifier is also called as voltage-driven Class-E resonant low dv/dt rectifier. The schematic of the rectifier is shown in Fig. 2.15 which consists of rectifying diode D, capacitor C, an inductor L, filter capacitor C_f and a load resistor R_L. The capacitor is connected in parallel with the rectification diode. The inductor is connected in series with the parallel combination of diode and capacitor. At the input of the rectifier, there is AC voltage whereas at the output DC power is delivered. The rectification is carried out by inductor L, capacitor C, and diode D. The rectified voltage is then further given to the first order low pass filter formed by filter capacitor and load resistor $C_f - R_L$. The high-frequency ripple in the output voltage is attenuated by first order low pass filter. The following advantages of this rectifier topology make it a better candidate than other class-E low dv/dt rectifiers:

1. If the transformer is coupled to this rectifier, then the leakage inductance, as well as the lead inductance, can be absorbed by the inductor L.

2. The diode junction capacitance formed due to irregularity in charges at pn junction can be absorbed by the capacitor C.

These advantages make the rectifier suitable for high-frequency applications, especially in DC-DC converters. The steady state operation of the voltage-driven Class-E low dv/dt (ZVS) rectifier is divided into two stages based on the diode ON and OFF condition.[8]

2.3.2 Principle of Operation

In this case, the duty cycle is equal to 0.5. When the diode is ON, a forward current starts flowing through it and when the diode is reverse biased or in OFF condition, it blocks any dc current. When the diode is ON, the capacitor C is short-circuited and

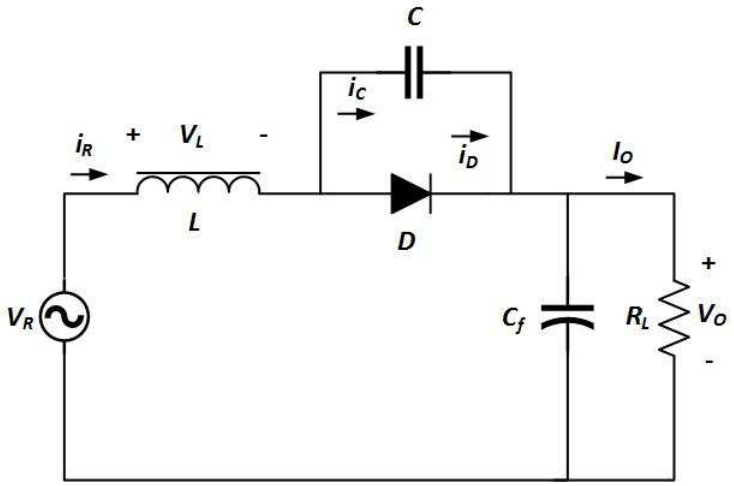

Figure 2.15: voltage-driven Class-E low dv/dt (ZVS) rectifier [8].

then the inductor L is in series with first order low pass filter. The inductor current is driven by the difference between sinusoidal input voltage and the DC output voltage $V_R - V_O$. The current through inductor and diode is equal to the current drawn by the source during ON time. The maximum forward current through the diode is equal to the peak value of current drawn by the source during ON time. When the diode current reaches to zero the turn OFF transition of the diode will commence.

Now, when the diode turns OFF, the inductor and the capacitor form a series resonant circuit connected in series with first order low pass filter. The difference between input sinusoidal voltage and DC output voltage will drive the series resonant circuit. As a result, the current through the inductor and the capacitor will be a portion of the sinusoid. The voltage across the diode is dependent on the current through the capacitor as in the case of the current-driven Class-E low dv/dt (ZVS) rectifier. The capacitor current can be given as $i_C = C\frac{dv_c}{dt}$ i.e. capacitor current is equal to the product of capacitance and the rate of change of capacitor voltage with respect to time. At ωt=0, capacitor current goes to zero which in turn makes $\frac{dv_c}{dt} = 0$. Here, the capacitor and diode voltage are equal i.e. $V_C = V_D$. Now, when the capacitor current goes negative, both capacitor and diode voltage starts decreasing

gradually. The minimum diode voltage is obtained when capacitor current goes to zero. When the capacitor current increases on the positive side, the diode voltage along with capacitor voltage starts increasing gradually. When the diode reaches its threshold voltage it turns ON. The diode and capacitor voltages are sinusoidal in nature and have the slope equal to zero during the transition of the diode from ON to OFF. In other words, the diode turns ON and OFF at low $\frac{dv_D}{dt}$. During the transition, the capacitor adds delay to the rising voltage across diode to achieve soft switching (ZVS) which further reduces switching losses and noise. In case of class E rectifiers, the reverse recovery characteristics of the pn junction diode should be considered so as to get insights of the reverse recovery current at diode turn ON and OFF instances.[8]

2.3.3 Reverse Recovery Characteristics of the PN Junction Diode

When the diode is forward biased, the current associated with it is made up of both majority and minority carriers. Once the forward current is established, there will be free minority carriers in the pn junction. Ideally, we know that when the forward current of the diode reaches to zero it stops conducting, but due to free minority carriers present in the pn junction and also in the bulk semiconductor material diode continues to conduct for a small amount of time. When the forward current goes to zero, the diode is said to be reversed biased. As per diode characteristics, there should be no reverse current ignoring the leakage current. But practically, diode does exhibit reverse characteristics for a small amount of time. In order to neutralize the minority carriers, they should be combined with opposite charges. This process requires a finite period of time, known as reverse recovery time t_{rr}.

When the diode exhibits the reverse recovery characteristics then the reverse current reaches its maximum value on a negative side (i.e. maximum reverse current) and again gradually rising it settles down to zero as per the characteristics. The reverse

recovery time is measured at initial zero crossing of the diode current from forward to reverse biased condition of the diode to 25% of the maximum reverse current. The time difference between initial zero crossing of the diode current at forward to reverse biased condition and maximum reverse current is called as storage time. Generally, there are two types of reverse recovery characteristics as follows.

1. Soft reverse recovery characteristic and

2. Abrupt reverse recovery characteristic.

Generally, the characteristic is classified on the basis of the time required for the diode to reach 25% of the maximum reverse current from the maximum reverse current. This time is dependent on the charge stored in the bulk semiconductor material and also on the minority charge carriers. If the diode takes a longer time to reach 25% of the maximum reverse current from maximum reverse current, then the diode is said to have soft reverse recovery characteristics. Whereas, if the diode quickly settles to 25% of maximum reverse current then the diode is said to have abrupt reverse recovery characteristics. The magnitude of the maximum reverse current is dependent on certain factors such as junction temperature, the rate of fall of forward current and amount of forward current before commutation. When the diode experiences the change over from forward conduction mode to reverse blocking mode a certain amount of charge carriers flow across diode known as reverse recovery charge carriers. The amount of the reverse charge carriers is nothing but the area enclosed by path of reverse recovery current.[9]

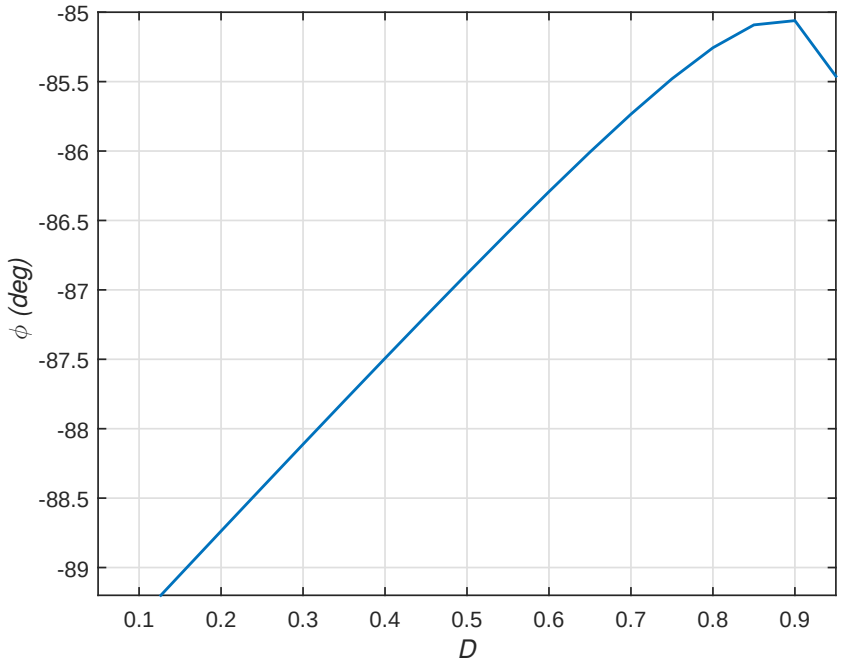

Figure 2.16: Phase angle as a function of duty cycle.

2.3.4 Effect of Variation in Duty Cycle on Phase Angle and AC-to-DC Current and Voltage Transfer Function

The equations for phase angle, AC-to-DC voltage transfer function, and loaded quality factor are followed from "Resonant Power Converters" by Kazimierczuk [7]. Fig. 2.16 shows the relation between duty cycle and the phase of the rectifier. The variations in duty cycle have corresponding changes in turn ON and OFF transitions as well as on other parameters including phase, AC-to-DC current transfer function and normalized load resistance or loaded quality factor. The phase angle of the rectifier is given as,

$$\phi = \tan^{-1} \frac{[4 + 4\pi^2 D(1-D)]\cos(2\pi D) + 2\pi(2D-1)\sin 2\pi D + \sin^2(2\pi D) - 4}{2\pi(1-D) - [1 + 4\pi^2 D(1-D)]\sin 2\pi D - [2\pi(1-D) - \sin 2\pi D]\cos 2\pi D} \tag{2.13}$$

where, ϕ is the initial phase and D is the duty cycle of the rectifier. As we increase the duty cycle from 0 to 1 the phase angle of the rectifier also increases from $-89°$ to $-85°$.

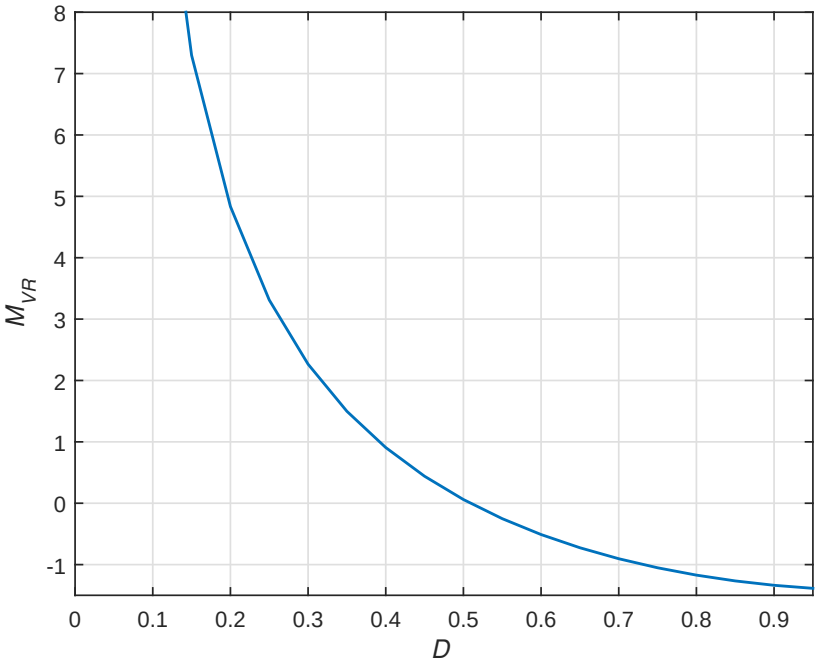

Figure 2.17: AC-to-DC voltage transfer function as a function of duty cycle.

Fig. 2.17 shows the relation between duty cycle and AC-to-DC voltage transfer function of the rectifier. The AC-to-DC voltage transfer function M_{VR} can be given as the ratio of DC output voltage to the RMS value of input voltage.

$$M_{VR} = \frac{V_O}{V_{rms}} \tag{2.14}$$

When the average current across the capacitor reaches zero, the AC-to-DC voltage transfer function can also be given in terms of duty cycle and phase as follows.

$$M_{VR} = \sqrt{2}\frac{\pi(1-D)\sin 2\pi D \sin\phi + [\frac{1}{2}\sin 2\pi D + \pi(1-D)\cos 2\pi D]\cos\phi}{\cos 2\pi D - 1} \tag{2.15}$$

where, ϕ is the phase and D is the duty cycle of the rectifier. When the duty cycle increases from 0 to 1 the AC-to-DC voltage transfer function decreases.

Fig. 2.18 shows the relation between the loaded quality factor and duty cycle. In order to obtain the component values of the rectifier we need to relate normalized load resistance, AC-to-DC voltage transfer function, phase and duty cycle of the rectifier.

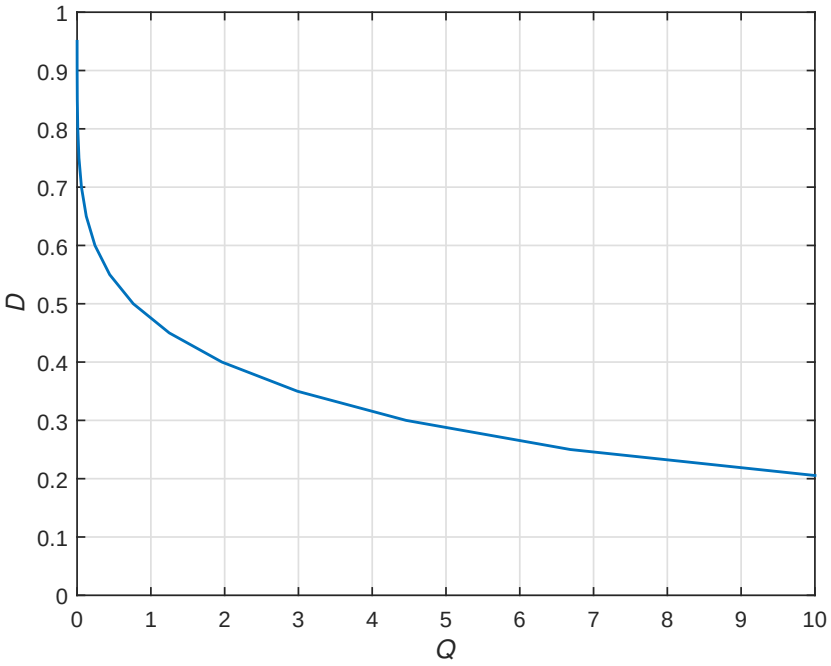

Figure 2.18: Duty cycle as a function of loaded quality factor.

The normalized load resistance is also called as loaded quality factor and can be given as follows.

$$Q = \frac{M_{VR}}{\frac{\cos 2\pi D - 1}{\sqrt{2}\pi} + \sqrt{2}(D - \frac{\sin 2\pi D}{2\pi})\cos\phi + \pi D^2 M_{VR}} \tag{2.16}$$

where, Q is the loaded quality factor, M_{VR} is the AC-to-DC- voltage transfer function, ϕ is the phase and D is the duty cycle of the rectifier. When the loaded quality factor increases the corresponding duty cycle decreases.

Fig. 2.19 shows the relation between the loaded quality factor and the AC-to-DC-voltage transfer function.

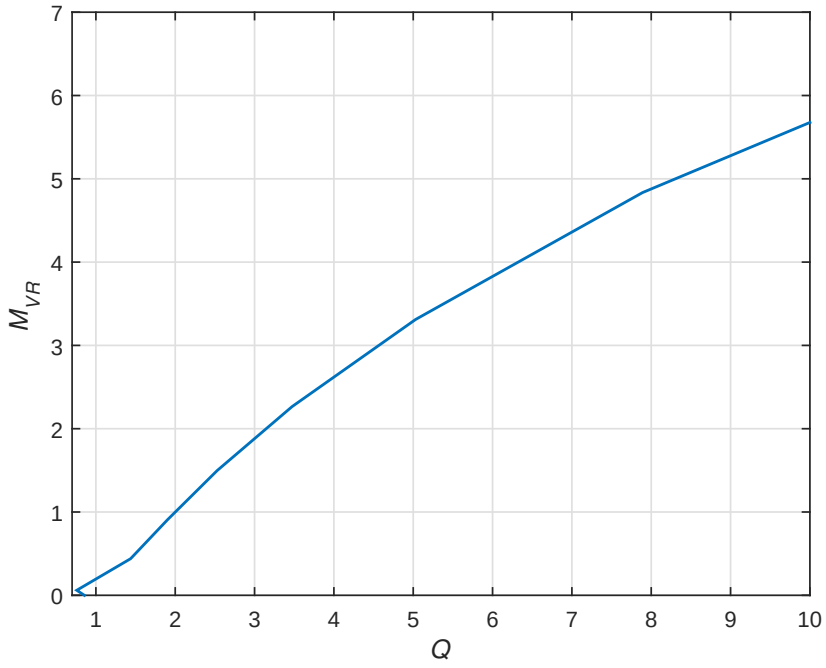

Figure 2.19: AC-to-DC- voltage transfer function as a function of loaded quality factor.

2.3.5 Parameters of the Voltage-Driven Class-E Low dv/dt (ZVS) Rectifier

Table 2 comprises of values of parameters of the voltage-driven Class-E low dv/dt (ZVS) rectifier such as duty cycle, phase angle, AC-to-DC voltage transfer function and loaded quality factor.

Table 2: Parameters of the Voltage-Driven Class-E Low dv/dt (ZVS) Rectifier.

Duty Cycle (D)	**Phase** ($^\circ$)	**Quality factor** (Q)	M_{VR}
0	0	∞	∞
0.05	-89.68	127.12	26.17
0.1	-89.36	31.72	12.09
0.15	-89.05	41.06	7.29
0.2	-88.73	7.89	4.83
0.25	-88.42	5.03	3.31
0.3	-88.11	3.47	2.26
0.35	-87.80	2.52	1.49
0.4	-87.49	1.90	0.90
0.45	-87.18	1.43	0.43
0.5	-86.88	0.75	0.06
0.55	-86.58	1.25	-0.25
0.6	-86.29	0.96	-0.51
0.65	-86.00	0.97	-0.72
0.7	-85.73	0.67	-0.9
0.75	-85.47	0.58	-1.05
0.8	-85.25	0.51	-1.17
0.85	-85.09	0.45	-1.26
0.9	-85.06	0.40	-1.33
0.95	-85.46	0.36	-1.38
1	0	0	$-\infty$

2.3.6 Component Values

The voltage-driven Class-E low dv/dt (ZVS) is designed following the design example from "Resonant Power Converters" by Kazimierczuk [7] to obtain DC output voltage

between 12 V to 15 V, output power between 25 W to 40 W for 6.78 MHz frequency. Initially, the maximum amplitude of input voltage V_M can be given as follows.

$$V_M = \frac{\sqrt{2}V_O}{M_{VR}} = 57.58 \text{ V}. \tag{2.17}$$

where V_O is the DC output voltage and M_{VR} is the AC-to-DC voltage transfer function. Observing the above equation, we can say that the maximum amplitude of input voltage is inversely proportional to the AC-to-DC voltage transfer function.

The minimum value of the filter capacitance can be obtained assuming maximum allowable peak to peak voltage ripple in filter capacitor is 5% of the output voltage as follows.

$$C_{fmin} = \frac{1}{\omega}\sqrt{\frac{1}{\frac{V_r^2}{4(I_{DM}-I_O)} - r_c^2}} = 312.65 \text{ nF}. \tag{2.18}$$

where ω is the angular frequency, V_r is the peak to peak voltage ripple, I_{DM} is the maximum diode current, I_O is the DC output current and r_c is the ESR of the filter capacitor.

The value of inductance and capacitance can be obtained with the help of load resistance as follows.

$$L = \frac{R_{Lmin}}{\omega_o Q} = 0.339 \ \mu\text{H}. \tag{2.19}$$

And,

$$C = \frac{Q}{\omega_o R_{Lmin}} = 1.162 \text{ nF}. \tag{2.20}$$

where Q is the loaded quality factor, R_{Lmin} is the minimum load resistance and ω_O is the angular frequency of the rectifier.

Considering the output voltage and output power as 15 V and 40 W respectively, we can obtain parameters of the voltage-driven class-E low dv/dt (ZVS) rectifier as follows.

Maximum output current:

$$I_{Omax} = \frac{P_{Omax}}{V_O} = 2.667 \text{ A}. \tag{2.21}$$

Minimum load resistance:

$$R_{Lmin} = \frac{V_O}{I_{Omax}} = 5.624\ \Omega. \tag{2.22}$$

Maximum diode voltage for $D = 0.5$:

$$V_{DM} = 3.601 V_O = 54.015\ \text{V}. \tag{2.23}$$

Maximum diode current for $D = 0.5$:

$$I_{DM} = 2.777 I_{Omax} = 7.406\ \text{A}. \tag{2.24}$$

2.3.7 Results

The simulation results for the voltage-driven Class-E low dv/dt (ZVS) rectifier are shown as follows. The capacitor voltage and current for the corresponding input voltage of the rectifier are shown in Fig. 2.20. We know that when the diode is OFF the current across the capacitor is a portion of the sinusoid. This current shapes the voltage across the capacitor. The capacitor current decreases gradually and when it reaches zero, the capacitor voltage attains its maximum value (on the negative side). Next, the capacitor current starts increasing as a result of which the diode voltage starts increasing (since, $V_C = V_D$). When the diode voltage reaches its threshold value diode turns ON. The maximum and average capacitor current measured is 4.9681 A and -0.019 A respectively. The maximum and average capacitor voltage and current measured is 0.6478 V and -15.061 V respectively.

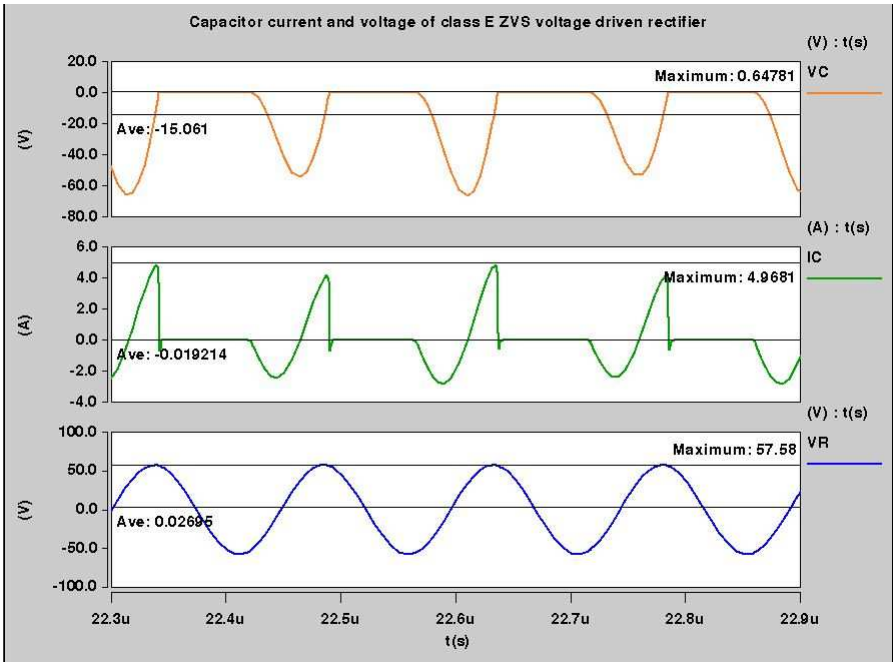

Figure 2.20: Capacitor current, voltage and input voltage of voltage-driven Class-E low dv/dt rectifier.

The diode voltage and current waveforms for the corresponding input voltage of the voltage-driven Class-E low dv/dt (ZVS) rectifier are shown in Fig. 2.21. When the diode is OFF, inductor and the shunt capacitance form a series resonant circuit. The voltage across the resonant circuit is the difference between sinusoidal input voltage and DC output voltage. As the current across the capacitor is a portion of sinusoid it shapes the voltage across diode and capacitor and makes their magnitude equal i.e. $(V_C = V_D)$. The waveforms of diode current and voltage complement each other. When the diode current reaches zero, the turn OFF transition of the diode will commence. The maximum and average value of diode current measured is 10.595 A and 2.7613 A respectively. The maximum and average value of diode voltage measured is 0.6478 V and -15.061 V respectively.

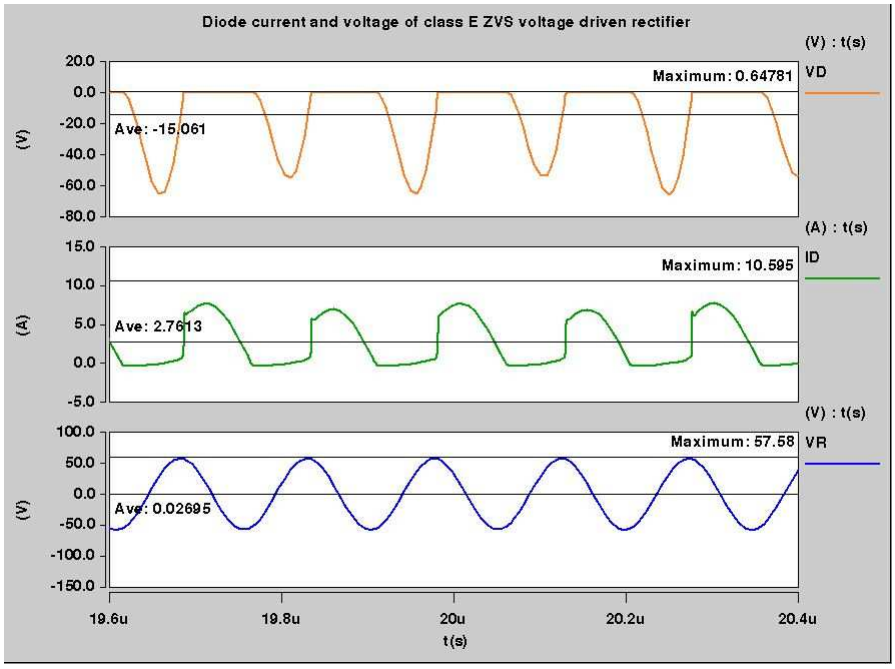

Figure 2.21: Diode current, voltage and input voltage of voltage-driven Class-E low dv/dt rectifier.

The inductor voltage and current waveforms for the corresponding input voltage of the voltage-driven Class-E low dv/dt (ZVS) rectifier are shown in Fig. 2.22. When the capacitor current starts increasing then the capacitor voltage along with the diode voltage starts increasing. When the diode voltage reaches its threshold value (0.7 V for pn junction diode and 0.4 V for Schottky diode) it turns ON and at this instance, the capacitor will be short-circuited. The voltage difference between sinusoidal input voltage and the DC output voltage ($V_R - V_O$) will be responsible for driving the inductor current. The maximum and average value of inductor current measured is 10.595 A and 2.7421 A respectively. The maximum and average value of inductor voltage measured is 93.787 V and 0.1983 V respectively.

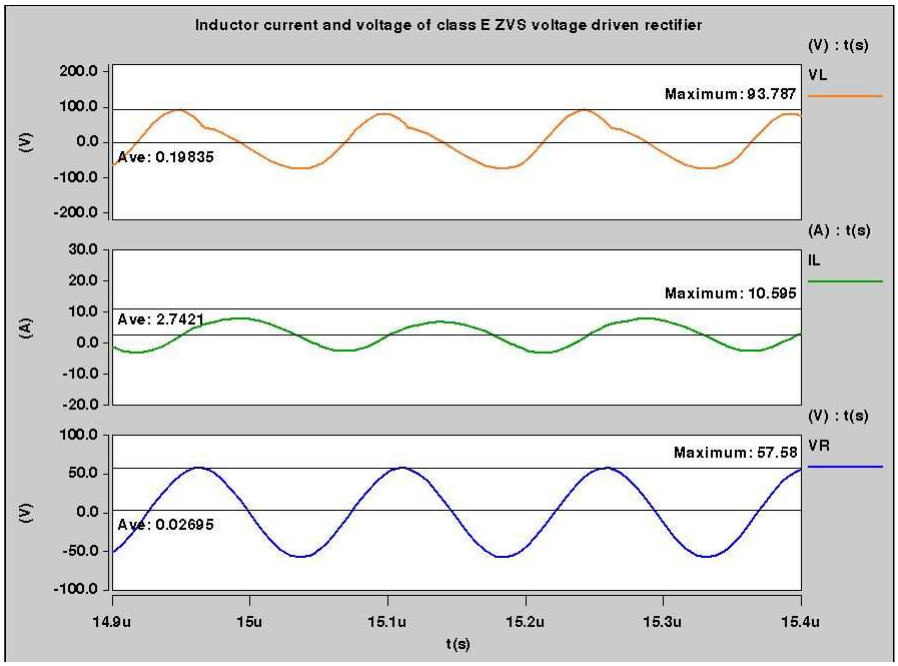

Figure 2.22: Inductor current, voltage and input voltage of voltage-driven Class-E low dv/dt rectifier.

The output voltage and current waveforms for the corresponding input voltage of the voltage-driven Class-E low dv/dt (ZVS) rectifier are shown in Fig. 2.23. The voltage-driven class-E low dv/dt (ZVS) rectifier has sinusoidal voltage source at the input whereas at the output DC voltage is obtained. The desired DC output voltage for the given specifications is 15 V. We obtained the maximum and average DC output voltage of the rectifier as 15.726 V and 14.862 V respectively. The maximum and average output current measured is 2.7963 A and 2.6426 A respectively.

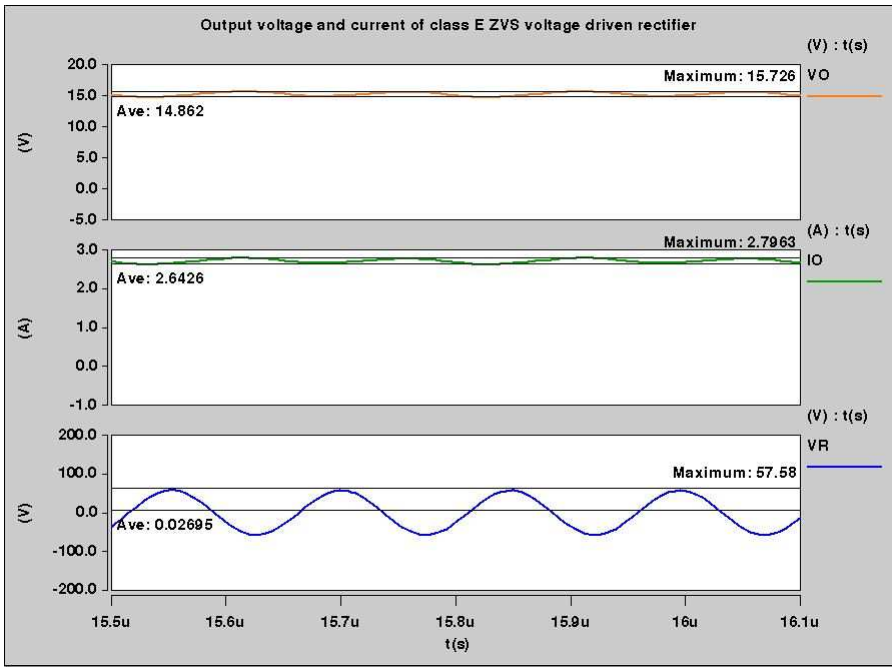

Figure 2.23: Output voltage, current and input voltage of voltage-driven Class-E low dv/dt rectifier.

The output and input power waveforms for the corresponding input voltage of the voltage-driven Class-E low dv/dt (ZVS) rectifier are shown in Fig. 2.24. The voltage-driven Class-E low dv/dt (ZVS) rectifier has sinusoidal voltage source at the input whereas at the output DC power is delivered to the load. The desired DC output power for the given specifications is 40 W. We know that power is the product of voltage and current. The maximum and average value of the input power is obtained as 422.98 W and -45.831 W respectively. Whereas, the maximum and average value of the output power is obtained as 43.976 W and 39.742 W respectively. The efficiency of the rectifier is defined as ratio of the average output power to the input power which can be given as follows.

Efficiency

$$\eta = \frac{P_O}{P_I} = \frac{39.742}{|45.831|} = 86.71\ \%. \tag{2.25}$$

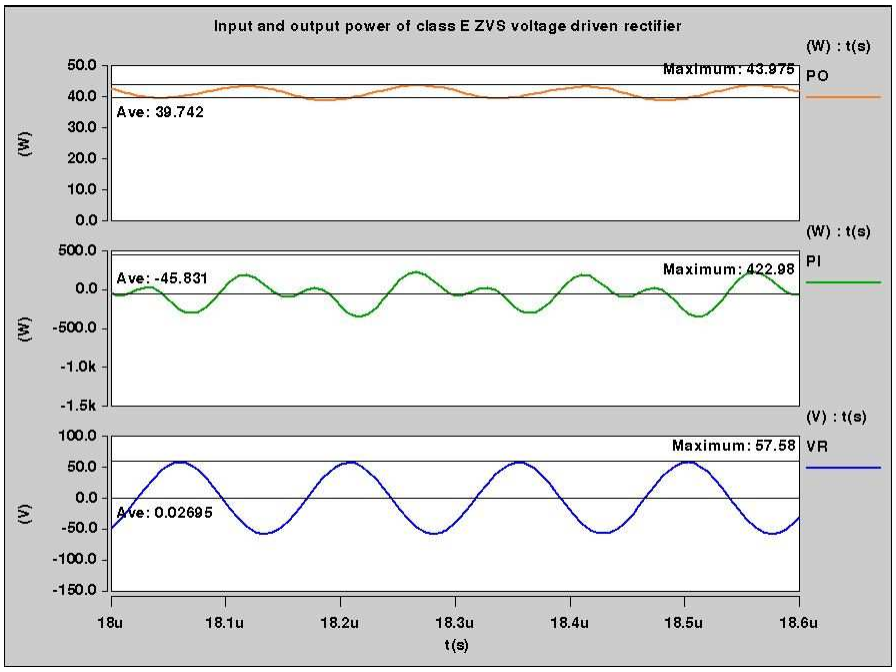

Figure 2.24: Output, input power and input voltage of voltage-driven Class-E low dv/dt rectifier.

The ZVS operation of the voltage-driven Class-E low dv/dt rectifier is shown in Fig. 2.25. The diode voltage waveform of the rectifier is reversed and superimposed on the diode current waveform. The condition for the zero voltage switching is that the switch voltage should be equal to zero at the turn ON instance of the diode. When the switch voltage goes to zero, the diode current starts increasing and the diode turns ON. If the diode voltage is non-zero at the turn ON instance, the diode voltage and diode current waveform overlap on each other causing switching losses. The switching losses lead to power loss. Therefore, the switching losses have an adverse effect on the efficient operation of the rectifier.

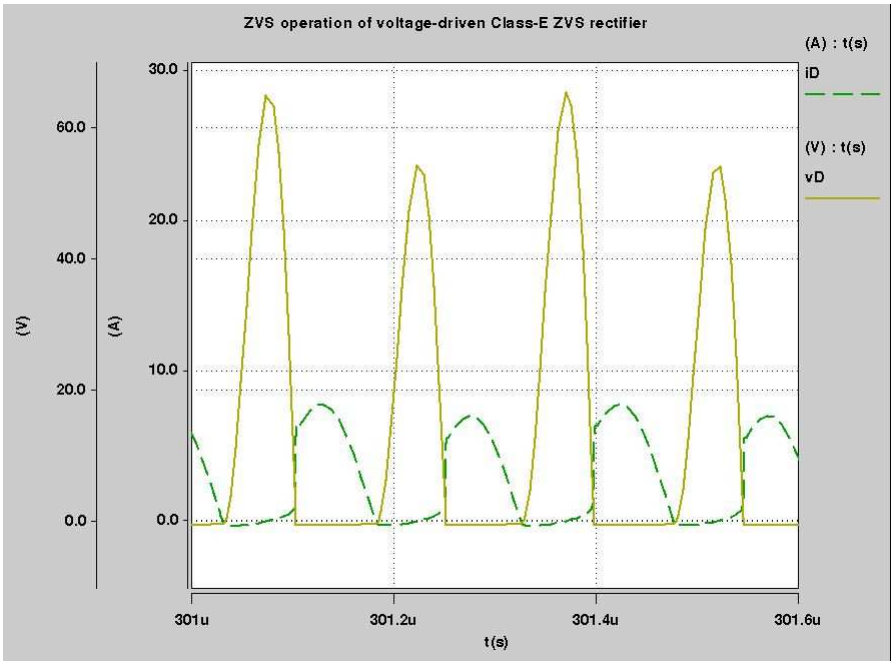

Figure 2.25: ZVS operation of voltage-driven Class-E low dv/dt rectifier.

2.3.8 Effect of Change in Load Resistance on the Efficiency of the Voltage-Driven Class-E Low dv/dt (ZVS) Rectifier

We know that the load at the output of the rectifier can vary depending on the applications. We calculated the optimum load resistance based on the specifications. The following Fig. 2.26 shows change in efficiency of the voltage-driven Class-E low dv/dt (ZVS) rectifier when there is variation in load resistance from 1 Ω to 60 Ω in the intervals of 5Ω. The rectifier satisfies the ZVS condition from $R_L = 1$ Ω to $R_L = 5.624$ Ω and beyond that, it operates in non-ZVS mode. As we increase the load resistance, the output power and the efficiency of the rectifier starts decreasing. The highest efficiency is obtained at $R_L = 5.624$ Ω. Therefore, $R_L = 5.624$ Ω can be called as the optimum load resistance for the given specifications.

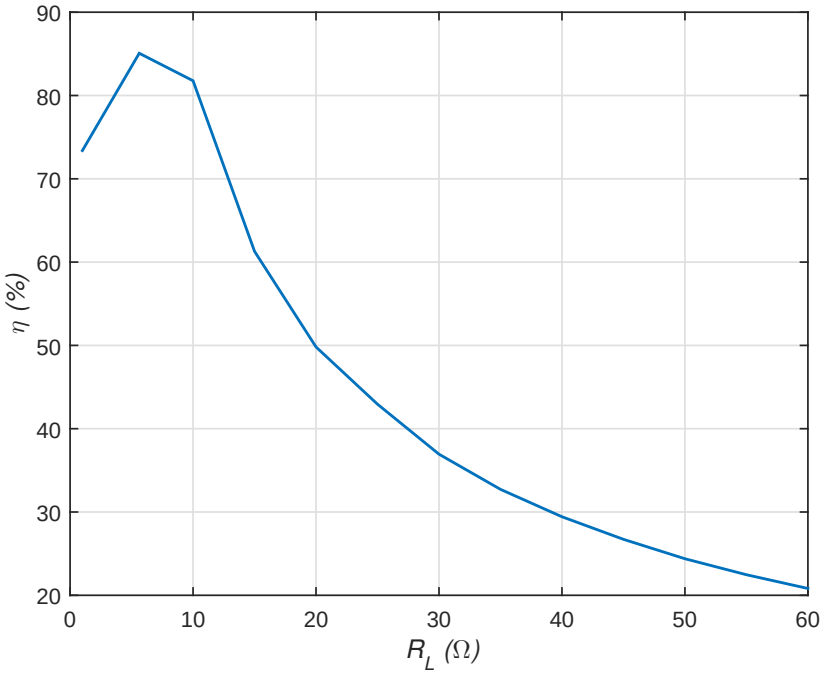

Figure 2.26: Efficiency as a function of the load resistance of the rectifier.

2.4 Current-Driven Class-E Low di/dt (ZCS) Rectifier

2.4.1 Circuit Description

The Class-E low di/dt (ZCS) rectifier is driven by a sinusoidal current source I_R. The schematic of the rectifier is shown in Fig. 2.27 which consists of a rectifying diode D, an inductor L, a filter capacitor C_f and a load resistor R_L. A first order low-pass filter is formed at the output by the duo of filter capacitor and load resistor. The first order low pass filter at the output maintains the ripple voltage below a specified level. Now, we can assume that the ripple voltage is much lower than the DC component of output voltage (V_O). As a result, the first order low pass filter formed by filter capacitor and load resistor can be termed as a DC voltage source. The steady state operation of the current-driven Class-E low di/dt (ZCS) rectifier is divided into two stages based on the diode ON and OFF condition.[10]

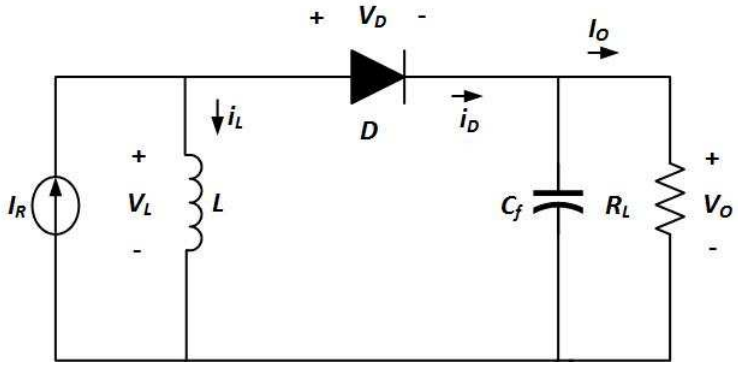

Figure 2.27: current-driven Class-E low di/dt rectifier [10].

2.4.2 Principle of Operation

In this case, duty cycle is equal to 0.75. when the diode is ON, voltage across inductor is equal to the DC voltage source formed by duo of filter capacitor and load resistor. Therefore, the inductor current i_L starts to increase linearly with a slope of $\frac{V_O}{L}t$. The difference between sinusoidal input current I_R and inductor current i_L constitutes the diode current i_D. When the diode current approaches zero, diode turn OFF transition will commence. At turn ON transition, the derivative of diode current is zero and at turn OFF its absolute value is small so, we can say that zero current switching is executed efficiently reducing the switching noise and losses.

Now, when the diode is OFF, diode current i_D will be zero and the inductor current i_L is equal to the sinusoidal input current I_R. As a result, the inductor voltage v_L will be sinusoidal in nature. The difference between the DC output voltage source V_O and the voltage across inductor v_L is equal to diode reverse voltage v_D. In this case, the average value of diode current i_D and diode reverse voltage v_D is equal to the DC output current I_O and DC output voltage V_O respectively.[10]

2.4.3 Effect of Variation in Duty Cycle on Phase Angle and AC-to-DC Current and Voltage Transfer Function

The equations for phase angle, AC-to-DC voltage and current transfer function, and normalized load resistance are followed from "Resonant Power Converters" by Kazimierczuk [7]. Fig. 2.28 shows relation between duty cycle D and initial phase ϕ of the current-driven Class-E low di/dt (ZCS) rectifier. We know that variations in duty cycle will cause corresponding changes in turn ON and OFF transitions of the diode. As a result, it will also have an effect on AC-to-DC current and voltage transfer functions. The phase angle of the rectifier is given as follows.

$$\phi = \tan^{-1} \frac{\sin(2\pi D) - 2\pi D}{1 - \cos 2\pi D} \tag{2.26}$$

where D is the duty cycle of the rectifier and is inversely proportional to the phase angle of the rectifier. When we increase the duty cycle from 0 to 1, the phase angle starts decreasing from 0° to -90°.

Fig. 2.29 shows the relation between duty cycle D and AC-to-DC current transfer function M_{IR} of the rectifier. We know that AC-to-DC current transfer function is defined as the ratio of DC output current to the RMS value of input current. It can be given in terms of phase and load resistance as follows.

$$M_{IR} = \frac{I_O}{I_{RMS}} = \frac{\sqrt{2}\cos\phi}{\frac{R_L}{\omega L}} \tag{2.27}$$

where, ϕ is the phase angle of the rectifier, R_L is the load resistance and ω is the angular frequency. The duty cycle and the AC-to-DC current transfer function share a direct relation i.e. when the duty cycle increases from 0 to 1 the AC-to-DC current transfer function also increases from 0 to 1.3.

Fig. 2.30 shows relation between duty cycle and normalized load resistance $\frac{R_L}{\omega L}$. This relationship gives us idea about variation in load resistance for the corresponding changes in duty cycle at a constant value of ωL. This relationship can be expressed

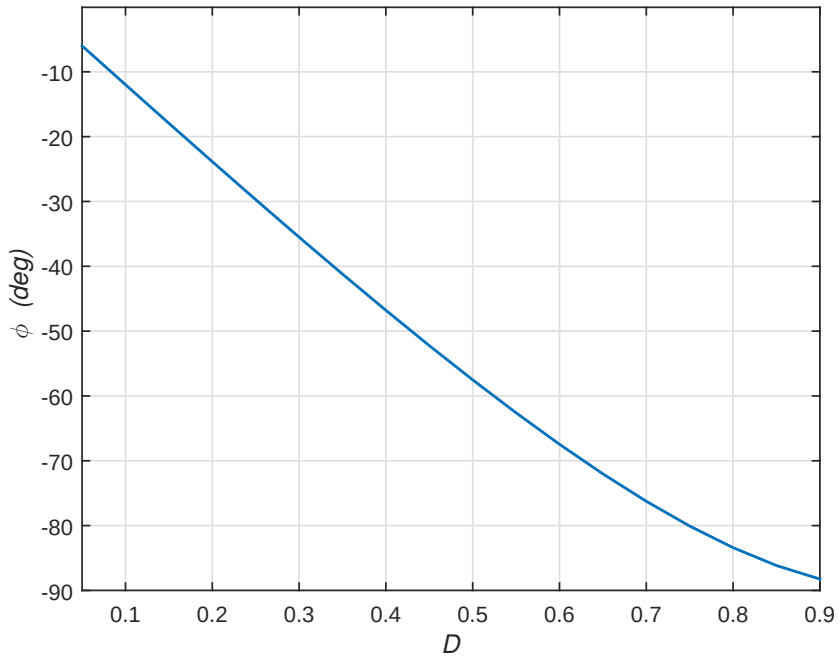

Figure 2.28: Phase angle as a function of duty cycle.

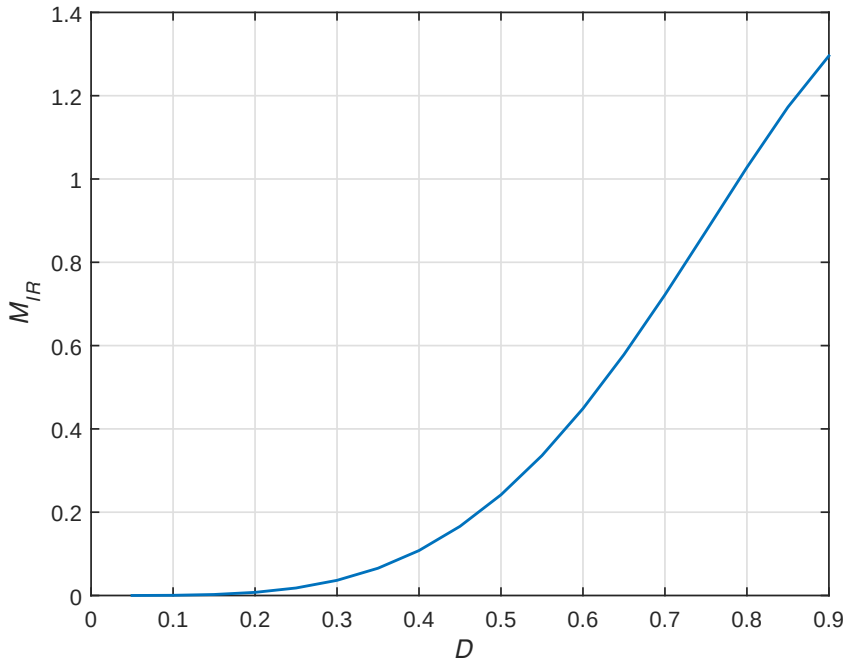

Figure 2.29: AC-to-DC current transfer function as a function of duty cycle.

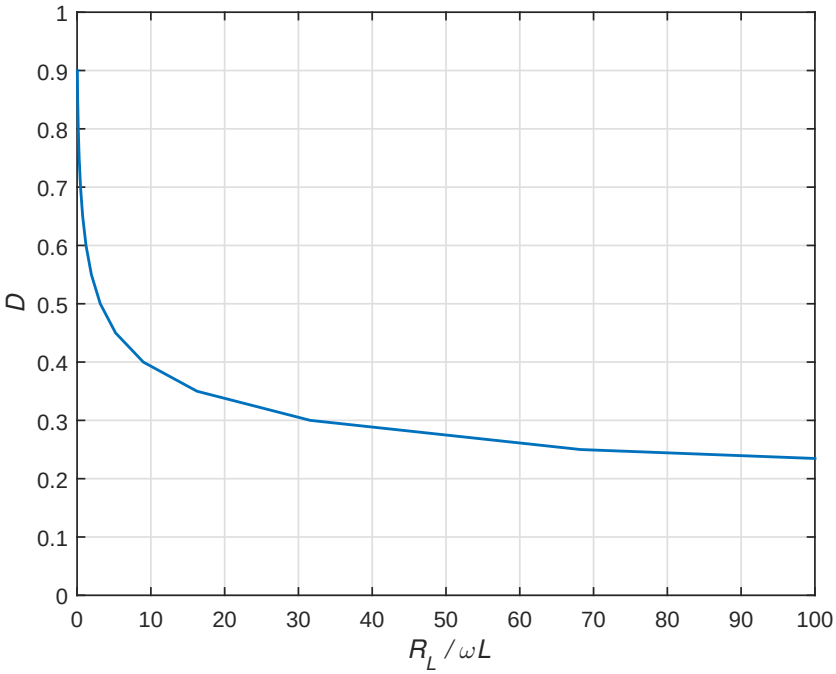

Figure 2.30: Normalized load resistance as a function of duty cycle.

as follows.

$$\frac{R_L}{\omega L} = \frac{2\pi}{1 - 2\pi^2 D^2 - \cos 2\pi D + \frac{(\sin 2\pi D - 2\pi D)^2}{1 - \cos 2\pi D}} \tag{2.28}$$

where, D is the duty cycle and R_L is the load resistance of the rectifier. The load resistance shares inverse relation with duty cycle at a constant value of ωL i.e. when load resistance increases from 0 to 100 it can be seen that duty cycle decreases from 1 to 0.

Fig. 2.31 shows relation between duty cycle D and AC-to-DC voltage transfer function M_{VR} of the rectifier. We know that AC-to-DC voltage transfer function is defined as the ratio of DC output voltage to the RMS value of input voltage. It can be given in terms of input resistance and load resistance as follows.

$$M_{VR} = \frac{V_O}{V_{RiRMS}} = \sqrt{\frac{R_L}{R_i}} \tag{2.29}$$

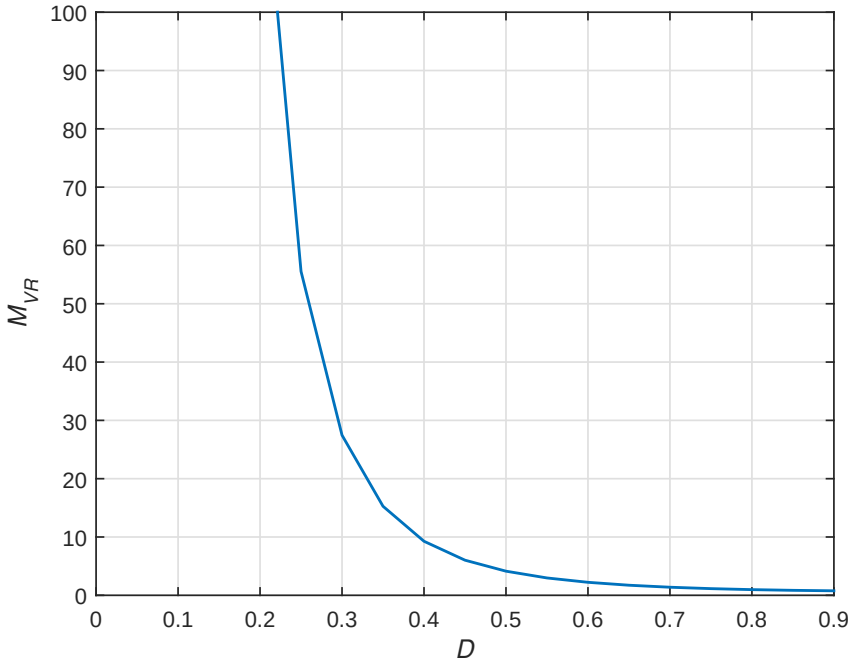

Figure 2.31: AC-to-DC voltage transfer function as a function of duty cycle.

where, ratio of load resistance to the input resistance can be given as follows.

$$\frac{R_L}{R_i} = \frac{2\pi^2}{\cos^2\phi}\left[\frac{1}{1-2\pi^2D^2-\cos 2\pi D+\frac{(\sin 2\pi D-2\pi D)^2}{1-\cos 2\pi D}}\right] \tag{2.30}$$

So, AC-to-DC voltage transfer can be given in terms of load resistance and input resistance as follows.

$$M_{VR} = \sqrt{\frac{2\pi^2}{\cos^2\phi}\left[\frac{1}{1-2\pi^2D^2-\cos 2\pi D+\frac{(\sin 2\pi D-2\pi D)^2}{1-\cos 2\pi D}}\right]} \tag{2.31}$$

where, ϕ is the phase angle of the rectifier, R_L is the load resistance of the rectifier. The duty cycle and the AC-to-DC voltage transfer function share an inverse relation between them i.e. when the duty cycle increases from 0 to 1, the AC-to-DC voltage transfer function decreases from 100 to 0.

2.4.4 Parameters of Current-Driven Class-E Low di/dt (ZCS) Rectifier

Table 3 comprises of values of parameters of the current-driven Class-E low di/dt (ZCS) rectifier such as duty cycle, phase angle, AC-to-DC voltage and current transfer

function and loaded quality factor, the ratio of load resistance to input resistance and normalized load resistance.

Table 3: Parameters of Current-Driven Class-E Low di/dt (ZCS) Rectifier.

Duty Cycle (D)	**Phase** ($^\circ$)	R_L/R_i	R_L/ω_L	M_{IR}	M_{VR}
0	0	∞	∞	0	∞
0.05	-5.99	$1.08\text{X}10^{9}$	$4.628\text{X}10^{4}$	$3.03\text{X}10^{-5}$	$3.29\text{X}10^{4}$
0.1	-11.98	$4.28\text{X}10^{6}$	$2.864\text{X}10^{3}$	$4.82\text{X}10^{-4}$	$2.07\text{X}10^{3}$
0.15	-17.94	$1.71\text{X}10^{5}$	556.40	0.002	413.54
0.2	-23.85	$1.76\text{X}10^{4}$	171.88	0.007	132.89
0.25	-29.71	$3.08\text{X}10^{3}$	68.21	0.018	55.54
0.3	-35.50	753.94	31.61	0.036	27.45
0.35	-41.20	233.11	16.24	0.065	15.26
0.4	-46.78	85.87	8.97	0.107	9.26
0.45	-52.23	36.26	5.21	0.166	6.02
0.5	-57.51	17.11	3.14	0.241	4.13
0.55	-62.60	8.85	1.93	0.336	2.97
0.6	-67.45	4.96	1.20	0.448	2.22
0.65	-72.02	2.98	0.75	0.578	1.72
0.7	-76.24	1.91	0.46	0.722	1.38
0.75	-80.07	1.30	0.27	0.874	1.14
0.8	-83.40	0.94	0.15	1.027	0.97
0.85	-86.16	0.72	0.08	1.172	0.85
0.9	-88.24	0.59	0.03	1.295	0.77
0.95	-89.55	0.52	0.008	1.381	0.72
1	-90	0.50	0	1.41	0.70

2.4.5 Component Values

The current-driven Class-E low di/dt (ZCS) is designed following the design example from "Resonant Power Converters" by Kazimierczuk [7] to obtain DC output voltage between 12 V to 15 V, output power between 25 W to 40 W for 6.78 MHz frequency. Initially, maximum amplitude of input current I_M can be given as follows.

$$I_M = \frac{\sqrt{2} I_{Omax}}{M_{IR}} = 4.313 \text{ A}. \tag{2.32}$$

where, I_{Omax} is the maximum output current and M_{IR} is the AC-to-DC current transfer function. Observing the above equation, we can say that the maximum amplitude of input current is inversely proportional to the AC-to-DC current transfer function.

The minimum value of the filter capacitance can be obtained assuming maximum allowable peak to peak current ripple in filter capacitor is 5% of the output current as follows.

$$C_{fmin} = \frac{I_{DM}}{\omega(V_r - I_{DM} r_C)} = 242.40 \text{ nF}. \tag{2.33}$$

where, ω is the angular frequency, V_r is the peak to peak voltage ripple, I_{DM} is the maximum diode current and r_c is the ESR of the filter capacitor.

The value of inductance can be obtained with the help of load resistance as follows.

$$L = \frac{R_{Lmin}}{0.2789\ \omega} = 473.35 \text{ nH}. \tag{2.34}$$

where, R_{Lmin} is the minimum load resistance and ω is the angular frequency of the rectifier.

Considering the output voltage and output power as 15 V and 40 W respectively, we can obtain parameters of the current-driven Class-E low di/dt (ZCS) rectifier as follows.

Maximum output current:

$$I_{Omax} = \frac{P_{Omax}}{V_O} = 2.667 \text{ A}. \tag{2.35}$$

Minimum load resistance:

$$R_{Lmin} = \frac{V_O}{I_{Omax}} = 5.624 \ \Omega. \tag{2.36}$$

Maximum diode voltage for $D = 0.75$:

$$V_{DM} = 6.712 V_O = 100.68 \text{ V}. \tag{2.37}$$

Maximum diode current for $D = 0.75$:

$$I_{DM} = 2.4071 I_{Omax} = 6.419 \text{ A}. \tag{2.38}$$

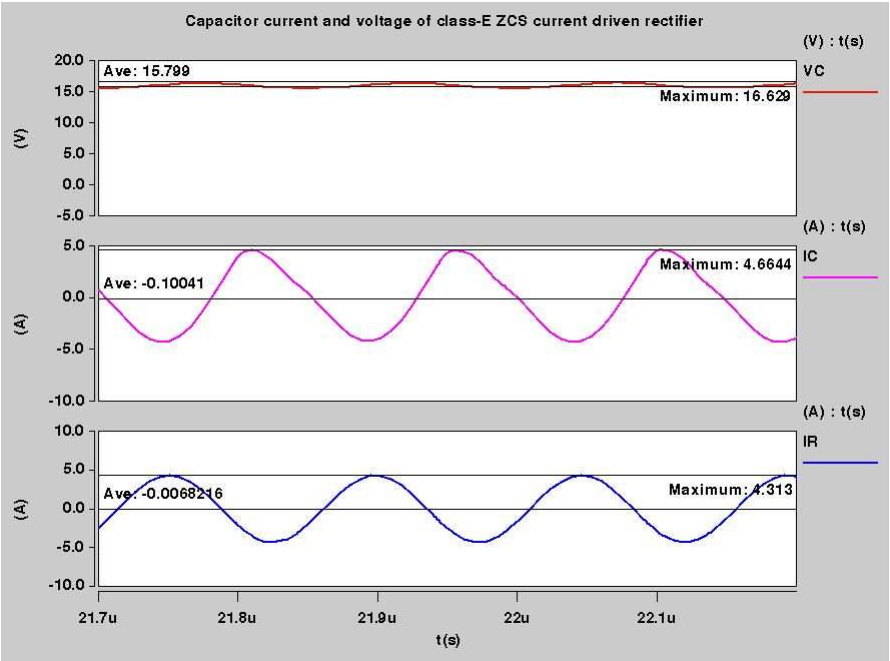

Figure 2.32: Capacitor current, voltage and input current of current-driven Class-E low di/dt rectifier.

2.4.6 Results

The simulation results of the current-driven Class-E low di/dt (ZCS) rectifier are as follows. The capacitor voltage and current waveforms for the corresponding input current of the rectifier are shown in Fig. 2.32. We know that the rectifier is driven by the sinusoidal input current and at the output a DC voltage is obtained. When the diode is ON, the circuit is left with inductor along with voltage source formed by filter capacitor and load resistor $C_f - R_L$. As a result, the inductor current increases linearly. The capacitor voltage and current is almost sinusoidal in nature. The maximum and average capacitor current measured is 4.6644 A and 0.1004 A respectively. The maximum and average capacitor voltage obtained is 16.629 V and 15.799 V respectively.

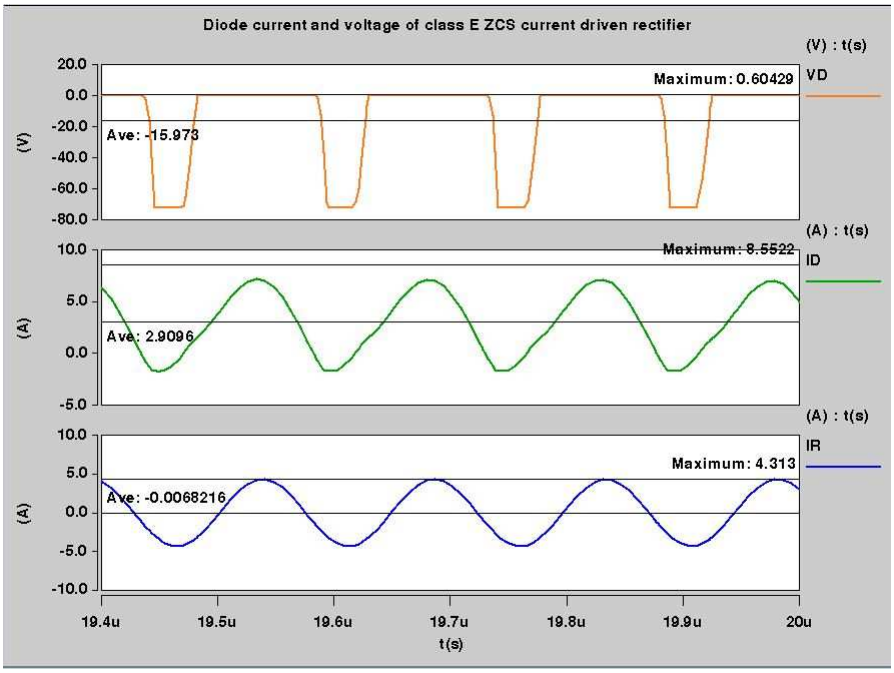

Figure 2.33: Diode current, voltage and input current of current-driven Class-E low di/dt rectifier.

The diode voltage and current waveforms for the corresponding input current of the current-driven Class-E low di/dt (ZCS) rectifier are shown in Fig. 2.33. The diode current constitutes the difference between input current I_R and inductor current i_L. The zero current switching condition is totally based on the diode current and voltage. We can observe from above figure that when diode current reaches zero (i.e. Diode turns OFF) then reverse diode voltage starts flowing. Again, when reverse diode voltage starts increasing and reaches zero we obtain a non-zero diode current and in this way, diode turns ON. If the turn ON and OFF transition of the diode occurs at low $\frac{di_D}{dt}$ then zero current switching (ZCS) is said to be achieved. The maximum and average diode current measured is 8.5522 A and 2.9096 A respectively. The maximum and average diode voltage measured is 0.6042 V and -15.973 V respectively.

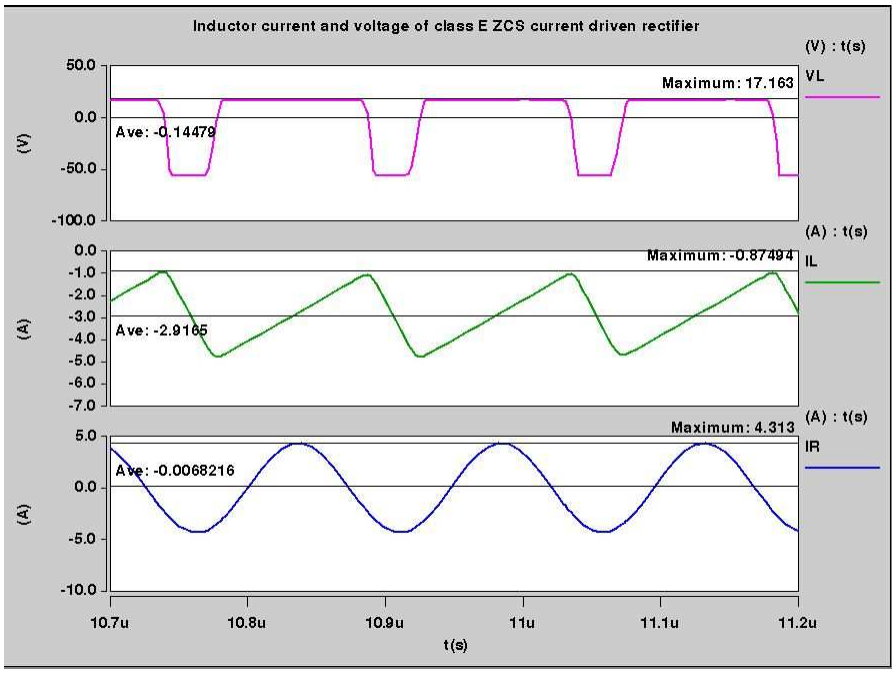

Figure 2.34: Inductor current, voltage and input current of current-driven Class-E low di/dt rectifier.

The inductor voltage and current waveforms for the corresponding input current of the current-driven Class-E low di/dt (ZCS) rectifier are shown in Fig. 2.34. When the diode is ON, the inductor current increases linearly with slope equal to $i_L = \frac{V_O}{L}t$. The turn ON and OFF transition of the diode is partially dependent on inductor current since the diode current is the difference between input current and inductor current. When the diode turns OFF, the inductor current is equal to the input current and as a result of which the inductor voltage resembles a part of the sinewave. The maximum and average inductor current measured is -0.8749 A and -2.9165 A respectively. The maximum and average inductor voltage measured is 17.163 V and -0.1447 V respectively.

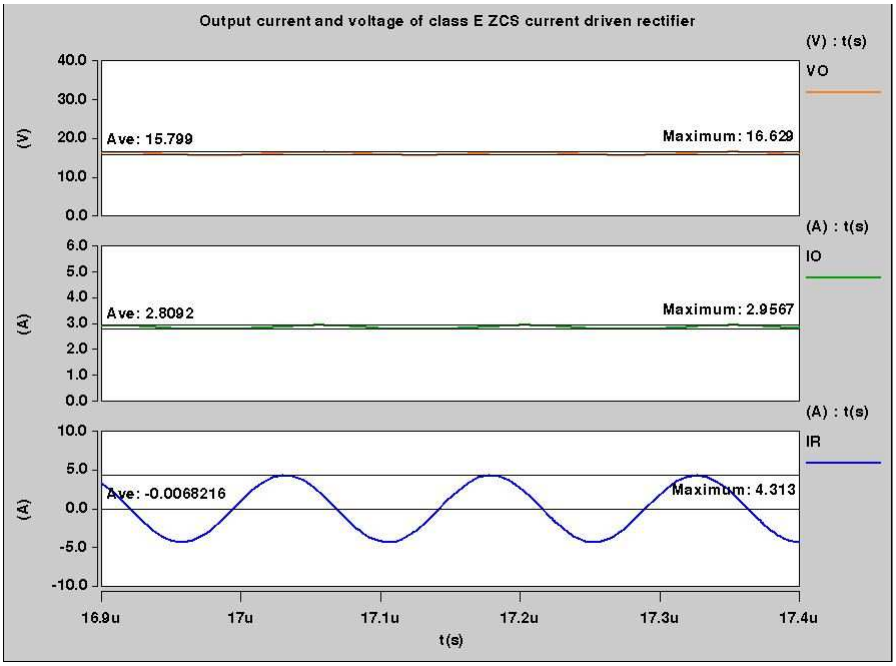

Figure 2.35: Output voltage, current and input current of current-driven Class-E low di/dt rectifier.

The output voltage and current waveforms for the corresponding input current of the current-driven Class-E low di/dt (ZCS) rectifier are shown in Fig. 2.35. The Class-E low di/dt (ZCS) rectifier is driven by a sinusoidal current and at the output, we get DC voltage. The desired DC output voltage for the given specifications is 15 V. We obtained the maximum and average DC output voltage of the rectifier as 16.629 V and 15.799 V respectively. The maximum and average output current measured is 2.9867 A and 2.8092 A respectively.

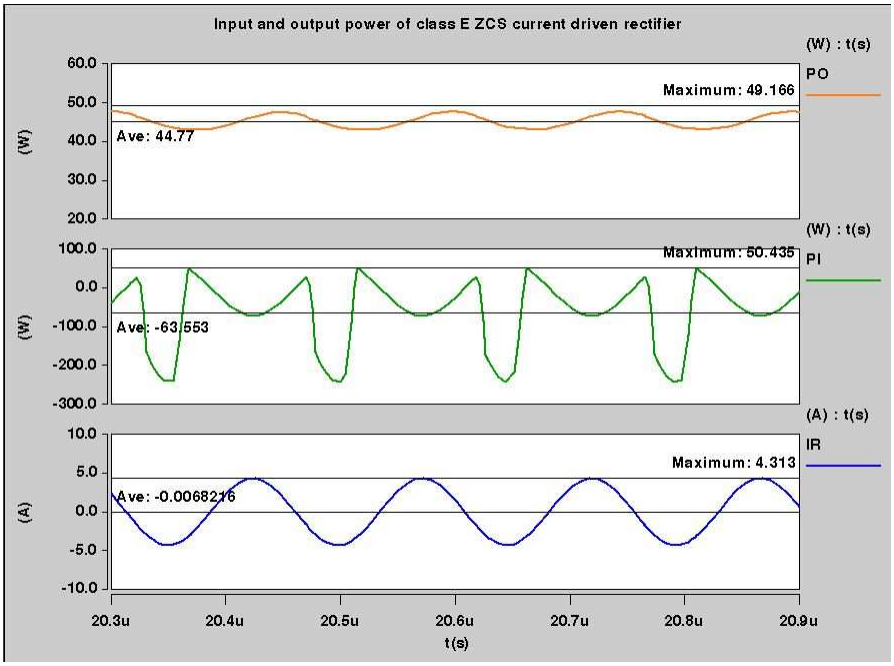

Figure 2.36: Output, input power and input current of current-driven Class-E low di/dt rectifier.

The output and input power waveforms for the corresponding input current of the current-driven Class-E low di/dt (ZCS) rectifier are shown in Fig. 2.36. The Class-E low di/dt (ZCS) rectifier has sinusoidal current source at the input whereas at the output DC power is delivered to the load. The desired DC output power for the given specifications is 40 W. We know that power is the product of voltage and current. The maximum and average value of the input power is obtained as 50.435 W and -63.553 W respectively. The maximum and average value of the output power is obtained as 49.166 W and 44.77 W respectively. The efficiency of the rectifier is defined as ratio of the average output power to the input power which can be given as follows.

Efficiency:

$$\eta = \frac{P_O}{P_I} = \frac{44.77}{|63.553|} = 70.44\ \%. \tag{2.39}$$

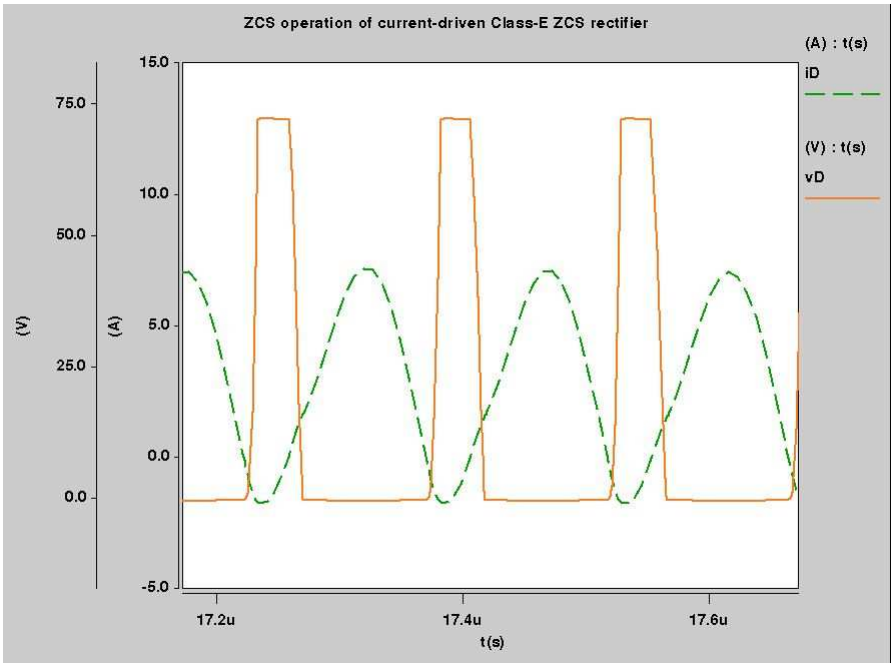

Figure 2.37: ZCS operation of current-driven Class-E low di/dt rectifier.

The ZCS operation of the current-driven Class-E low di/dt rectifier is shown in Fig. 2.37. The diode voltage waveform of the rectifier is reversed and superimposed on the diode current waveform. The condition for the zero current switching is that the current across the switch should be equal to zero at the turn OFF instance of the diode. When the switch current goes to zero, the diode voltage starts increasing and the diode turns OFF. If the diode current is non-zero at the turn OFF instance, the diode voltage and diode current waveform overlap on each other causing switching losses. The switching losses lead to power loss. Therefore, the switching losses have an adverse effect on the efficient operation of the rectifier.

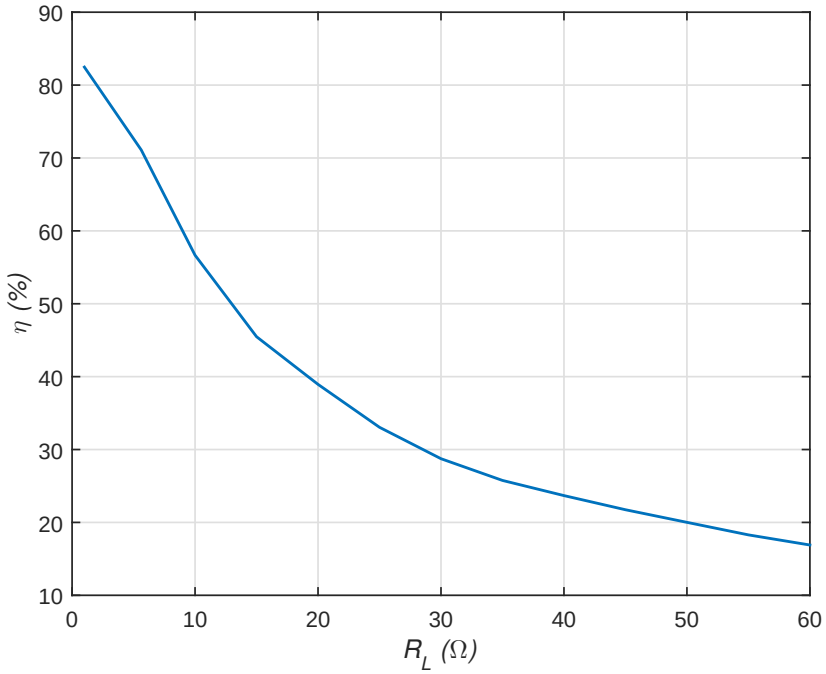

Figure 2.38: Efficiency as a function of the load resistance of the rectifier.

2.4.7 Effect of Change in Load Resistance on the Efficiency of the Current-Driven Class-E Low di/dt (ZCS) Rectifier

We know that the load at the output of the rectifier can vary depending on the applications. We calculated the optimum load resistance based on the specifications. The following Fig. 2.38 shows change in efficiency of the current-driven Class-E low di/dt (ZCS) rectifier when there is variation in load resistance from 1 Ω to 60 Ω in the intervals of 5 Ω. The rectifier satisfies the ZCS condition from $R_L = 1$ Ω to $R_L = 5.624$ Ω and beyond that it operates in non-ZCS mode. As we increase the load resistance, the output power and the efficiency of the rectifier starts decreasing.

2.5 Voltage-Driven Class-E Low di/dt (ZCS) Rectifier

2.5.1 Circuit Description

The Class-E low di/dt (ZCS) rectifier is driven by sinusoidal voltage source V_R. The schematic of the rectifier is shown in Fig. 2.39 which consists of rectifying diode D, an inductor L, filter capacitor C_f and load resistor R_L. The zero current switching (ZCS) is carried out by the diode current i_D which maintains the switching losses and noise along with reverse recovery current. Due to diode current pulses, there will be the generation of harmonics which may affect the efficiency of the rectifier. In order to avoid harmonics, the rectifier is driven at a duty cycle of 0.5. If we drive the rectifier at full load resistance R_{Lmin}, a duty cycle of 0.5 can be obtained keeping the minimum ripple voltage at the output. The combination of filter capacitor C_f and the load resistor R_L form a first order low pass filter. Since the ripple voltage is maintained at a low level as compared to DC component of output voltage we can treat the first order low pass filter formed by filter capacitor and load resistor as a DC voltage source V_O. Now, If the rectifier is connected to the ac source using the isolation transformer, it can lead to the generation of transformer leakage inductance or diode lead inductance. But, in this rectifier topology, the inductance is designed in such a way that it absorbs all the transformer leakage inductance as well as diode lead inductance into L. The steady state operation of the rectifier is categorized based on diode ON and OFF transitions.[11]

2.5.2 Principle of Operation

When the diode is ON, the circuit will be left with an inductor and the DC voltage source. At this instance, diode voltage will be zero and a finite amount of diode current and inductor voltage will occur. The difference between input sinusoidal voltage and the DC output voltage $(V_R - V_O)$ will determine the amount of diode current and the voltage across the inductor. The diode current is partially sinusoidal and linearly

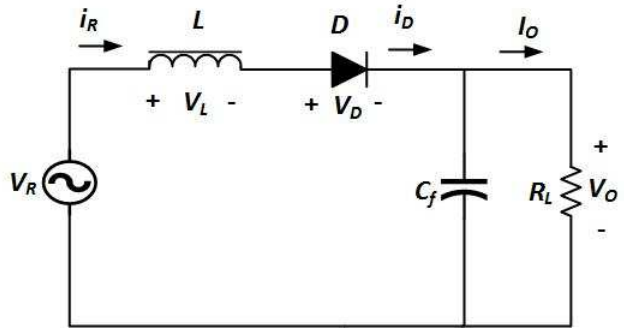

Figure 2.39: voltage-driven Class-E low di/dt rectifier [11].

decreasing in nature. The relation between the voltage across inductor and diode current can be expressed by following equation $V_L = L\frac{di_D}{dt}$ i.e. while turn ON transition of the diode, diode current increases gradually with inductor voltage. When the voltage across inductor reaches zero, diode current attains its maximum value I_{DM}. Again, when the voltage across inductor goes to negative, diode current reaches zero turning OFF the diode. At the diode turn OFF instance, the voltage across inductor was negative which results in a reduced peak value of reverse recovery current avoiding the reverse recovery effect. When the diode is OFF, the voltage across the diode is nothing but the difference between sinusoidal input voltage and the dc output voltage $(V_R - V_O)$. Whereas, the diode current reaches zero. The maximum voltage across diode is given by V_{DM}. When the magnitude of diode voltage reaches its threshold voltage diode turn ON transition occurs. When the diode is OFF, inductance and the junction capacitance form a series resonant circuit which may cause oscillations in the diode voltage.[11]

2.5.3 Effect of Variation in Duty Cycle on Phase Angle and AC-to-DC Current and Voltage Transfer Function

The equations for phase angle, AC-to-DC voltage transfer function, and normalized load resistance are followed from "Resonant Power Converters" by Kazimierczuk [7]. Fig. 2.40 shows the relation between duty cycle D and initial phase ϕ of the voltage-

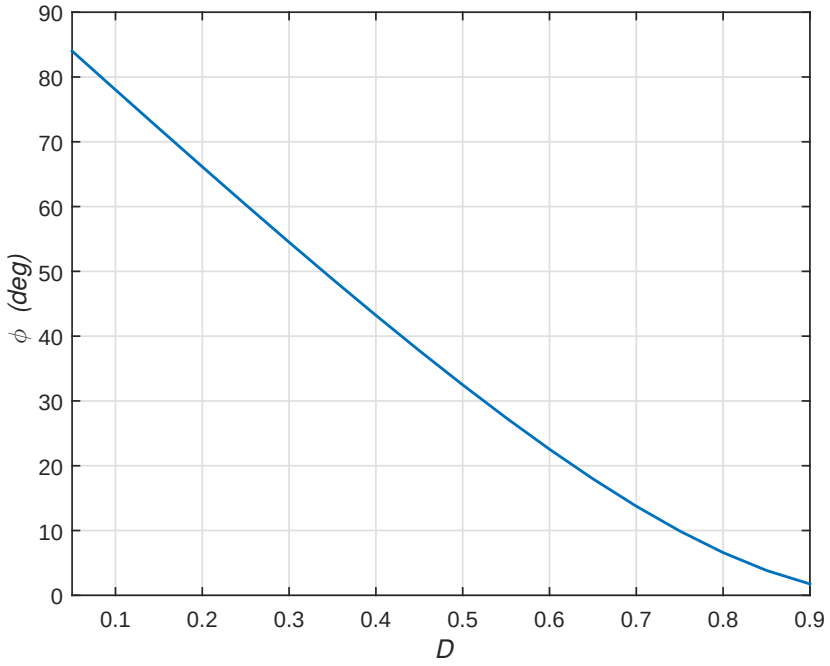

Figure 2.40: Phase angle as a function of duty cycle.

driven Class-E low di/dt (ZCS) rectifier. We know that duty cycle is the important parameter in regards in with turn ON and OFF transitions of the diode. We can express the relation of duty cycle and the initial phase of the rectifier with the help of the following equation.

$$\phi = \tan^{-1} \frac{\sin 2\pi D - 2\pi D}{1 - \cos 2\pi D} \tag{2.40}$$

where ϕ is the phase angle and D is the duty cycle of the rectifier. As we increase the duty cycle from 0 to 1 the phase angle decreases from 90° to 0° so, we can say that phase angle of the rectifier is inversely proportional to the duty cycle.

Fig. 2.41 shows the relation between duty cycle D and normalized load resistance $\frac{R_L}{\omega L}$. The objective behind realizing this relation is to get insight about change in load resistance for the corresponding variation in the duty cycle for a constant value of ωL. We can express the relation of duty cycle and the normalized load resistance of

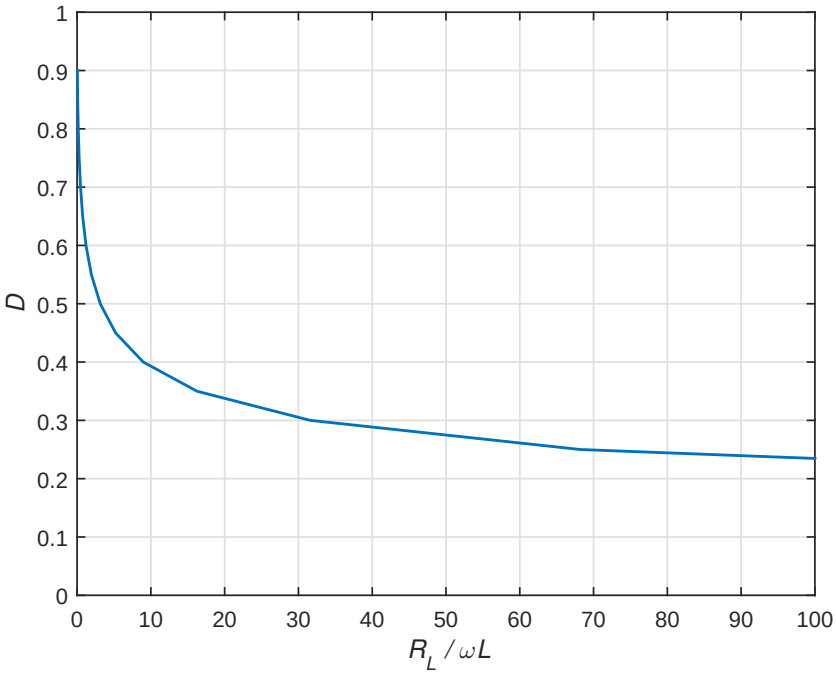

Figure 2.41: Duty cycle as a function of normalized load resistance.

the rectifier with the help of the following equation.

$$\frac{R_L}{\omega L} = \frac{2\pi}{1 - 2\pi^2 D^2 - \cos 2\pi D + \frac{(\sin 2\pi D - 2\pi D)}{\tan \phi}} \tag{2.41}$$

where R_L is the load resistance, D is the duty cycle and ϕ is the phase angle of the rectifier. As we increase the normalized load resistance from 0 to 100 the duty cycle of the rectifier starts decreasing from 0.8 to 0.2 so, we can say that the duty cycle is inversely proportional to the normalized load resistance.

Fig. 2.42 shows the relation between duty cycle D and AC-to-DC voltage transfer function M_{VR}. We know that AC-to-DC voltage transfer function is nothing but the ratio of DC output voltage to the RMS value of input voltage. Duty cycle is an important parameter regarding the diode turn ON and OFF transition which further gives us an idea about AC-to-DC voltage transfer function. We can express the relation of duty cycle and AC-to-DC voltage transfer function of the rectifier with

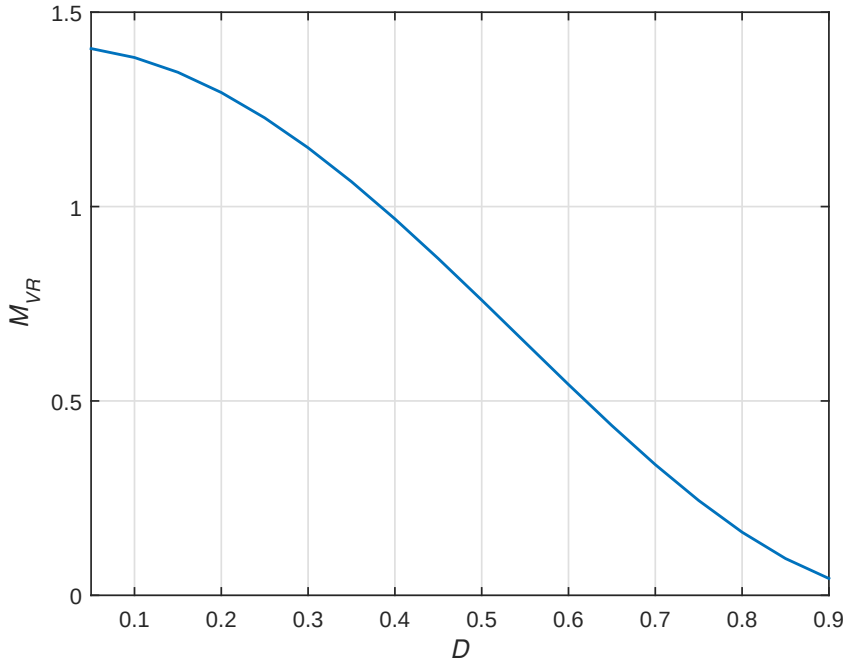

Figure 2.42: AC-to-DC voltage transfer function as a function of duty cycle.

the help of the following equation.

$$M_{VR} = \frac{V_O}{V_{iRMS}} = \sqrt{2}\sin\phi \tag{2.42}$$

where V_O is the DC output voltage, V_{iRMS} is the RMS value of input voltage and ϕ is the phase angle of the rectifier. As we increase the duty cycle from 0 to 1 the AC-to-DC voltage transfer function starts decreasing from 1.4 to 0 so, we can say that the duty cycle is inversely proportional to the AC-to-DC voltage transfer function.

2.5.4 Parameters of Voltage-Driven Class-E Low di/dt (ZCS) Rectifier

Table 4 comprises of values of parameters of the voltage-driven Class-E low di/dt (ZCS) rectifier such as duty cycle, phase angle, AC-to-DC voltage transfer function and normalized load resistance.

Table 4: Parameters of Voltage-Driven Class-E Low di/dt (ZCS) Rectifier.

Duty Cycle (D)	**Phase** ($^\circ$)	R_L/ω_L	M_{VR}
0	90	∞	1.41
0.05	84.00	$4.62\text{X}10^4$	1.40
0.1	78.01	$2.86\text{X}10^3$	1.38
0.15	72.05	556.40	1.34
0.2	66.14	171.88	1.29
0.25	60.28	68.21	1.22
0.3	54.49	31.61	1.15
0.35	48.79	16.24	1.06
0.4	43.21	8.97	0.96
0.45	39.76	5.21	0.86
0.5	32.48	3.14	0.75
0.55	27.39	1.93	0.65
0.6	22.54	1.20	0.54
0.65	17.97	0.75	0.43
0.7	13.75	0.46	0.33
0.75	9.29	0.27	0.24
0.8	6.59	0.15	0.16
0.85	3.83	0.08	0.09
0.9	1.75	0.03	0.04
0.95	0.44	0.008	0.01
1	0	0	0

2.5.5 Component Values

The voltage-driven Class-E low di/dt (ZCS) is designed following the design example from "Resonant Power Converters" by Kazimierczuk [7] to obtain DC output voltage between 12 V to 15 V, output power between 25 W to 40 W for 6.78 MHz frequency. Initially, the maximum amplitude of input voltage V_M can be given as follows.

$$V_M = \frac{\sqrt{2}V_O}{M_{VR}} = 27.92 \text{ V}. \tag{2.43}$$

where, V_O is the output voltage and M_{VR} is the AC-to-DC voltage transfer function. Observing the above equation, we can say that he maximum amplitude of input current is inversely proportional to the AC-to-DC voltage transfer function.

The minimum value of the filter capacitance can be obtained assuming maximum allowable peak to peak voltage ripple in filter capacitor is 5% of the output voltage as follows.

$$C_{fmin} = \frac{I_{DM}}{\omega(V_r - I_{DM}r_C)} = 398.2 \text{ nF}. \tag{2.44}$$

where, ω is the angular frequency, V_r is the peak to peak voltage ripple, I_{DM} is the maximum diode current and r_c is the ESR of the filter capacitor.

The value of inductance can be obtained with the help of load resistance as follows.

$$L = \frac{R_{Lmin}}{2\pi^2 f} = 0.0420 \ \mu\text{H}. \tag{2.45}$$

where, R_{Lmin} is the minimum load resistance and f is the frequency of the rectifier. Considering the output voltage and output power as 15 V and 40 W respectively, we can obtain parameters of voltage-driven Class-E low di/dt (ZCS) rectifier as follows.

Maximum output current:

$$I_{Omax} = \frac{P_{Omax}}{V_O} = 2.667 \text{ A}. \tag{2.46}$$

Minimum load resistance:

$$R_{Lmin} = \frac{V_O}{I_{Omax}} = 5.624 \ \Omega. \tag{2.47}$$

Maximum diode voltage for $D = 0.5$:

$$V_{DM} = 2.862 V_O = 42.93 \text{ V}. \tag{2.48}$$

Maximum diode current for $D = 0.5$:

$$I_{DM} = 3.5621 I_{Omax} = 9.4989 \text{ A}. \tag{2.49}$$

2.5.6 Results

The simulation results of the voltage-driven Class-E low di/dt (ZCS) rectifier are shown as follows. The capacitor voltage and current waveforms for the corresponding input voltage of the rectifier are shown in Fig. 2.43. We know that the rectifier is driven by the sinusoidal input voltage and at the output a DC voltage is obtained. When the diode is ON, the circuit consists of inductor along with voltage source formed by filter capacitor and load resistor $C_f - R_L$. The capacitor voltage and current is almost sinusoidal in nature. The maximum and average capacitor current measured is 9.2385 A and 0.049 A respectively. The maximum and average capacitor voltage obtained is 15.56 V and 14.482 V respectively.

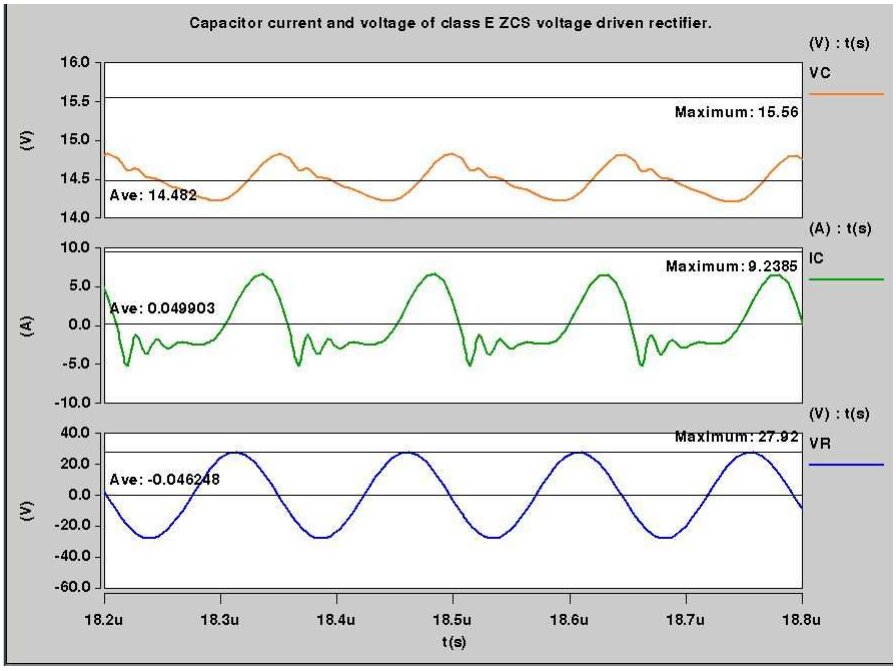

Figure 2.43: Capacitor voltage, current and input voltage of voltage-driven Class-E low di/dt rectifier.

The diode voltage and current waveforms for the corresponding input voltage of the rectifier are shown in Fig. 2.44. The zero current switching (ZCS) condition is totally based on the diode current and voltage. We can observe from above figure that when there is a non-zero diode current (i.e. Diode turns ON) the diode voltage is zero. But, when the diode current reaches zero (i.e. Diode turns OFF) the reverse diode voltage starts increasing and in this way diode turns OFF. If the turn ON and OFF transition of the diode occurs at low $\frac{di_D}{dt}$, then zero current switching (ZCS) is said to be achieved. The maximum and average diode current measured is 11.97 A and 2.625 A respectively. The maximum and average diode voltage measured is 0.6760 V and -14.667 V respectively.

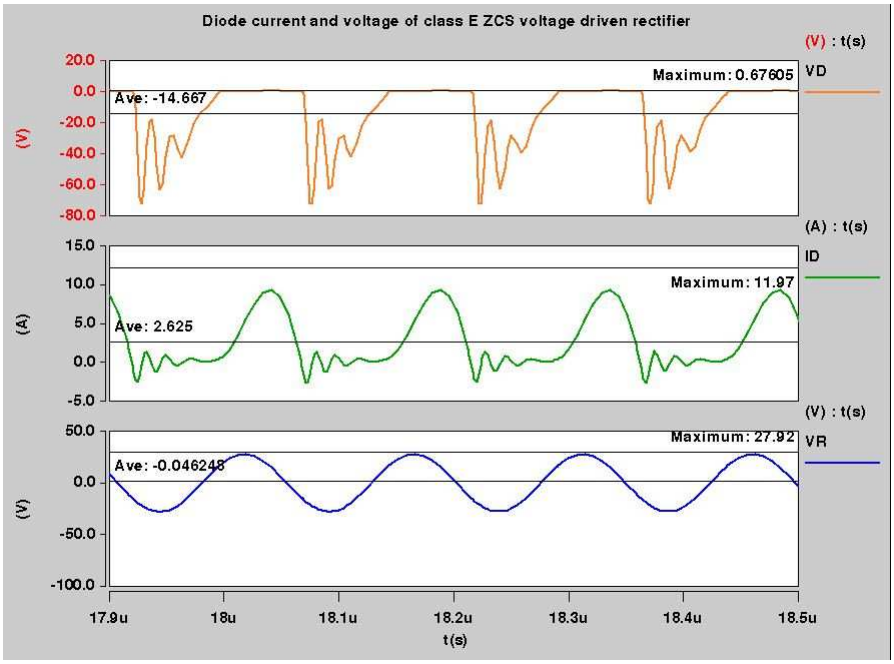

Figure 2.44: Diode voltage, current and input voltage of voltage-driven Class-E low di/dt rectifier.

The inductor voltage and current waveforms for the corresponding input voltage of the rectifier are shown in Fig. 2.45. We know that the inductor voltage and the diode current are related by the equation $V_L = L\frac{di_D}{dt}$. As a result of this, when the voltage across the inductor is positive the diode current starts increasing gradually turning the diode ON. When the voltage across the inductor turns zero the diode current reaches its peak value. Again, when the voltage across inductor goes to negative the diode current reaches to zero turning the diode OFF. Since the inductor voltage has a negative finite value at the turn OFF we can say that the diode turned OFF at low $|\frac{di_D}{dt}|$ achieving zero current switching (ZCS). Due to the zero current switching (ZCS) effect reduces the diode reverse recovery current which eventually helps the rectifier in getting rid of the diode reverse recovery problem. The maximum and average inductor current measured is 11.97 A and 2.625 A respectively. The maximum and average inductor current measured is 36.936 V and 0.1126 V respectively.

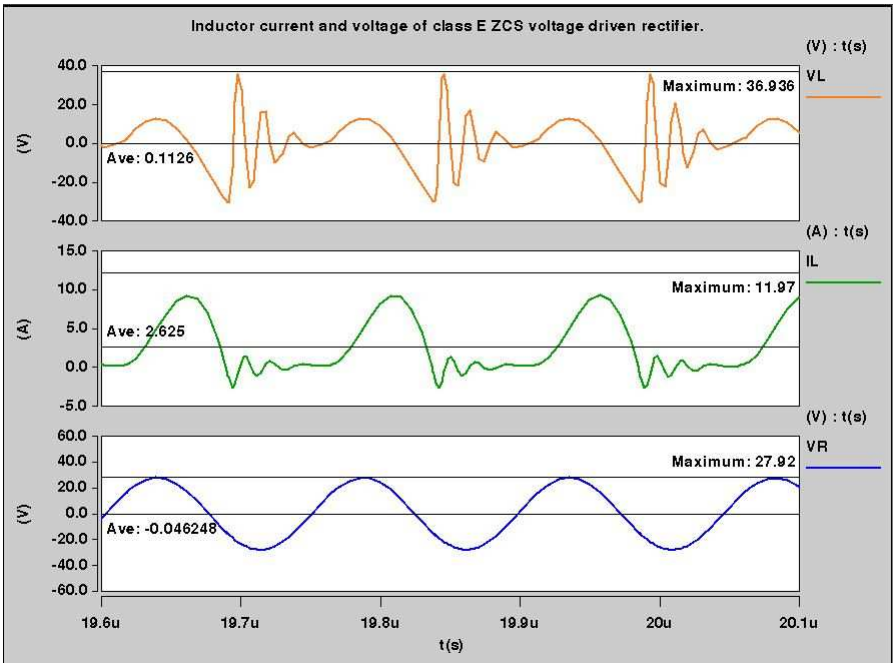

Figure 2.45: Inductor voltage, current and input voltage of voltage-driven Class-E low di/dt rectifier.

The output voltage and current waveforms for the corresponding input voltage of the voltage-driven Class-E low di/dt (ZCS) rectifier are shown in Fig. 2.46. The Class-E low di/dt (ZCS) rectifier is driven by a sinusoidal voltage and at the output, we get DC voltage. The desired DC output voltage for the given specifications is 15 V. We obtained the maximum and average DC output voltage of the rectifier as 15.56 V and 14.482 V respectively. The maximum and average output current measured is 2.7666 A and 2.5751 A respectively.

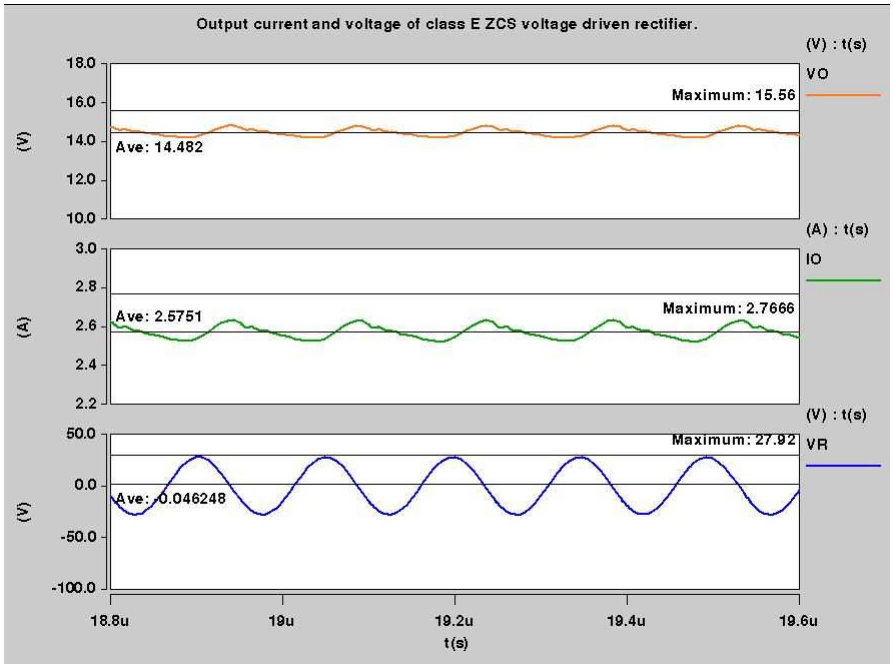

Figure 2.46: Output voltage, current and input voltage of voltage-driven Class-E low di/dt rectifier.

The output and input power waveforms for the corresponding input voltage of the voltage-driven Class-E low di/dt (ZCS) rectifier are shown in Fig. 2.47. The Class-E low di/dt (ZCS) rectifier has sinusoidal voltage source at the input whereas at the output DC power is delivered to the load. The desired DC output power for the given specifications is 40 W. We know that power is the product of voltage and current. The maximum and average value of the input power is obtained as 46.684 W and -43.56 W respectively. Whereas, the maximum and average value of the output power is obtained as 43.048 W and 37.3 W respectively. The efficiency of the rectifier is defined as ratio of the average output power to the input power which can be given as follows.

Efficiency:

$$\eta = \frac{P_O}{P_I} = \frac{37.3}{|43.56|} = 85.62\ \%. \tag{2.50}$$

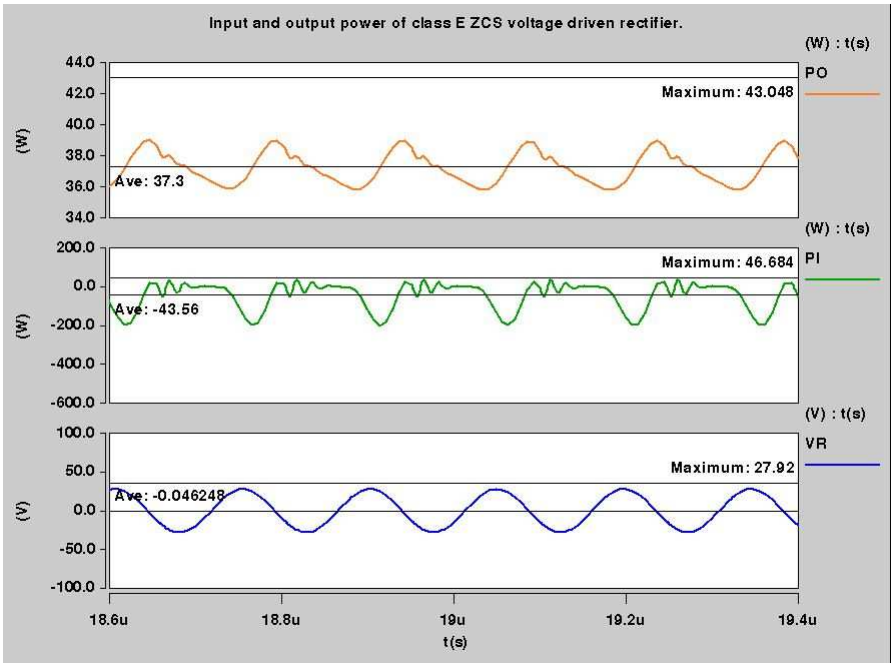

Figure 2.47: Input, output power and input voltage of voltage-driven Class-E low di/dt rectifier.

The ZCS operation of the voltage-driven Class-E low di/dt rectifier is shown in Fig. 2.48. The diode voltage waveform of the rectifier is reversed and superimposed on the diode current waveform. The condition for the zero current switching is that the current across the switch should be equal to zero at the turn OFF instance of the diode. When the switch current goes to zero, the diode voltage starts increasing and the diode turns OFF. If the diode current is non-zero at the turn OFF instance, the diode voltage and diode current waveform overlap on each other causing switching losses. The switching losses lead to power loss. Therefore, the switching losses have an adverse effect on the efficient operation of the rectifier.

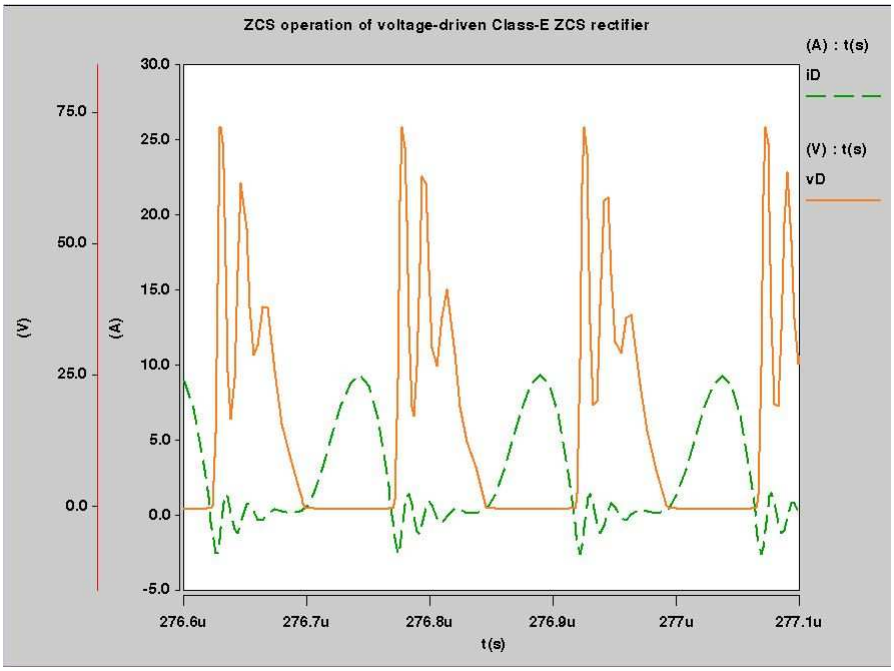

Figure 2.48: ZCS operation of voltage-driven Class-E low di/dt rectifier.

2.5.7 Effect of Change in Load Resistance on the Efficiency of the Voltage-Driven Class-E Low di/dt (ZCS) Rectifier

We know that the load at the output of the rectifier can vary depending on the applications. We calculated the optimum load resistance based on the specifications. The following Fig. 2.49 shows change in efficiency of the voltage-driven Class-E low di/dt (ZCS) rectifier when there is variation in load resistance from 1 Ω to 60 Ω in the intervals of 5 Ω. The rectifier satisfies the ZCS condition from $R_l = 1\ \Omega$ to $R_l = 5.624\ \Omega$ and beyond that it operates in non-ZCS mode. As we increase the load resistance, the output power of the rectifier starts decreasing.

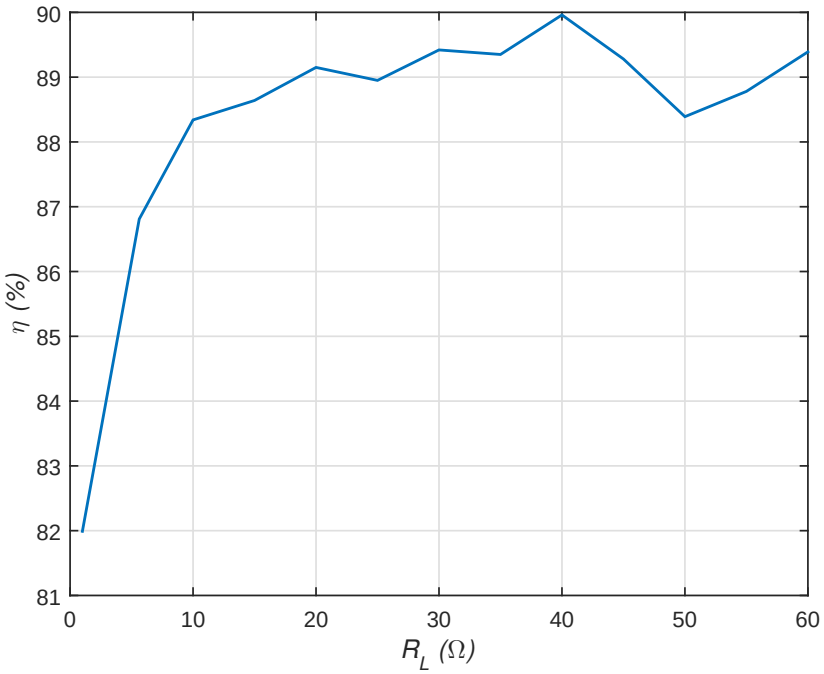

Figure 2.49: Efficiency as a function of the load resistance of the rectifier.

3 Transformer

3.1 Magnetic Relationships

3.1.1 Magnetomotive Force

In an electric circuit, the current flows due to the existence of an electromotive force (EMF). Similarly, in the case of magnetic circuits, the magnetic pressure which sets up magnetic flux is called as magnetomotive force (MMF). The unit for magnetomotive is Ampere-turns (A.t). The magnetomotive force can be given as follows.

$$MMF = F = Ni \text{ A.t} \tag{3.1}$$

where N are the number of turns of an inductor and i is an AC current flowing through the inductor. [12]

3.1.2 Magnetic Field Intensity

Magnetic field intensity is also known as magnetic field strength. The magnetic field intensity can be defined as the ratio of magnetomotive force (MMF) to the length of the inductor. The unit for magnetic field intensity is Ampere/meter (A/m). Magnetic field intensity is denoted by H and can be given as follows.

$$H = \frac{MMF}{l} = \frac{F}{l} = \frac{Ni}{l} \text{ A/m} \tag{3.2}$$

where N denotes the number of turns and l denotes the length of the inductor [12]

3.1.3 Magnetic Flux

Magnetic flux is nothing but the product of magnetic field and the area perpendicular to the magnetic field. The unit of magnetic flux is Weber Wb. The relation between the surface and the magnetic flux density is very crucial. The relation depends on

the angle between magnetic flux density and the surface. If an angle θ_B is formed between the magnetic flux density B and the surface S, then the amount of magnetic flux is given as,

$$\phi = B.S\cos(\theta_B) \text{ Wb} \tag{3.3}$$

However, if the magnetic flux density is uniform and perpendicular to the surface or parallel to the surface then angle $\theta_B = 90°$ or $\theta_B = 0°$ respectively [12].

3.1.4 Magnetic Flux Density

Magnetic flux density is nothing but the ratio of magnetic flux to the surface area. Magnetic flux density is also called as Induction. The unit of magnetic flux density is Tesla (T). Magnetic flux density is denoted by B and is given as,

$$B = \frac{\phi}{S} \text{ T} \tag{3.4}$$

The magnetic flux density B and the magnetic field intensity H are related as follows.

$$B = \mu H \tag{3.5}$$

where μ is the permeability of the magnetic material. Permeability is a property that describes the magnetic flux conductivity of a magnetic material. It can be given as the product of relative and the free space permeability i.e. $\mu = \mu_r\mu_0$. The permeability of the free space μ_0 has a constant value of $4\pi * 10^{-7}$ H/m and the value of relative permeability μ_r is dependent on the magnetic material. The magnetic flux ϕ follows the path of highest permeability.

3.1.5 Magnetic Flux Linkage

Magnetic flux linkage is nothing but the product of magnetic flux and the number of turns in a given coil. The unit of magnetic flux linkage is Weber.Turn Wb.turn.

Magnetic flux linkage is denoted by λ and is given as,

$$\lambda = N\phi = NA_cB \text{ Wb.turn} \tag{3.6}$$

where N is the number of turns of the coil, ϕ is the magnetic flux, A_c is the cross-sectional area of the core through which magnetic flux passes and B is the magnetic flux density.

3.1.6 Mutual Inductance

Mutual inductance and coupling coefficient are the most important parameters which characterize the link or coupling between two transformer windings. If current flows through the primary winding, it results in the magnetic flux in primary winding and some portion of it also pass through the secondary winding. The current flowing through primary winding results in flux linkage inside the conductor and also which links the windings known as internal self-inductance and external self-inductance respectively. The sum of internal and external self-inductance is nothing but the leakage inductance. The flux linkage which links the secondary winding and quantifies the change in the current in secondary winding due to the change in current in the primary winding is called as Mutual Inductance. The mutual inductance is denoted by M.

3.1.7 Magnetizing Inductance

When the coupling coefficient between the windings of the transformer is 1, the transformer is said to be perfectly coupled. As a result, there is no leakage flux and the entire amount of magnetic flux at the primary links to the secondary side. However, apart from coupling coefficient, there are many other parameters which can introduce

leakages in transformer such as permeability and reluctance of the core. The permeability of the core should be infinite and the core reluctance should be zero in order to avoid leakages. In practice, core permeability and the core reluctance are finite. Therefore, magnetizing inductance comes into the picture. The magnetizing inductance can be placed on either primary or secondary side of the transformer. When the output of the transformer is open circuited, an input current flows through the magnetizing inductance on the primary side called as magnetizing current. Magnetizing current can be denoted by L_m.

3.1.8 Coupling Coefficient

The coupling coefficient is a dimensionless quantity which characterizes the distance between the magnetic fields of two inductors. The value of coupling coefficient ranges between 0 to 1. When the value of coupling coefficient is close to 1 then the windings are said to be tightly coupled. In the case of tightly coupled transformers, mutual flux is maximum and a very small amount of leakage flux is present. When the value of coupling coefficient is close to 0 then the windings are said to be loosely coupled and therefore the mutual flux is low and leakage flux is large. The coupling coefficient is denoted by k.

3.1.9 Leakage Inductance

When there are irregularities in the coupling of the windings of transformer i.e. if coupling coefficient is less than 1 i.e. $(k < 1)$, leakage inductances are introduced. Primary side and secondary side leakage inductance can be denoted as L_{l1} and L_{l2} respectively. The leakage inductances are characterized by connecting in series configuration with the windings of transformer. If the transformer is coupled with a

circuit containing diode or transistor, then the leakage inductance may form a resonant circuit with the diode junction capacitances or transistor capacitance which can lead to distorted signals and eventually resulting in reduced transformer output. The leakage inductances can be reduced by efficiently designing the cores and windings. The windings should be as wide as possible and the insulation between them should be low. If the windings are to be placed on one another then the overlapping should be perfect. The thickness of the winding is directly proportional to the leakage inductance i.e. lower the thickness of the winding, lower the leakage inductance. Leakage inductance are closely related to the coupling coefficient and primary and secondary inductance as shown below.

$$L_{l1} = (1 - k)L_1 \tag{3.7}$$

And,

$$L_{l2} = (1 - k)L_2 \tag{3.8}$$

where, k is the coupling coefficient, L_1 and L_2 are the primary and secondary inductances of the transformer.

3.1.10 Magnetic Permeability

Magnetic permeability is a very important aspect of magnetics. Magnetic permeability is a property of magnetic material which restores its domains in the magnetic field. Magnetic permeability is also known as Electromagnetism. Permeability can be expressed in various ways according to the applications.

Absolute permeability is defined as ratio of magnetic flux density B to the intensity of magnetic field H. Absolute permeability is also known as Induced capacity. Relative permeability is defined as the ratio of permeability of a specific medium or absolute permeability to the permeability of free space. Permeability of free space is denoted by μ_0 and has constant value of $4\pi * 10^{-7}$H/m. Relative permeability is

a dimensionless quantity. Relative permeability can be denoted as μ_r. If magnetic resistance is introduced in the magnetic core of the transformer, then the effective permeability comes into existence. The effective permeability and the dimension of the magnetic resistance (air gap) are dependent on each other. The magnetic materials also experience diamagnetism which comes into picture when an external magnetic field is applied to an object. Basically, diamagnetism causes a repulsive effect by creating a magnetic field in opposition to the externally applied magnetic field. Unlike the diamagnets, paramagnets are attracted towards the magnetic material. The relative magnetic permeability of diamagnets is less than 1 whereas, paramagnets have relative magnetic permeability greater than 1 and that for free space, insulators and nonmagnetic materials relative magnetic permeability is equal to 1. Few examples for diamagnets are copper, lead, silver and gold and that of ferromagnetic material are iron, cobalt, nickel and their alloys.[13]

3.2 Magnetization and Hysteresis

The process of magnetization is nothing but aligning of the domains in the ferromagnetic material upon the presence of the external field. The magnetization is characterized by two most important parameters i.e. magnetic field density B and magnetic field strength H. When an external field is applied to the magnetic material, magnetic field strength of the material starts rising and in accordance, its magnetic field density also increases. However, the number of domain dipoles aligned and the ability of the magnetic material to respond to field strength are inversely proportional i.e. if the number of domain dipoles aligned are increased the magnetic material starts losing its capability to respond to its increased field strength. As a result, at some point, the magnetic material has no effect on increasing field strength. This situation is called magnetic core saturation.

The relationship between magnetic field density B and magnetic field strength H for a particular magnetic material is known as B-H curve or magnetization curve. The magnetization is also called as Hysteresis. The slope of the B-H curve is highly dependent on the magnetic dipoles. When there is no external field applied, dipoles are in arbitrary position as a result of which the magnetic field density B is zero at this condition. Now, when an external field is applied, domains start to align and the process of magnetization begins. At this point, the magnetic field density B increases with increasing magnetic field strength H. However, when the dipoles are perfectly aligned, the magnetic material starts saturating and the rate at which flux density increases goes down. If the external field is detached, the flux level doesn't go to its initial level instead it reduces to a residual level. This is called as residual flux density or remanence. In order to get the flux density to its initial level, demagnetization of the material needs to be done. Demagnetization is simply applying the opposite external field to the magnetic material, which can be achieved by reversing the spins of magnetic domains or shifting the domain walls. In the process of demagnetization, the dipoles are aligned in opposite fashion which leads to saturation of magnetic material in the opposite direction. The negative or opposite magnetic field intensity applied in order to reduce the flux density to zero is called as the coercive force. The magnetization curve represents low value of reluctance at low values of magnetic field strength H and high reluctance at the saturation region of the magnetic material. The magnetic flux of magnetic materials has the property of choosing the shortest magnetic path length (MPL) when excited from the demagnetized state. The nature of the hysteresis loop differs for soft and hard magnetic materials. For the hard ferromagnetic material such as permanent magnets, the area under the loop is wide because the magnetic walls cannot be moved easily whereas for the soft ferromagnetic materials the magnetic walls are easily adjustable which makes the area under the

loop narrow. The area under the hysteresis loop is a very significant parameter in calculating the hysteresis loss for a magnetic material. The area enclosed by the loop is an account of the energy required by the material to complete the hysteresis cycle. In other words, the area enclosed by the loop is equal to the energy loss per volume for one cycle. The energy loss also depends on the magnitude of magnetic flux density B and frequency. When the frequency and the magnitude of flux density increases so do the area enclosed by the loop increases which leads to increased energy loss. Hence, an ideal or lossless magnetic core for transformer should possess very narrow hysteresis.[13]

3.2.1 Losses in Magnetic Components

Hysteresis losses

Losses generally occur in the magnetic core of the transformer. These losses are known as core losses. In high-frequency applications, core losses and increased core temperature make the systems inefficient. Hysteresis loss, eddy current loss and conduction loss together form the core loss. In magnetic materials, when magneto motive force (MMF) is removed, not all the energy of magnetic field is returned to the circuit. This loss of energy loss associated with aligning and adjusting the magnetic moments in the core of the material is called as Hysteresis. Larger the area enclosed by the hysteresis loop, the more hysteresis loss. When the alternating current around the winding is varied, there is a flow of energy from source to the coil and vice versa. But, the flow flowing from the source to the coil is greater than the energy returned to source. This difference between energy is termed as core loss which can be further categorized into hysteresis and eddy current loss.

Hysteresis loop represents the behavior of magnetic flux density B and magnetic field strength H. When the magnetic field strength is increased from zero to its maxi-

mum value, the external circuit transfers the energy to the coil and when the magnetic field strength is decreased to zero from the maximum value, energy is returned from the coil to external circuit. However, there is a difference between energy supplied to the coil and energy returned to the coil. This energy difference is the energy lost in the core of magnetic material. There is alignment and adjusting of magnetic domains involved in the magnetic material which causes friction forces. As a result, to compensate the friction forces, some energy is absorbed into the core of the magnetic material.[13]

Eddy Current Losses

According to Faraday's law, a time-varying magnetic field induces a voltage in the coil which van be given as,

$$V = \frac{d\lambda}{dt} \tag{3.9}$$

This induced voltage generates currents in the core called as Eddy currents. The losses associated with eddy currents are called as eddy current losses. The eddy currents flow in a circular fashion. The resistivity of the core plays a very important role in the generation of the eddy currents. The variation in the magnetic field lets the eddy currents generate but the resistivity of the core is a controlling factor. In other words, if the core of the transformer is built using high resistivity material then the generation of eddy currents is lower. Eventually, eddy current losses are lower. The resistivity of the core is directly proportional to the temperature. As temperature increases, the collision between the electrons increases which in turn decreases the mobility of the electrons. As a result, the resistivity of the material increases. The effects of eddy current losses on the core of the transformer include increased core temperature, widening of the hysteresis and power dissipation. Since eddy currents are basically dependent upon the resistivity of the material they also rely on the ge-

ometry of the core. The magnitude and shape of the inductor current also have an impact of the eddy currents. There are two eddy current effects namely skin effect and proximity effect.[13]

Skin Effect

Skin effect is a self-inflicting effect caused by the magnetic field of its own induced current. At high frequencies, skin effect causes non-uniform density of current in the conductors. The occurrence of skin effect is due to the penetration of conductor carrying time-varying current in its own magnetic field which gives rise to eddy currents in the conductor itself. These eddy currents produce a secondary magnetic field that opposes the primary magnetic field and an extra circulating current is generated when a time-varying current flows through the conductor. However, the density of the current at the surface of the conductor is more and it gradually decreases as we move towards the center of the conductor. In other words, the interior of the wire or conductor is not involved in the conduction of current. At very high frequencies, the entire current flows through the narrow surface of the conductor leading to power loss. This phenomenon is known as Skin effect.

At high frequencies, the magnetic field does not penetrate into the interior of the conductor. The degree to which the magnetic field can penetrate into the interior of the conductor is known as depth of penetration or skin depth. Skin depth is dependent upon various parameters such as permeability, frequency, and resistivity of the material. Temperature of the conductor also has an impact on the skin depth since, temperature and the resistivity are proportional to each other.

The skin depth can be given a follows.

$$\delta_\omega = \sqrt{\frac{\rho_\omega}{\pi \mu f}} \tag{3.10}$$

where δ_ω is the skin depth, ρ_ω is the resistivity of the material, μ is the permeability and f is the operating frequency [12].

Proximity Effect

The electromagnetic induction in the conductor is caused due to its own time-varying current or due to other adjacent conductors. The literal meaning of proximity is closeness. The ability of the conductor to carry current at high frequency is affected by the closeness of the other current carrying conductor. In other words, proximity effect occurs when an alternating current in the nearby conductors results in a time-varying magnetic field and induces a circulating current inside the conductor. Proximity effect is inflicted by the currents in the nearby conductors whereas skin effect is a self-inflicting phenomenon. Eddy currents are inevitably introduced in the conductor by time-varying magnetic field regardless whether the conductor carries current or not. If the conductor carries current, both skin effect and proximity effect come into the picture, producing skin effect eddy current and proximity effect eddy current which collectively forms total eddy current. If the conductor does not carry current, then proximity effect eddy current is induced. The main drawback of the proximity effect is the non-uniform distribution of current density in the cross section of the conductor. The non-uniform distribution of current density causes an increase in winding loss at high frequency. The magnetic fields of the adjacent conductors may add or subtract when the conductors are brought into close proximity of each other. However, the degree of proximity effect depends on several parameters including frequency of operation, shape, and size of the conductor, configuration of conductors and spacing between them. If the winding has many layers, then the proximity effect dominates over the skin effect [12].

3.3 Transformer

Transformers are magnetic devices which are used to transfer energy from one circuit to another. They establish this transfer through the magnetic field. Transformers

are composed of two or more mutually coupled windings. Windings are nothing but the set of conductor turns that conduct same amount of current. If the windings are sharing a common magnetic flux, then they are said to be mutually coupled windings. Transformers can be designed with or without a magnetic core. The main purpose of the transformer is to step-up or step-down alternating voltage suitable for the application. The basic fundamentals of the transformer are based on Faraday's law and on ferromagnetic properties of the core. According to Faraday's law, if there is a change in the current of one winding, the mutually coupled windings will experience the change in magnetic flux which in turn induces the voltage between terminals of windings. The transformer has many different functions such as it can be used as an impedance matching circuitry. Furthermore, it can be used to provide DC electric isolation and also to store and transfer magnetic energy. The amount of energy transfer by the transformer is dependent on various parameters such as magnetic flux density, operating frequency, and temperature. Transformer can be constructed using two coils wound around on an iron or ferrite magnetic core. Generally, the coil with the source is referred to as primary winding and the coil with load is referred to as secondary winding. A time-varying current flows through the primary winding and produces a time-varying magnetic flux in both the windings. The time-varying magnetic flux further induces a voltage in the secondary winding. The common magnetic flux between primary and secondary winding is referred to as mutual flux. When two coils are in close proximity to each other such that the magnetic field from one links with the another resulting in the induced voltage into the second coil and this interaction between two coils is called as mutual inductance [12].

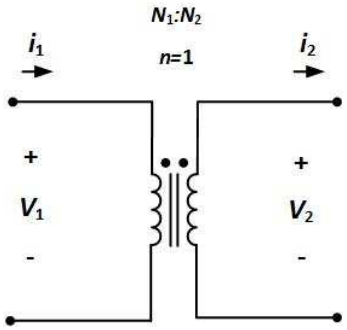

Figure 3.1: Ideal transformer [12]

3.3.1 Ideal Transformers

The Fig. 3.1 represents the ideal model of the transformer. Basically, real transformers experience losses such as core loss, copper loss, and winding loss. But, Ideal transformer does not exhibit any losses. Ideal transformers do not have any leakage inductance; it means that all the magnetic energy is transferred from primary to the secondary winding. The windings of the ideal transformer are purely inductive. The mutual inductance and the self-inductance of the ideal transformer are infinite. The coupling between the coils is a very important factor which affects the performance of the transformer. In the case of an ideal transformer, the coupling between the coils is perfect. The winding resistances are zero. The core permeability is infinite.[12]

3.3.2 Non-Ideal Transformers

The Fig. 3.2 represents the schematic of non-ideal transformer. Non-ideal transformers are nothing but the real transformers. Non-ideal transformers are not perfectly coupled as a result of which, several losses and leakages are occurred such as primary and secondary leakage inductances. The primary and secondary winding resistances are non-zero in case of non-ideal transformers. Due to weak coupling between the coils, the amount of flux delivered to the secondary winding is not equal to that of the primary which leads to leakage flux. Therefore, the total magnetic flux is the

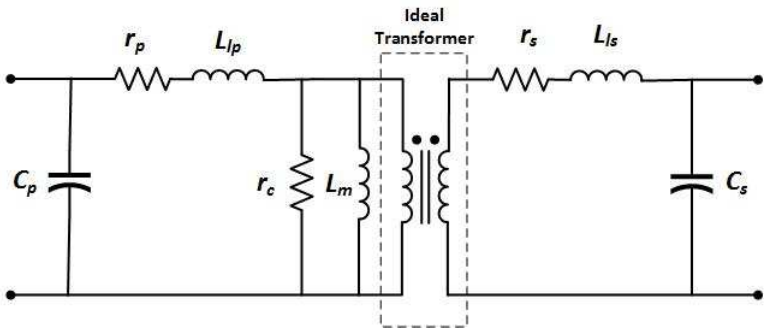

Figure 3.2: Non ideal transformer [12]

combination of mutual flux and the leakage flux. The efficiency of the non-ideal transformers is hampered due to the existence of winding resistances. The effect of winding resistances on the efficiency of the transformer is inevitable. Ideally, the voltage at the output of the transformer should be in accordance with the induced EMF at the input, but in the case of the non-ideal transformer, the output voltage is not equal to the induced EMF. However, one way to minimize the effect of winding resistance is an addition of lumped resistance in series with each winding. The magnitude of lumped resistance should be equal to the winding resistance.

As we discussed earlier, in the case of non-ideal transformers, out of the total flux produced on the primary side, a small fraction of the flux does not link to the secondary side, known as leakage flux. Even the leakage flux is a small fraction, the effect of the leakage flux on the efficiency of the transformer cannot be ignored. The leakage flux can occur in both primary as well as secondary windings. The fraction of flux which is common to both windings is known as mutual flux. Hence, the efficiency of the transformer degrades as more and more leakage flux is produced.

Apart from, the existence of winding resistance and the leakage flux, there is one more factor responsible for the inefficient operation of the transformer and i.e. finite permeability. Ideally, the permeability of the transformer should be infinite to achieve 100% efficiency but it is not practically possible. The practical transformers

have relatively high reluctance i.e. low or finite permeability. The permeability of the transformer simply defines the amount of current to be drawn from the mains which in turn produces the necessary MMF to establish the desired flux. Therefore, if the core of the transformer is of finite permeability then the current drawn from mains would be finite. The finite permeability of the core of the transformer results in the core losses eventually leading to inefficient operation[13] [12].

3.4 Magnetic Coil Design Considerations

The transformer design procedure involves many constraints such as output power, efficiency, weight, size and operating frequency. While designing the transformer, the requirements can be specified in terms of output power, efficiency or the operating frequency. Therefore, depending upon the specifications the approach to design transformer varies. The design procedure of the transformer starts with designing individual components to the best of their ability. One of the most important constraints is the output power of the transformer and can be given as the product of the voltage at which the transformer is operating and the maximum current demand. In the same way, the efficiency of the transformer is related to the losses incurred in the components of the transformer, the secondary winding of the transformer should be designed in such a way that it delivers to the load within the specified limits, the temperature of the environment in which the transformer is being used plays a very important role. The maximum permissible temperature rise should be taken into consideration while designing the transformer.

As we know, the material used to design the core of the transformer is one of the most vital parameters. Each core material has its unique characteristics such as cost, temperature requirement, size, cost, and efficiency range. While designing the transformer, the core material to be used is sometimes specified or it is expected

to be chosen according to the requirements. For example, the aerospace applications always aim for minimization of volume, and weight, so the designer should take into consideration these specific characteristics of the core material. Nowadays, almost all the electronics applications are built keeping in mind the cost, volume and weight minimization. Even the wire conductors which are wound over the core of the transformers are characterized according to the required applications. The wire conductors are categorized based on the size, diameter of the conductor, operating frequency, current carrying capacity etc. But, practically, it is not always possible for the designers to achieve balance between all the characteristics then there is a need of certain tradeoffs.

Depending upon the transformer applications, the significance of the parameters varies. For example, if it is desired for a transformer to have reduced volume and weight. Then one way to achieve this is operating the transformer at high frequencies but at the cost of degradation in efficiency. Another way to achieve the reduced volume and weight dimensions for the transformer, and also when using the high frequency is undesirable, is to choose an efficient core material which will not harm the efficiency. But, selecting an efficient core material may lead to increased cost of the design. In summary, many tradeoffs between the parameters are executed to achieve the desired design goals[13].

3.4.1 Magnetic Wire

The windings of the transformers are made up of magnetic wire. The magnetic wire can be wound around the conductor in any shape such as round, square, rectangular and foil. The magnetic wire has solid copper and coating of insulation. The layer of insulation coating provides thermal resistance to the magnetic wire. The coating of insulation of the magnetic wire remains exposed and may experience thermal

overloads based on the applications. Therefore, in order to have a long life of magnetic devices, the selection of the coating of insulation is very crucial. As per the applications, different shapes of the magnetic wire are employed. For example, the foil, square or rectangular shaped magnetic wires are best candidates for high-current applications. When the transformer is designed with a uneven number of turns of the windings, then the foil shaped copper winding establishes a good coupling between the windings. There are many electrical, mechanical and thermal advantages associated with the application of foil shaped copper winding. Generally, in high-frequency applications, there are several losses involved in the core of the transformer. The reason behind these losses is skin and proximity effect. In order to overcome these losses, a special kind of wire is developed with the help of many small strands known as Litz wire. The term Litz is a German word, meaning woven wire. Litz wire is constructed by insulating the small strands together and connecting them externally in a parallel fashion. One disadvantage of the Litz wire is that, it is three times expensive than the normal solid copper wire.[12]

3.4.2 Wire Insulation

The bare copper wire used for the windings in the transformers is vulnerable and may undergo several thermal shocks. Also, when the bare copper wire is wound in turns on the conductor, it may experience short circuits between the turns. Therefore, in order to overcome these problems, the bare copper wire is provided with an insulation film. The insulation film to be used is dependent on the thickness of the bare copper wire. There are several grades of the insulation film and those are

1. Single insulation
2. Heavy insulation
3. Triple insulation

4. Quad insulation

[12]

3.4.3 Wire Insulation Factor:

The wire insulation factor is dependent on the inner and outer diameter of the bare wire. The Fig. 3.3 represents the cross section of the magnetic wire. The inner diameter of the bare wire defines the cross sectional area and can be given as follows.

$$A_w = \frac{\pi d_i^2}{4} \tag{3.11}$$

since the total wire cross section comprises of bare copper wire as well as the corresponding insulation, the total wire cross section can be given as follows.[12]

$$A_{w0} = \frac{\pi d_o^2}{4} = \frac{\pi (d_i + 2t)^2}{4} \tag{3.12}$$

where, t is the thickness of the wire insulation, d_i and d_o is the inner and outer diameter of the wire respectively. The insulation factor can be defined as ratio of cross section of bare wire to the cross section of insulated wire and can be given as follows.

$$K_i = \frac{A_w}{A_w} = \left(\frac{d_i}{d_o}\right)^2 = \left(\frac{d_i}{d_i + 2t}\right)^2 \tag{3.13}$$

3.4.4 Air and Wire Insulation Factor

As we discussed earlier, the bare wire has many different shapes such as round, foil, square, rectangular etc. Depending upon the shape of the wire used, there are several ways in which the bare wire can be arranged. For example, the round bare wire can be arranged in triangular pattern or in square pattern. The area covered by the insulation of the bare wire and the air is known as cross section area of cell A_{cell}. The air and wire insulation factor can be defined as ratio of cross section area of bare wire

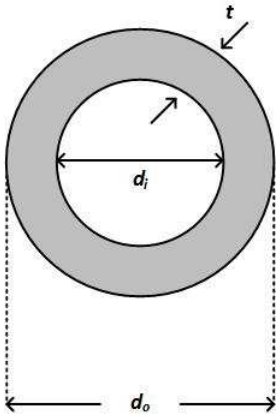

Figure 3.3: Cross section of the magnetic wire [12]

to the cross section area of the cell and can be expressed as follows.

$$K_{ai} = \frac{A_w}{A_{cell}} \tag{3.14}$$

The air and wire insulation factor varies according to the pattern implemented, quality of the wire and also on the tension provided in the wire. The cross section of the cell varies according to the pattern used. For example, the basic cell of the winding with triangular pattern can be shown in Fig. 3.4. The cross section of the cell for the triangular pattern can be given as follows [12].

$$A_{cell} = \frac{\sqrt{3}}{4}(d_i + 2t)^2 \tag{3.15}$$

And the total cross section area of the bare wire can be given as,

$$A_w = \frac{\pi d_i^2}{8} \tag{3.16}$$

Therefore, the air and wire insulation factor for the triangular pattern can be expressed as follows.

$$K_{ai} = \frac{A_w}{A_{cell}} = \frac{\pi}{2\sqrt{3}}\left(\frac{d_i}{d_o}\right)^2 = \frac{\pi}{2\sqrt{3}}\left(\frac{d_i}{d_i + 2t}\right)^2 \tag{3.17}$$

Similarly, the cross section of the cell for the square pattern of the wire can be given

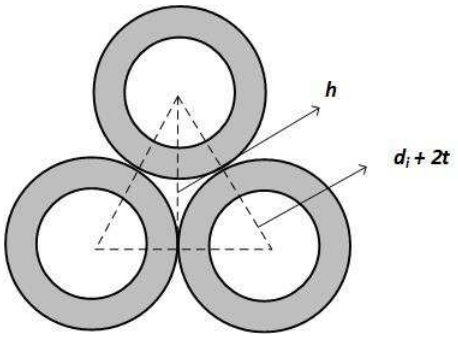

Figure 3.4: Cross section of cell of winding with triangular pattern [12]

as follows.

$$A_{cell} = (d_o)^2 = (d_i + 2t)^2 \tag{3.18}$$

And the total cross section for the bare wire can be given as,

$$A_w = \frac{\pi (d_i)^2}{4} \tag{3.19}$$

Hence, the air and wire insulation factor for the square pattern can be expressed as follows.

$$K_{ai} = \frac{A_w}{A_{cell}} = \frac{\pi}{4}\left(\frac{d_i}{d_o}\right)^2 = \frac{\pi}{4}\left(\frac{d_i}{d_i + 2t}\right)^2 \tag{3.20}$$

The basic cell of the winding with square pattern can be shown in Fig. 3.5

3.4.5 Air Factor

When the bare wire which is to be wound on the conductor of the transformer is provided with an insulation film, the area between the insulation film and the effective cell is filled with air. This area can be defined as ratio of cross section of the bare wire with insulation to the cross section of the cell and is known as air factor. Air factor can be expressed as follows[12].

$$K_a = \frac{A_{w0}}{A_{cell}} \tag{3.21}$$

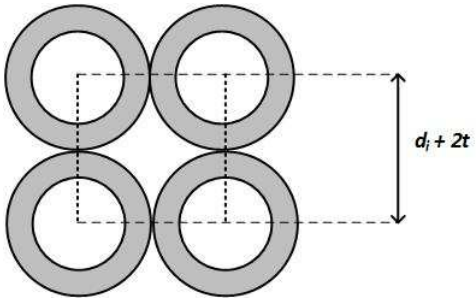

Figure 3.5: Cross section of cell of winding with square pattern [12]

Alternatively, the air factor can also be defined as ratio of wire and air insulation factor to the wire insulation factor and can be given as follows.

$$K_a = \frac{K_{ai}}{K_i} \tag{3.22}$$

Air factor for the triangular winding pattern can be expressed as,

$$K_a = \frac{A_{w0}}{A_{cell}} = \frac{\pi}{2\sqrt{3}} \tag{3.23}$$

And air factor for the square winding pattern can be expressed as,

$$K_a = \frac{A_{w0}}{A_{cell}} = \frac{\pi}{4} \tag{3.24}$$

3.4.6 Window Utilization Factor

Copper is the main conducting material in the transformer design. However, there are several designs available for the core of the transformer based on the shapes and sizes. For example, toroidal cores (TC), they offer a reduction in electromagnetic interference (EMI). These cores are the best candidates for designing coupled inductors and EMI filters. Pot cores (PC) consists of the plastic coil former known as the bobbin. PC are available in both with and without air gap provision. The applications dealing with high frequency and low current inductors and transformers are main clients for pot cores (PC). However, PC have poor heat removal factor. Power

quality (PQ) cores and rectangular modular (RM) cores are revised version of the pot cores (PC). These cores are best suitable for switch-mode power supplies (SMPS), DC-DC converters, matching transformers etc. EE cores are the widely used cores in transformers. EE cores are constructed using pairs of E cores. The construction of economical transformer design (ETD) cores is similar to the EE cores. The applications of the EE cores range from 5 W to 10 kW. Apart from these, there are cut cores which consist of two equal halves. The examples of cut cores are CC and UU cores. There are two important parameters associated with the cut cores and those are cross section area A_c and window area of the magnetic path W_a. The shapes of the corners of the cut cores differ depending upon the type of the core i.e. CC cores have round shaped corners and UU cores have sharp shaped corners. EI cores, EC cores, ER cores, UI cores and planer cores are some of the other examples of the magnetic cores[12].

While designing the core for the power transformer, it is very important to have insight into the amount of copper in the effective window area. The amount of copper deposited in the window area of the core is impacted by parameters like insulation film provided to the wire, the type of the core used because the window area varies with the core type, the insulation between the windings if multilayer winding is employed for the transformer. Even the quality of the wire and the workmanship are some of the factors affecting the amount of copper. The measure of the amount of the copper in the effective window area of the core of the transformer can be given by window utilization factor K_u. The window utilization factor K_u is dependent on all the above-mentioned parameters. Fig. 3.6 represents the window cross-sectional area and window utilization factor of EE core. The window utilization factor K_u can be described as ratio of bare conductor area A_{Cu} to the core window area W_a and can

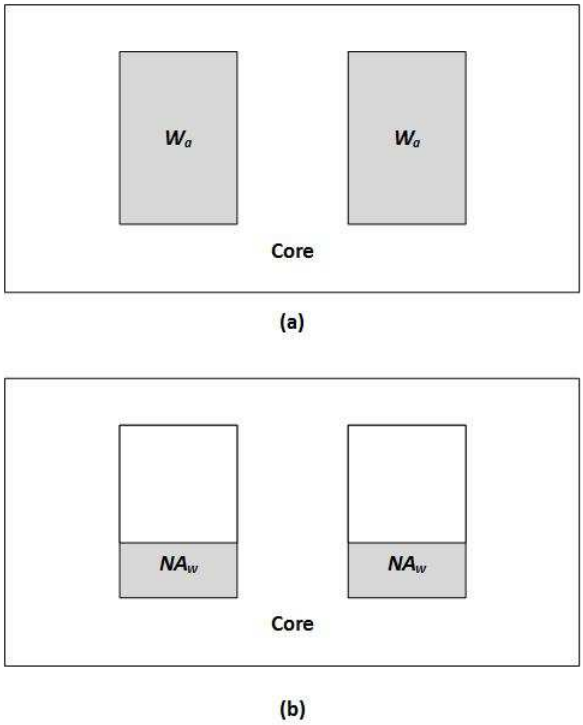

Figure 3.6: Window area of EE core (a) Window cross-sectional area. (b) Window utilization factor K_u [12]

.

be expressed as follows [12].

$$K_u = \frac{A_{Cu}}{W_a} \tag{3.25}$$

The bare conductor area A_{Cu} is nothing but the area acquired by the cross section of wire and number of turns implemented together i.e. $A_{Cu} = NA_w$, where, N denotes the number of turns and A_w is the cross section of the wire. Alternatively, the window utilization factor can be described as follows [12].

$$K_u = \frac{NA_w}{W_a} \tag{3.26}$$

We already discussed that the Litz wire is built combining multiple individual strands together. Therefore, if the transformer is built by the core consisting of Litz wire then the window utilization factor of the core mainly depends upon the number of strands and also on the cross section area of the individual strands. Therefore, the window

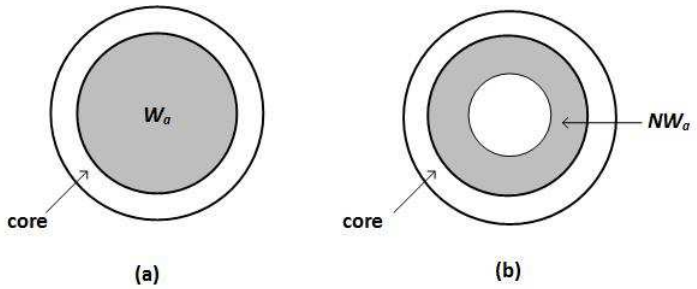

Figure 3.7: Window area of the toroidal core (a) Window cross-sectional area. (b) Window utilization factor K_u [12].

utilization factor for the core with the strands can be given as follows.

$$K_u = \frac{A_{Cu}}{W_a} = \frac{NS_nA_{wso}}{W_a} \tag{3.27}$$

where S_n indicates the number of strands used to build wire and A_{wso} indicates the area of the individual strand. The core window area W_a varies with the shape of the core employed and it also decides the current carrying capability of the transformer. The window utilization factor differs for the inductors and transformers i.e. generally the value for window utilization factor for the inductor is 0.3 and that for the transformer is 0.4. The value for the window utilization factor for the toroidal core ranges between 0.15-0.25. Fig. 3.7 represents the window cross -sectional area and window utilization factor of the toroidal core.

3.5 Area Product (A_p) Method

In the previous section, we discussed some of the considerations while designing the transformer. Now, we will look forward to some of the design procedures for the transformers. The design procedure for the inductor and the transformer comprises of choosing the method to select core, selection of core and winding conductor. There are some of the recognized strategies which can be implemented while selecting the core of the transformer such as Area product method A_p and Core geometry coefficient method k_g. Apart from the method to select the core, there are several parameters

such as core material, the relative permeability of the core, the maximum amplitude of the magnetic flux density and operating frequency, which should be taken into consideration. However, after selection of the core based upon one of the mentioned methods, the final step is the winding conductor selection, which comprises of choosing conductor size, conductor shape, conductor insulation, etc,.

The area product method mainly deals with the effective window area and cross section area of the core. The area product method is simple and straightforward. However, being simple, the method does not guarantee optimal design of magnetic elements. As we discussed earlier, there are several design requirements such as inductance, peak current and the RMS current which must be met while designing the inductors. Whereas, the frequency of operation, as well as the Volt-Ampere rating, should be kept in mind while designing the transformers. The material used while constructing the core and the windings of the transformers also play a very important role in the reduction of losses and core saturation. While selecting the material for winding conductor, the current density of the material J_m is one of the vital element. Current density J_m is dependent on the cross section area of the winding conductor A_w and the corresponding current. Another important consideration while selecting the core of the transformer is the flux density B_m. The optimum value of the flux density B_m ensures the designer that there would be minimum core saturation. Finally, while manufacturing the actual transformers, the factors such as window utilization factor, air and insulation factor, quality of the material and workmanship are some of the constraints.[14]

We will derive the equation for area product method for sinusoidal inductor current and operating frequency of 6.78 MHz. We earlier discussed the magnetic flux linkage in the transformer, which can be given as follows.[15]

$$\lambda = N\phi = NA_cB \tag{3.28}$$

But, we can represent the peak magnetic flux linkage as the product of maximum sinusoidal inductor current and the corresponding inductance. So, the magnetic flux linkage in terms of inductor current can be given as follows.

$$\lambda_{pk} = N\phi_{pk} = NA_cB_{pk} = LI_{Lmax} \tag{3.29}$$

The amplitude of the sinusoidal inductor voltage is the product of the angular frequency and the magnetic flux linkage and can be given as follows.

$$V_m = \omega N\phi = \omega NA_cB_m \tag{3.30}$$

It is important to know the current density while selecting the winding conductor. The value of the inductor current is related to the current density and can be given as follows.

$$J_m = \frac{I_L}{A_w} \tag{3.31}$$

The cross section area of the winding conductor for the transformer is dependent on the diameter of the bare conductor wire d_i. The cross section of the winding conductor can be given as follows.

$$A_w = \frac{\pi d_i^2}{4}$$

When the core and winding conductor both are selected, the next important task is to calculate the number of turns for the optimal design of the transformer. The number of turns N can be calculated with the help of cross section area of winding conductor, window utilization factor and window area of the core. A number of turns can be given as follows.

$$N = \frac{K_uW_a}{A_w} \tag{3.32}$$

The number of turns is also indirectly dependent on the current density and the current across the inductor. Alternatively, the number of turns can be also expressed

as follows.

$$N = \frac{K_u W_a J_m}{I_{Lmax}} = \frac{V_m}{\omega A_c B_m} = \frac{L I_L}{A_c B_m} \tag{3.33}$$

There is a magnetic field generated in the transformer and the maximum magnetic energy generated in the field is controlled by the inductance and the current through the inductor. The maximum magnetic energy generated can be expressed as follows.

$$W_m = \frac{1}{2} L I_{Lmax}^2 \tag{3.34}$$

The area product is also known as ferrite-copper area product. The value of the area product is widely used by manufacturers to estimate the dimensions of the core. In order to calculate the area product, it is necessary to determine the value of the window area of the core W_a and cross-section area of the core A_c. The cross-section area of the core can be calculated by rearranging the above equation (3.33) and can be given as follows.

$$A_c = \frac{L I_L}{N B_m} \tag{3.35}$$

The core window area must be sufficient enough to incorporate the bare conductor, insulation film on the wires, bobbin (if any), space between the turns for the air. The core window area can be expressed by rearranging the above equation (3.33) and can be given as follows.

$$W_a = \frac{N A_w}{K_u} = \frac{N I_L}{K_u J_m} \tag{3.36}$$

Now, the area product can be expressed as the product of the cross-section area of the core and the window area. Combining equations (3.35) and (3.36), we can determine the area product.

$$A_p = W_a A_c = \frac{L I_{Lmax}^2}{K_u J_m B_m} = \frac{2 W_m}{K_u J_m B_m} = \frac{V_m I_L}{\omega K_u J_m B_m} \tag{3.37}$$

the area product A_p is inversely proportional to the flux density, window utilization factor and the current density of the winding conductor. The maximum value of

flux density is not only affected by the losses occurred in the core but the rise in temperature of the core also reduces the flux density value. The winding area is a physical attribute of the core and it can be similar to different cores but, the values of dimensions like heights and widths of the cores may be different. It is obvious that if the window area of the core is narrow then there would be losses due to proximity effect. In order to minimize these losses, it is recommended that the window of the core should be wide. Moreover, the cores with wide window area also minimize the winding AC losses. The area product gives an insight of both current and magnetic flux conduction ability of the core. The current conduction capability of the core can be described by the window area parameter and the magnetic flux conduction capability is related to the cross-section area of the core.

Further, the magnetic energy stored W_m in the magnetic field proves very useful in calculating some of the important parameters such as apparent power and quality factor. The apparent power P_Q can be described by sinusoidal current and voltage through inductor and can be given as follows.[15]

$$P_Q = \frac{1}{2} V_m I_L = f W_m \tag{3.38}$$

where V_m and I_L denotes the sinusoidal voltage and current through inductor respectively. f is the operating frequency and W_m is the magnetic energy stored in the magnetic field.

Generally, the loaded quality factor deals with the resonant circuits. We know that the resonant circuits can be series or parallel depending upon the placement of the passive components like inductor, capacitor, and resistor. The Fig. 3.8 illustrates the series and parallel resonant circuits. The loaded quality factor for the resonant circuits can be described by the following expression,

$$Q_L = \frac{\omega L}{R} = \frac{\omega L I_L^2}{2P_o} = \frac{\omega W_m}{P_o} \tag{3.39}$$

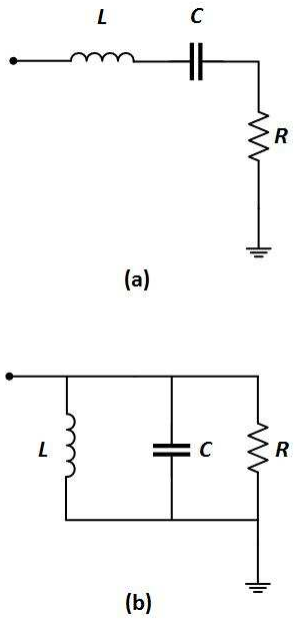

Figure 3.8: Resonant Circuits. (a) Series resonant circuit. (b) Parallel resonant circuit. [15]

where P_o is the power delivered at the output of the transformer and ω is the angular frequency of operation. For the resonant inductors, the value for the loaded quality factor value is same irrespective of the fact that, whether the circuit is series resonant or parallel resonant.[15]

3.6 Component Values

We will consider Fig. 3.2 for the calculation of component values. The component values for the design of the transformer are calculated following the design example from [12]. The first step to calculate the area product is to have knowledge about the amount of magnetic energy stored in the magnetic field of the transformer. We know that the magnetic energy in the magnetic field is dependent on the value of the inductor and the current through the inductor. Therefore, the magnetic energy

stored in the magnetic field can be calculated as follows.

$$W_m = \frac{1}{2} L I_{Lmax}^2 \tag{3.40}$$

since we now calculated the magnetic energy, the next step is to know the typical values of the parameters such as window utilization factor, optimum flux density and current density of the wiring conductor. The typical value of the window utilization factor ranges from 0.2 to 0.8. The low value of the window utilization factor indicates that the coil is wound loosely and there is a large free space for the winding arm. The example for the loosely wound coil is the core with bobbin. On the contrary, when the value of the window utilization factor is high as 0.8, it indicates that the coil is wound very tightly and there is not much free space left in the window area. The example for the tightly wound coil is the toroidal core [16]. The value of window utilization factor for the current design is considered as 0.3.

The magnetic flux density is measured in Tesla (T). The magnetic flux density is a very important parameter considering the core saturation losses in the transformer. The maximum value of the magnetic flux density B_m should be less than that of saturation magnetic flux density B_s (i.e. $B_m < B_s$). The magnetic flux density is related to temperature. Specifically, the magnetic flux density is inversely proportional to the temperature i.e. when the temperature increases, the magnetic flux density decreases for example, the magnetic flux density for the ferrite core at room temperature is around 0.5 T and as temperature is increased to 100° then the magnetic flux density reduces to 0.3 T. The value of the magnetic flux density for the current design of the transformer is considered as 0.25 T.

The value of the current density majorly depends on the type of winding wire chosen. The length of wire and also the number of turns also have the significant impact on the value of current density. Generally, the uniform current density is measured in terms of A/mm^2 . When the length of wire is less than 1 m and even the

number of turns are less, then the value of maximum RMS uniform current density ranges from $J_{rms(max)}$= 6-10 A/mm^2 . On the other hand, when the length of wire is greater than 1m and the number of turns are greater, then the value of maximum RMS uniform current density is $J_{rms(max)}$= 5 A/mm^2 . The value of the maximum RMS uniform current density for the current design is considered as 5 A/mm^2 . Initially, the area product defined in is restricted to the resonant inductors. Therefore, the area product for the transformer can be expressed as follows,

$$A_p = W_a A_c = \frac{4W_m}{K_u J_m B_m} \tag{3.41}$$

Since the value of the area product is determined, there are several important aspects to be taken care of while selecting the core. These parameters include type of the core, the material of the core, the shape of the core, the cross-section of the core, volume and length of the core. Even the relative permeability of the material is essential. Once the area product is determined, the window area of the core can be calculated with the help of cross-section area of the core. The window area of the core is the ratio of area product to the cross section of core. The window area of the core is,

$$W_a = \frac{A_p}{A_c} \tag{3.42}$$

Furthermore, the self-inductances of the primary and secondary windings of the transformer can be calculated with the help of the magnetizing inductance L_m and the coupling coefficient k. The value of the coupling coefficient k also has an impact on the distance between two coils. The value of coupling coefficient ranges from 0 to 1. The primary self-inductance of the transformer can be given as follows,

$$L_1 = \frac{L_m}{k} \tag{3.43}$$

The secondary side of the transformer can be reflected on the primary side by the reflection principle. The reflection principle needs the turns ratio of the windings.

The turns ratio n is related to the ratio of self-inductance and also to the number of turns associated with primary and secondary windings. The value of the turns ratio n is expected to be around 1. The turns ratio n can be given as follows,

$$n = \frac{N_1}{N_2} = \sqrt{\frac{L_1}{L_2}} \tag{3.44}$$

Since we know the value of turns ratio, the secondary self inductance can be determined as follows,

$$L_2 = \frac{L_1}{n^2} \tag{3.45}$$

The leakage inductances for both primary and secondary can be determined with the help of self-inductances and coupling coefficient. The primary leakage inductance can be given as follows,

$$L_{l1} = (1 - k)L_1 \tag{3.46}$$

Similarly, the secondary leakage inductance can be given as follows,

$$L_{l2} = (1 - k)L_2 \tag{3.47}$$

We know that the magnetizing inductances are part of non-ideal transformers. When the coupling between the coil is not perfect then the magnetizing inductances arises in the transformer. The magnetizing inductances can be on either sides of the windings. The value of the magnetizing inductance mainly depends on the relative permeability, the cross-section area of the core, the number of turns, length of the core and air gap. The primary magnetizing inductance can be given as follows.

$$L_{mp} = \frac{\mu_0 \mu_{rc} A_c N_1^2}{l_c \left(1 + \frac{\mu_{rc} l_g}{l_c}\right)} \tag{3.48}$$

where μ_0 and μ_{rc} are the absolute and relative permeability of the core respectively. The value of the absolute permeability is constant at $\mu_0 = 4\pi * 10^{-7}$ H/m and the value of the relative permeability of the core is material dependent. N_1 are the number

of turns of the primary side winding. l_c and l_g denote the length of the core and the length of the air gap.

Similarly, the magnetizing inductance of the secondary winding can be determined. All the parameters for the determination of the secondary magnetizing is similar to that of primary except the number of turns. The secondary magnetizing inductance can be given as follows.

$$L_{ms} = \frac{\mu_0 \mu_{rc} A_c N_2^2}{l_c \left(1 + \frac{\mu_{rc} l_g}{l_c}\right)} \tag{3.49}$$

N_2 are the number of turns of the secondary side winding.

The selection of winding wire is the next step. The selection of the wire incorporates several aspects such as the cross section area of the wire, length, and diameter of wire. The cross section area of the winding wire can be defined as current through the inductor to the current density and can be given as follows.

$$A_w = \frac{I_L}{J_m} \tag{3.50}$$

The bare diameter of the wire is dependent on the cross section area of the wire. The bare diameter of the winding area can be given as follows.

$$d_i = \sqrt{\frac{4A_w}{\pi}} \tag{3.51}$$

We know that the current flows through the skin of the conductor. The effective resistance of the conductor mainly controls the current flow on the skin of the conductor. At high frequencies, the effective resistance increases which result in decrease effective cross section of the conductor. However, the magnetic field produced due to the induced current does not penetrate completely into the conductor. The measure of the degree of penetration of the magnetic field into the conductor is known as skin depth. The skin depth is frequency dependent quantity. The skin depth can be given

as follows.

$$\delta_{\omega} = \sqrt{\frac{\rho_{\omega}}{\pi \mu f}} = \frac{66.2}{\sqrt{f}} \tag{3.52}$$

where ρ_{ω} is the resistivity of the material, μ is the permeability and f is the operating frequency.

There are several parameters involved in choosing the winding wire of the appropriate gauge such as resistance, current carrying capability, the number of turns and the cross section area. The turns of the winding area have an impact on the size of the transformer. Therefore, a parameter, mean turn length is essentially calculated. Mean turn length (MTL) is nothing but the measure of the average amount of length of wire is required to complete turn. The mean turn length (MTL) varies according to the shape of the core. For toroidal cores, the mean turn length can be given as follows.

$$MTL = l_T = \frac{\pi(outer\,diameter + inner\,diameter)}{2} \tag{3.53}$$

On the other hand, for EE cores, the mean turn length can be given as follows.

$$MTL = l_T = 4(outer\,diameter) \tag{3.54}$$

since the average length of the winding wire is calculated. Now, the total length of the primary and secondary winding needs to be determined. The length of the primary and secondary winding can be calculated with the help of mean turn length and the number of turns. The length of the primary winding can be given as follows.

$$l_{wp} = N_1 l_T \tag{3.55}$$

Similarly, the length of the secondary winding can be given as follows.

$$l_{ws} = N_2 l_T \tag{3.56}$$

where N_1 and N_2 are the number of turns for primary and secondary windings respectively.

The resistance of the winding wire can be defined with the help of mean turn length (MTL), the cross section of wire, the number of turns and resistivity of the winding wire material. In most of the cases, copper is used as winding wire material. The resistivity of the copper is $\rho_{cu} = 1.724 * 10^{-8}$ $(\Omega.m)$. The resistance for the primary winding wire can be given as follows.

$$r_{wp} = \rho_{cu}\frac{l_{wp}}{A_w} = \rho_{cu}\frac{N_1 l_T}{A_w} \tag{3.57}$$

Similarly, the resistance of the secondary winding wire can be given as follows.

$$r_{ws} = \rho_{cu}\frac{l_{ws}}{A_w} = \rho_{cu}\frac{N_2 l_T}{A_w} \tag{3.58}$$

where A_w is the cross section area of the wire.

The table 5 comprises of component values of transformer designed for current-driven Class-E low dv/dt (ZVS) rectifier and voltage-driven Class-E low di/dt (ZCS) rectifier. *CD-Current-driven, VD-Voltage-driven

Table 5: Component values of transformer.

Parameters (D)	**CD ZVS rectifier**	**VD ZCS rectifier**
Area product (A_p)	0.59 cm^4	0.59 cm^4
Magnetic energy (W_m)	0.5531 mJ	0.5531 mJ
Magnetizing inductance (L_m)	22.43 μH	72.61 μH
Primary self-inductance (L_1)	45 μH	150 μH
Secondary self-inductance (L_2)	30 μH	100 μH
Primary leakage inductance (L_{l1})	22.43 μH	72.61 μH
Secondary leakage inductance (L_{l2})	15 μH	50 μH
Number of primary turns (N_1)	36	66
Number of secondary turns (N_2)	30	56
Turns ratio (n)	1.2	1.17
Area of primary winding wire (A_{wp})	1.404 mm^2	0.7806 mm^2
Diameter of conductor (d_i)	1.3372 mm	0.9969 mm
Window area of core (W_a)	70.91 mm^2	70.91 mm^2
Skin depth (δ_ω)	0.0254 mm	0.0254 mm
Peak magnetic flux density (B_{pk})	0.0507 T	0.0517 T
Mutual inductance (M)	18.37 μH	61.23 μH
Mean turn length (MTL)	37.6 mm	37.6 mm
Length of primary winding (l_{wp})	1400 mm	2500 mm
Length of secondary winding (l_{ws})	1200 mm	2200 mm
Primary winding resistance (r_{wp})	0.0293 Ω	0.0523 Ω
Secondary winding resistance (r_{ws})	0.0251 Ω	0.0460 Ω

3.7 Maximum Efficiency Criterion

The efficiency of the transformer is hindered by losses such as magnetic losses and copper losses. The magnetic losses are generally caused by the improper selection of material for the core, core cross-sectional area or shape of the core. Due to this reason, magnetic losses can be also termed as core losses. As we discussed earlier, the eddy current loss and the hysteresis loss fall under the core loss category. We know that, while designing the transformer the frequency of operation, flux density and the material used for the core remains constant. Therefore, the losses emerging from these parameters are bound to occur. For this reason, the magnetic losses of the transformer can be also termed as fixed losses. However, the core losses can be minimized by choosing the material with optimum magnetic characteristics for the core design and also by minimizing the thickness of the lamination.

The copper losses are also known as electric-power loss. When there is a dissipation of power from the primary and secondary windings then the copper losses are said to have occurred. The copper losses are dependent on the current flowing through the windings and also on the corresponding resistance. Due to this reason, the copper losses are also known as I^2R losses. However, as the number of windings or the load increases so the square of the current will increase resulting in increased core losses. Generally, the copper losses are termed as variable losses.

In order to account the efficiency of the transformer, it is necessary to have the measure of losses occurred in the transformer. The equivalent series resistance (ESR) associated with the components of the transformer accounts for the respective losses. When the transformer is not having any load at the output, then the efficiency of the transformer is zero. However, When the load is introduced, the efficiency of the transformer increases with the increasing load. The efficiency of the transformer has a definite value and so any further increase in the value of load not only limits the

efficiency but also forces it to drop off. The condition for achieving the maximum efficiency of the transformer is that the amount of copper losses and the core losses are equal. The load at which the amount of copper losses and core losses are equal is said to be the optimum load.

We know that the total input power is a combination of output power and the total losses incurred in the individual components. The efficiency of the transformer can be given as the ratio of the output power to the input power. The efficiency of the transformer can be expressed as follows.

$$\eta_t = \frac{P_O}{P_I} = \frac{P_O}{(P_O + P_{LS})} \tag{3.59}$$

where P_{LS} denotes the total power loss incurred in the transformer. [17]

4 Inverter

4.1 Introduction

The resonant inverters which includes switching of semi-conductor switches at zero voltage (ZVS) or zero current (ZCS) are perfect examples of energy-saving converter systems. They can operate at higher frequencies. Basically, there two types of Class-E dc-ac inverters namely Class-E Zero Voltage Switching (ZVS) and Class-E Zero Current Switching (ZCS) Inverters. The resonant inverters have wide applications in high-frequency operations. Class-E inverters are termed as most efficient inverters till date for power levels up to several kilowatts. The switching losses are virtually zero since the switch voltage and current waveforms do not overlap each other which leads to high efficiency. The Class-E inverter is easy to construct and has large power handling capacity as compared to other inverters. The capability of Class-E inverter to operate at high efficiency at fixed values of load and switching frequency makes it a very good candidate for Wireless Power Transfer (WPT) applications. It is generally used as a coil driver in an inductive link Wireless Power Transfer (WPT) applications. The switching element is a very vital part of the Class-E inverter since it can directly lead to displacement of the coils from optimum position. If the switching of Class-E inverter is not initiated at optimum conditions, then large current and voltage spikes may be developed leading to permanent damage of the switching elements. In addition, if the Class-E inverter is operated at non-optimum conditions, then the overall efficiency of the inverter will be degraded resulting in reduced output power at the load. In order to resolve this problem certain tuning mechanisms can be implemented.

If the wireless power transfer (WPT) system is to be build using the Class-E inverter, then there are certain parameters which should be taken into account regarding the design of inverter. The distance between the coils, misalignment of coils,

coupling coefficient etc. are some of the parameters which influence the efficiency of the overall system. There are three ways to adjust the output power of WPT system which are mentioned as follows:

1. By varying the switching frequency
2. By varying the duty cycle and
3. By varying the DC input voltage.

But, the efficiency of the system may be compromised if the method involving the switching frequency variation is considered at light load conditions. The other two methods deliver efficient results at light load conditions.[18] [19]

4.2 Class-E Resonant ZVS Inverter

4.3 Circuit Description

The basic circuit of the Class-E resonant ZVS inverter is shown in fig. 4.1 which consist of DC input voltage V_I, MOSFET S, which acts a switch, dc-feed inductance or choke inductor L_f, $L - C - R_i$ series resonant circuit, and a voltage shaping shunt capacitance C_1. The switching of the MOSFET (switch) is determined by the driver's operating frequency given by $f = \frac{\omega}{2\pi}$. The shunt capacitance absorbs all the capacitances in the circuit such as transistor output capacitance, choke parasitic capacitance and stray capacitance. The load resistor R_i in the series resonant circuit is an AC load. In order to neglect AC ripple on the DC supply current I_I, the choke inductance is assumed to be high. When the switch is ON, the shunt capacitance C_1 gets short circuited and only the series resonant circuit $L-C- R_i$ comes in action and the voltage across switch falls to approximately zero and a non-zero switch current flows through MOSFET. When the switch is in OFF condition, the series resonant circuit includes shunt capacitance i.e. $C_1 - L - C - R_i$ and the difference between currents through choke inductance and series resonant filter flows through the shunt capacitance C_1 producing the pulse shape voltage. The switching condition of the MOSFET characterizes the load network of Class-E resonant ZVS inverter consisting of two resonant frequencies and two loaded quality factors. When the switch is ON, the resonant frequency and the loaded quality factor can be expressed as,

$$f_{o1} = \frac{1}{2\pi\sqrt{LC}} \tag{4.1}$$

and

$$Q_{L1} = \frac{\omega_{o1}L}{R_i} = \frac{1}{\omega_{o1}CR_i} \tag{4.2}$$

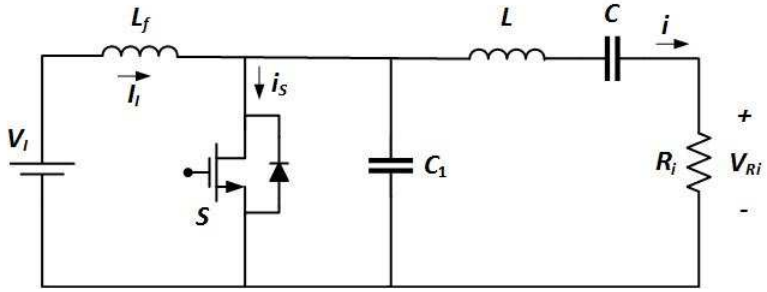

Figure 4.1: Class-E resonant ZVS inverter.

respectively. When the switch is OFF, the resonant frequency and the loaded quality factor can be expressed as,

$$f_{o2} = \frac{1}{2\pi\sqrt{LC_{eq}}} \tag{4.3}$$

and

$$Q_{L2} = \frac{\omega_{o2}L}{R_i} = \frac{1}{\omega_{o2}C_{eq}R_i} \tag{4.4}$$

respectively, where, $C_{eq} = \frac{CC_1}{C+C_1}$. The most important function of the inverter is the zero voltage switching (ZVS) at the turn ON of switch and one of the condition to achieve the ZVS is that the operating frequency should be greater than the resonant frequency i.e. $f > f_{o1}$. In this situation, the series resonant circuit $L - C - R_i$ signifies the inductive load on the operating frequency. Therefore, the inductance can be divided into two separate inductances namely, L_a and L_b. Out of the two separate inductances, L_a resonates with capacitance C and the operating frequency and loaded quality factor can be expressed as,

$$f = \frac{1}{2\pi\sqrt{L_aC}} \tag{4.5}$$

and

$$Q_L = \frac{\omega L}{R_i} = \frac{\omega(L_a + L_b)}{R_i} = \frac{1}{\omega C R_i} + \frac{\omega L_b}{R_i} \tag{4.6}$$

[18]

4.4 Principle of Operation

There are basically three modes of operation of Class-E resonant ZVS inverter. The modes of operation are dependent on the switch voltage and current waveforms. The derivative of the switch voltage with respect to time is a vital parameter which sets modes of zero voltage switching (ZVS) of Class-E inverter. The three modes of operation can be expressed as $\frac{dv_s(\omega t)}{d(\omega t)} = 0$, $\frac{dv_s(\omega t)}{d(\omega t)} < 0$ and $\frac{dv_s(\omega t)}{d(\omega t)} > 0$. The zero voltage switching (ZVS) condition is satisfied when the switch voltage and the voltage across shunt capacitance C_1 goes to zero when the switch turns ON. As a result of this, the energy stored in the shunt capacitance C_1 goes to zero reducing the turn-ON switching loss. The zero voltage switching (ZVS) can be given as $v_s(2\pi) = 0$. The mode in which the derivative of the switch voltage with respect to time is equal to zero i.e. $\frac{dv_s(\omega t)}{d(\omega t)} = 0$ is known as optimum mode of operation because it satisfies the ZVS condition. Whereas, the other two modes fall under sub-optimum mode of operation as they impose some losses in the Class-E ZVS inverter. In the ZVS operation, the operating frequency falls between the two resonant frequencies i.e. $f > f_{o1}$ and $f < f_{o2}$ where f is the operating frequency and f_{o1} and f_{o2} are the resonant frequencies. As we discussed earlier, the shape of the current and voltage waveforms also determines the modes of operation of Class-E inverter, the main parameter involved in shaping the current waveform is loaded quality factor (Q_L). The shape of the current waveform is nearly sinusoidal when the value of loaded quality factor is high i.e. $Q_L > 2.5$ and the shape of current waveform becomes nearly exponential function when the loaded quality factor is low i.e. $Q_L < 2.5$.[18]

4.4.1 Optimum Operation

In Class-E resonant ZVS inverter, zero voltage switching (ZVS) is said to be achieved when the voltage across switch goes to zero at the turn-ON instance of MOSFET (switch) i.e. $v_s(2\pi) = 0$. The waveforms for the optimum operation are shown in

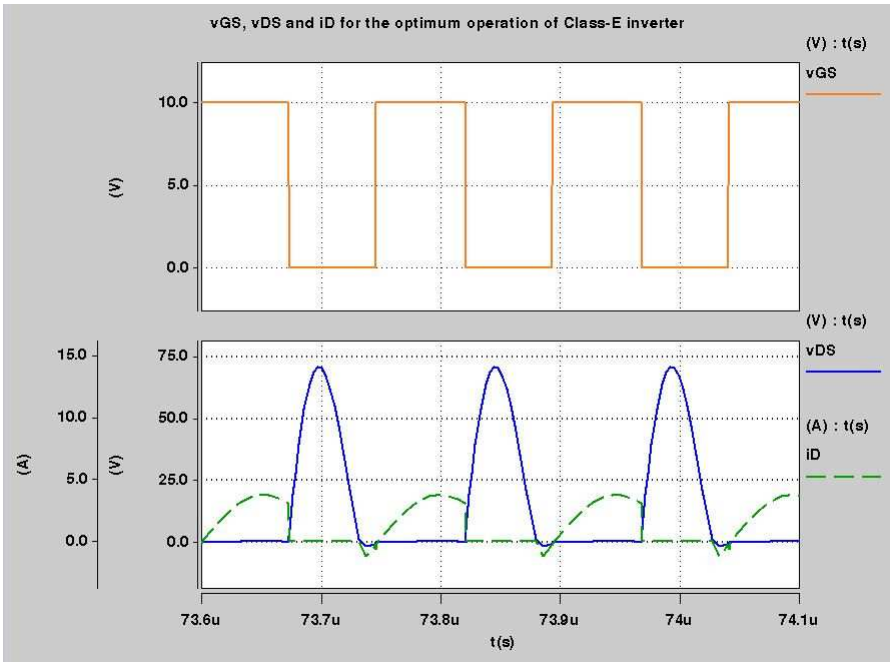

Figure 4.2: Optimum operation of the Class-E resonant ZVS inverter.

Fig. 4.2. In addition, if the derivative of the switch voltage with respect to time goes to zero at turn-ON of switch, then zero derivative switching (ZDS) of the Class-E resonant inverter is said to be achieved. The zero derivative switching (ZDS) is also known as zero-slope switching. Both, the zero voltage switching (ZVS) and the zero derivative switching (ZDS) fall under 'nominal' condition. The operating conditions at which maximum drain efficiency is achieved, nullifying all the losses is said to be 'optimum' condition. In practical situations, the components used in the design of Class-E resonant inverter are non-ideal which results in reduced efficiency. Therefore, the system is incapable of performing in optimum condition. One way to get the nominal and optimum conditions closer is to choose components with smaller parasitic. When the switch is ON, the switch current i_s starts increasing gradually from zero. The maximum switch current is denoted by I_{SM}. When the turn-OFF transition of the switch occurs, the switch current goes to zero and the switch voltage starts increasing gradually from zero, reaching its maximum value i.e. V_{SM} goes to

zero at next turn-ON instance of switch. In the optimum mode of operation, the switch voltage and switch current is maintained on the positive side. The relation between several components of the Class-E resonant inverter like the shunt capacitor C_1, inductance L_b, AC load resistance R_i and also operating frequency and duty cycle all together determine the optimum operation. The AC load resistance R_i is a very important parameter when the optimum operation of the Class-E resonant inverter is desired. The AC load resistance R_i controls the amplitude of current I_M of the series resonant circuit $L - C - R_i$ and also the voltage across the shunt capacitor C_1. As a result, the AC load resistance R_i should be optimum to achieve the optimum operation of Class-E resonant inverter. The optimum AC load resistance can be termed as R_{opt}. Therefore, the condition to achieve the optimum operation is $R_i = R_{opt}$. But, in practical situations, either the AC load resistance R_i is less than the optimum AC load resistance R_{opt} i.e. $R_i < R_{opt}$ or the AC load resistance R_i is greater than the optimum AC load resistance R_{opt} i.e. $R_i > R_{opt}$ which presents a problem for the optimum operation of the Class-E resonant inverter. When $R_i < R_{opt}$, the amplitude of current I_M through the series resonant circuit $L - C - R_i$ as well as the voltage drop across the shunt capacitor C_1 goes higher than that for optimum operation. As a result, at turn-ON transition, the voltage across switch goes less than zero. On the other hand, when $R_i > R_{opt}$, the amplitude of current I_M through the series resonant circuit $L - C - R_i$ as well as the voltage drop across the shunt capacitor C_1 is lower than that for optimum operation. As a result, at turn-ON transition, the voltage across switch goes greater than zero. These situations impose turn-ON switching losses in transistor, because the energy stored in the shunt capacitor C_1 during the turn-on transition is dissipated in the form of heat. The turn-ON switching losses contradict the zero voltage switching (ZVS) operation of the class E resonant inverter. A small modification in the switch of Class-E inverter can be used to overcome the turn-ON

switching losses in the inverter or to achieve zero voltage switching (ZVS) operation. The modification includes adding an anti-parallel or series diode to the transistor which guarantees the turn-ON of switch at zero voltage for $R_i \leq R_{opt}$.

The zero derivative switching (ZDS) for the Class-E resonant inverter can be achieved by nullifying the Miller's effect. Miller's effect is basically dependent on the instantaneous voltage gain and the coupling capacitance. Miller's capacitance can be represented as $C_M = (1 - A_v)C$ where, A_v is the instantaneous voltage gain and C is the coupling capacitance. Therefore, the instantaneous voltage gain for the Class-E resonant inverter can be given as ratio of change in drain to source voltage Δv_{DS} to the change in gate to source voltage Δv_{GS}. The change in the drain to source voltage for the Class-E resonant inverter coupled with current-driven Class-E ZVS rectifier is zero i.e. $\Delta v_{DS} = 0$ and so the instantaneous voltage gain can be given as $A_v = \frac{\Delta v_{DS}}{\Delta v_{GS}} = 0$. Since, the instantaneous voltage gain is zero, the gate to drain capacitance (C_{gd}) is said to be reflected on the gate to source terminals of the inverter. Hence, the Miller's capacitance for the Class-E resonant inverter can be expressed as $C_M = (1 - A_v)C_{gd} = C_{gd}$.

4.4.2 Sub-optimum Operation

Basically, the main difference between optimum and sub-optimum operation is that the optimum operation guarantees the zero voltage switching (ZVS) as well as the zero derivative switching (ZDS) for Class-E resonant inverter. On the other hand, the sub-optimum operation ensures only the zero voltage switching (ZVS) for Class-E resonant inverter for a certain range of load resistance i.e. $0 \leq R_i \leq R_{opt}$. The waveforms for the sub-optimum operation are shown in Fig. 4.3. For the sub-optimum operation, the condition for zero voltage switching (ZVS) is expressed as $v_s(2\pi) = 0$ and for zero derivative switching (ZDS) there are two cases in which either the derivative of the switch voltage with respect to time is less than zero i.e. $\frac{dv_s(\omega t)}{d(\omega t)} < 0$ or it is

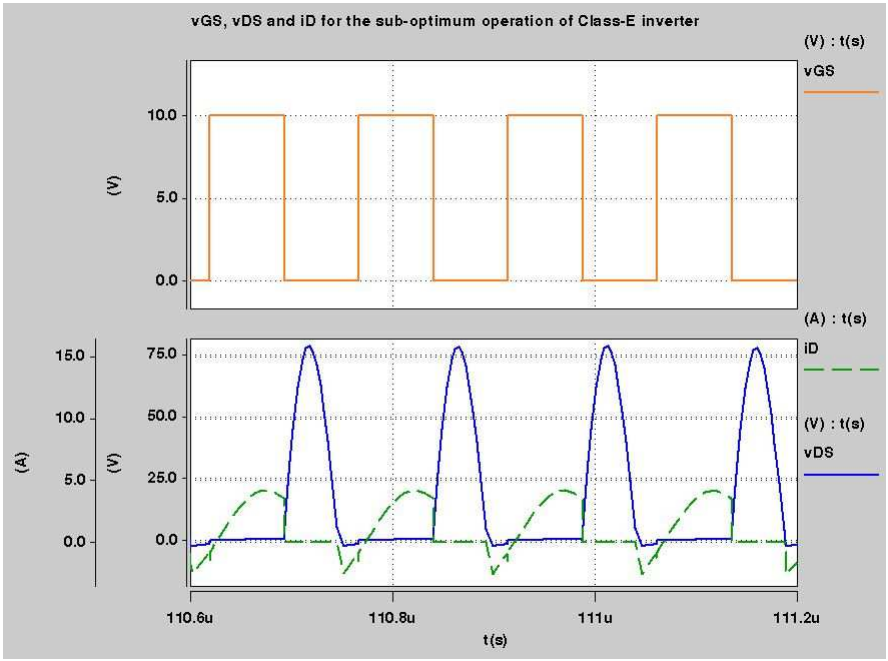

Figure 4.3: Sub-optimum operation of the Class-E resonant ZVS inverter.

greater than zero i.e. $\frac{dv_s(\omega t)}{d(\omega t)} > 0$ and $v_s(2\pi) = 0$. We know that, in general, the time at which the switch turns ON is determined by gate to source voltage but, when $\frac{dv_s(\omega t)}{d(\omega t)} < 0$, the anti-parallel diode connected in series with the switch has impact on switching the transistor (switch). Basically, the diode accelerates the switching time of the transistor. However, the switching losses are zero since the switch turns ON at zero voltage resulting high efficiency. The condition for achieving such an operation is $0 \leq R_i \leq R_{opt}$. Since the AC load resistance R_i is less than optimum load resistance R_{opt}, there are some irregularities in operating frequency and also in transistor on switch duty cycle D_t which results in negative and positive values of switch current. The negative value of current simply means that the transistor can be either ON or OFF, but the anti-parallel diode is ON. In other words, the diode duty cycle D is greater than the transistor on switch duty cycle. On the other hand, when the switch current is positive, the transistor is turned ON and the anti-parallel diode is OFF. Therefore, the transistor on switch duty cycle D_t ranges between minimum transistor

on switch duty cycle D_{tmin} and diode duty cycle D i.e. $D_{tmin} \leq D_t \leq D$.

When $\frac{dv_s(\omega t)}{d(\omega t)} > 0$ and $v_s(2\pi) = 0$. In this case, the switch current is always positive but the switch voltage can have either positive or negative values. Therefore, to overcome this problem, it is recommended to have a unidirectional switch for the current and bidirectional switch for voltage. The bidirectional switch has capability of conducting in both the directions. The bidirectional switch can be built by simply adding a diode in series with the transistor. The diode in series with the transistor basically delays the turn-ON instance of the switch. As a result, the transistor on switch duty cycle D_t is greater than or equal to the diode duty cycle D but less than or equal to the maximum diode duty cycle D_{tmax} i.e. $D \leq D_t \leq D_{tmax}$. However, there are several drawbacks of having diode in series with transistor. The drawbacks include higher conduction losses, higher on-voltage, losses associated with transistor output capacitance. The increased switch voltage charges the transistor output capacitance to its peak value via series diode. Since, the diode is in OFF condition, the charge remains on the transistor output capacitance until the transistor turns ON. Now, when the transistor turns ON, the transistor output capacitance gets discharged via on-resistance of the MOSFET, dissipating the stored energy and eventually reducing the overall efficiency.

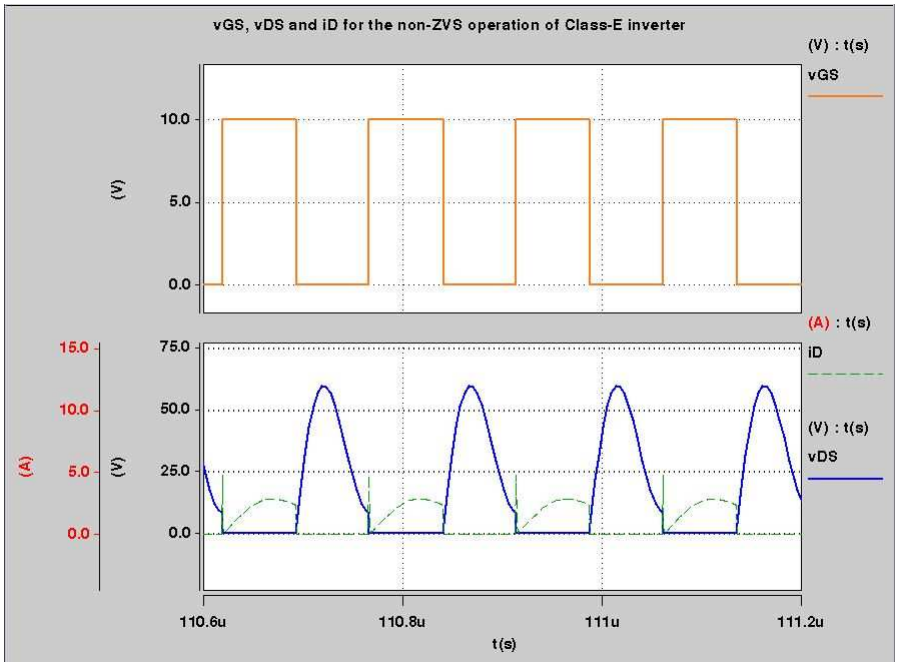

Figure 4.4: Non-ZVS operation of the Class-E resonant ZVS inverter.

Fig. 4.4 represents the non-ZVS operation of the Class-E resonant ZVS inverter. The load resistance is made greater than the optimum load resistance (i.e. $R_i > R_{opt}$) [18].

Effect of variation in duty cycle on the phase angle of Class-E resonant ZVS inverter

Fig. 4.5 shows the relation between the duty cycle and the phase angle of the Class-E inverter. The phase angle of the Class-E inverter can be given as,

$$\phi = \pi + \tan^{-1} \frac{\cos(2\pi D) - 1}{2\pi(1 - D) + \sin(2\pi D)} \tag{4.7}$$

where, D is the duty cycle and ϕ is the phase angle of the inverter. The duty cycle is varied from 0 to 1 and the corresponding decrease in the phase angle is observed. The duty cycle and the phase angle are inversely proportional to each other.

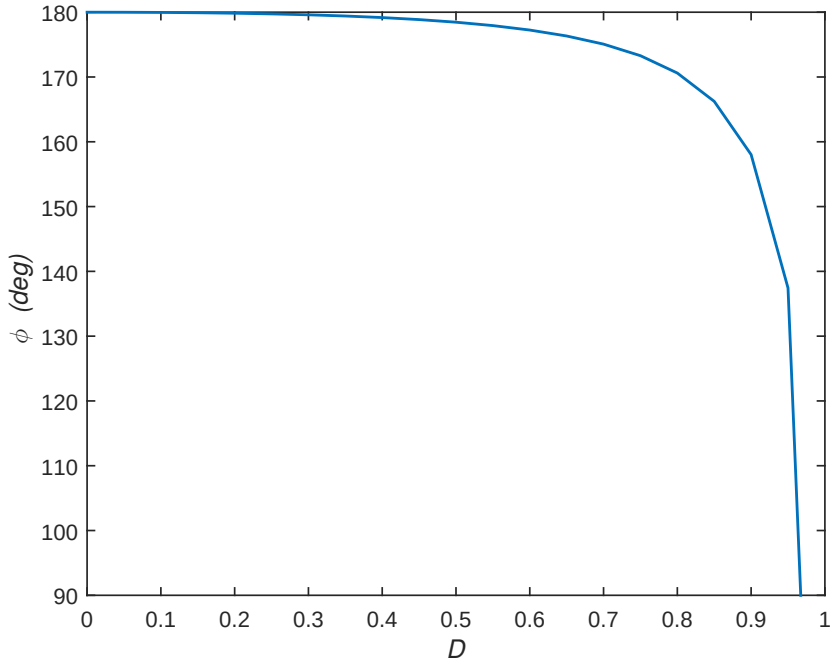

Figure 4.5: Phase angle as a function of duty cycle.

4.5 Component Values

We will consider the transformer version of the Class-E resonant inverter for the calculation of the component values shown in Fig. 4.6 comprising of DC input voltage V_I, power MOSFET S, voltage shaping shunt capacitance C_1, choke inductance L_f. The transformer part consists of primary and secondary self-inductances denoted by L_p and L_s respectively, magnetizing inductance L_m, primary leakage inductance L_{lp} and secondary leakage inductance L_{ls}. The capacitor C and the inductance L_1 form a series resonant circuit. The resonant inductance L_1 is the series combination of two inductances namely external inductance L_{ext} and the primary leakage inductance L_{lp} i.e. $L_1 = L_{ext} + L_{lp}$. In order to cancel the leakages on the secondary side of the transformer for higher efficiency, a capacitor is placed in series with the secondary winding leakage inductance, C_s. The coupling coefficient is denoted by k. The distance between the two coils of the transformer can be variable, as a result of this the

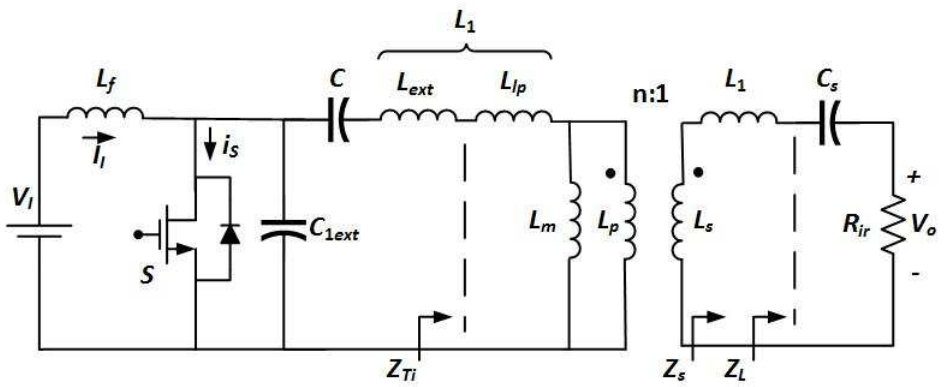

Figure 4.6: Transformer version of Class-E Resonant ZVS Inverter [20].

value of the coupling coefficient also varies. The turns ratio is denoted by n and can be defined as ratio of number of primary turns N_1 to the number of secondary turns N_2. The AC load resistance R_{ir} is nothing but the equivalent resistance of the rectifier across which the DC output voltage is desired. We will design the Class-E resonant inverter to obtain the DC output voltage between 12 V to 15 V, output power between 25 W to 40 W for 6.78 MHz frequency. Initially, the AC load resistance R_{ir} of the Class-E resonant inverter can be calculated with the help of DC input voltage V_I and the output power P_O and can be given as follows.[20]

$$R_{ir} = \frac{8}{(\pi^2 + 4)} \frac{V_I^2}{P_O}. \tag{4.8}$$

The magnetizing inductance L_m can be calculated with the help of primary self-inductance L_p and the coupling coefficient of the transformer k and can be expressed as follows.

$$L_m = kL_p. \tag{4.9}$$

The primary and secondary leakage inductances can be calculated using the primary and secondary self-inductances respectively. The primary leakage inductance can be represented as follows.

$$L_{lp} = (1 - k)L_p. \tag{4.10}$$

The primary leakage inductance can also be expressed in terms of magnetizing inductance a follows.

$$L_{lp} = \frac{(1-k)}{k} L_m. \tag{4.11}$$

And the secondary leakage inductance can be represented as follows.

$$L_{ls} = (1-k) L_s. \tag{4.12}$$

The secondary leakage inductance can be expressed in terms of magnetizing inductance and the turns ratio n as follows.

$$L_{lp} = \frac{(1-k)}{n^2 k} L_m. \tag{4.13}$$

In order to overcome the leakage inductance on the secondary side of the transformer, it is necessary to add a capacitor in series with the winding. The series capacitor C_s can be calculated taking into account the secondary leakage inductance and can be represented as follows.

$$C_s = \frac{1}{\omega^2 L_{ls}} = \frac{1}{4\pi^2 f_s^2 L_{ls}} = \frac{n^2}{4\pi^2 f_s^2 (1-k) L_p}. \tag{4.14}$$

where ω is the angular operating frequency which can be also expressed as $\omega = 2\pi f_s$ and f_s is the switching frequency of the inverter, n is the turns ratio of the transformer, L_{ls} is the secondary leakage inductance, L_p is the primary self-inductance and k is the coupling coefficient of the Class-E resonant inverter.

4.5.1 Impedance of Class-E Resonant ZVS Inverter

The conventional Class-E resonant inverter delivers specified amount of power at the corresponding DC voltage at the output. But, the requirement of the output power as well as the DC output voltage can vary according to the applications. In order to obtain a specific amount of power at the specified DC voltage, the Class-E resonant

inverter should be coupled with matching resonant circuits. Basically, matching resonant circuits are responsible for achieving impedance matching. Impedance matching is a process of achieving harmony between two terminations of the circuit. The AC load resistance, output power and the DC output voltage are important quantities while designing the resonant inverter. But, in some cases, the AC load resistance of the inverter is already specified and at the output of the inverter a particular amount of power and DC output voltage is desired. Therefore, it becomes necessary for the inverter to incorporate a matching resonant circuit and achieve impedance transformation. There are basically two methods of achieving the impedance transformation either by tapping the resonant capacitance C or by tapping resonant inductance L. There are four types of matching resonant circuit obtained by each method and those are 1. π1a 2. π2a 3. π1b and 4. π2b. The matching resonant circuits π1a and π1b can be built by tapping the resonant capacitance C and π2a and π2b circuits can be built by tapping the resonant inductance L. The matching resonant circuits are shown in Fig. 4.7.[18] The impedance transformation in the Class-E resonant inverter is achieved by implementing π2a impedance matching circuit. Therefore, the modified circuit of Class-E resonant inverter with π2a impedance matching circuit can be represented in Fig. 4.8. We can see observe from figure that, the primary portion of the transformer version of the Class-E resonant inverter remains the same. On the other hand, the secondary side of the inverter is transferred to the primary by the reflection principle which basically depends on the turns ratio of the transformer n. The fig. shows the equivalent load resistance R_i which is obtained by applying reflection principle to the AC load resistance and is given as,

$$R_i = n^2 R_{ir}. \tag{4.15}$$

The input impedance of the Class-E resonant inverter is closely related to the several parameters such as distance between the coils, primary and secondary self-

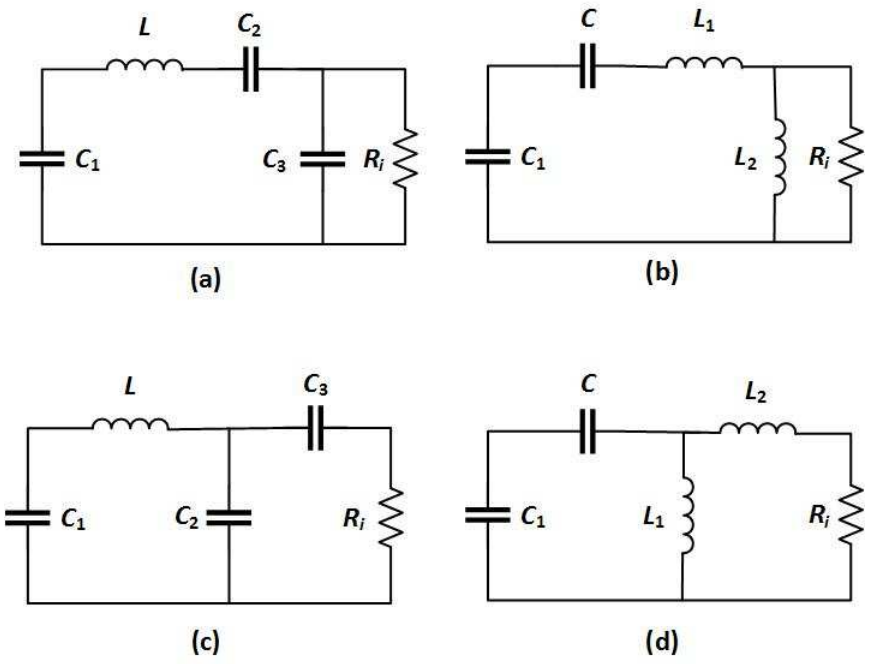

Figure 4.7: Matching Resonant Circuits. (a) Resonant circuit π1a. (b) Resonant circuit π2a. (c) Resonant circuit π1b. (d) Resonant circuit π2b. [18].

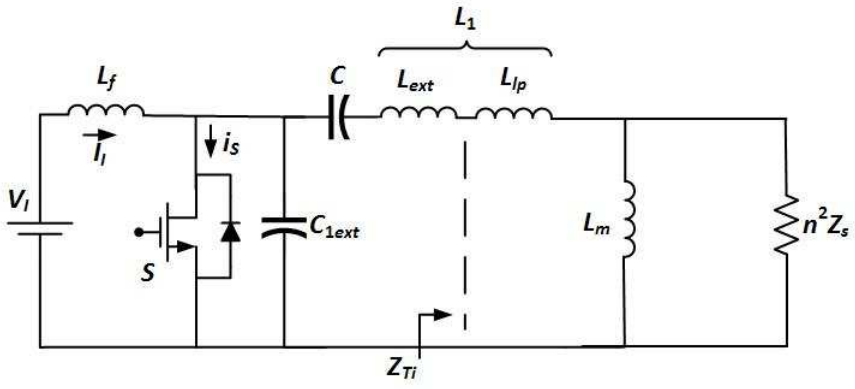

Figure 4.8: Class-E Resonant ZVS Inverter with π2a Impedance Matching Circuit [20].

inductances and AC load resistance. The distance between the coils of the transformer defines the coupling coefficient k. The coupling coefficient ranges between 0 and 1. For the ideal transformers, the value of coupling coefficient k is equal to or close to 1. The input impedance can be characterized as series combination of coupling dependent resistance R_{Ti} and coupling dependent inductance L_{Ti} and can be described as,

$$Z_{Ti} = sL_{lp} + (sL_m||R_i) = sL_{lp} + \frac{sL_mR_i}{sL_m + R_i}. \tag{4.16}$$

Solving the above equation, we get

$$Z_{Ti} = \frac{s^2(1-k)kL_p^2 + sL_pR_i}{(skL_p + R_i)}. \tag{4.17}$$

And substituting $s = j\omega$ into above equation, we get

$$Z_{Ti} = \frac{\omega^2L_p^2k^2R_i}{R_i^2 + \omega^2L_p^2k^2} + j\frac{\omega^3(1-k)k^2L_p^3 + \omega L_pR_i^2}{R_i^2 + \omega^2L_p^2k^2}. \tag{4.18}$$

Observing the above equation, we can say that the real part of the equation constitutes the equivalent input resistance R_{Ti} and can be represented as follows.

$$R_{Ti} = \frac{\omega^2L_p^2k^2R_i}{R_i^2 + \omega^2L_p^2k^2}. \tag{4.19}$$

And the imaginary part of the equation constitutes the equivalent input reactance X_{Ti} which can be represented as follows.

$$X_{Ti} = L_{Ti}\omega = \frac{\omega^3(1-k)k^2L_p^3 + \omega L_pR_i^2}{R_i^2 + \omega^2L_p^2k^2}. \tag{4.20}$$

where L_{Ti} is the equivalent input inductance, ω is the angular operating frequency, R_i is the equivalent load resistance, L_p is the primary self-inductance and k is the coupling coefficient. The equivalent input resistance and the equivalent input inductance both are functions of coupling coefficient k and can be termed as R_{Ti} and L_{Ti} respectively. The coupling coefficient proves to be a very important parameter in the zero voltage switching (ZVS) operation of Class-E inverter since it decides the value of

equivalent input resistance R_{Ti} and the condition to achieve ZVS is $0 \leq R_{Ti} \leq R_{opt}$. Fig. 4.9 shows Class-E resonant inverter comprising of coupling dependent resistance and inductance. Now, the total resonant inductance can be given as combination of external inductance L_{ext} and coupling dependent inductance L_{Ti} i.e.

$$L = L_{ext} + L_{Ti}. \tag{4.21}$$

The determination of the values of external inductance L_{ext}, magnetizing inductance L_m and the total resonant inductance L is basically dependent on the impedance transformation circuitry of Class-E resonant inverter. The reactance of inductances L_1 and L_m for the π2a impedance transformation can be given as follows.

$$X_{L1} = \omega L_1 = \left(Q_L - \sqrt{\frac{R_i}{R_{Ti}} - 1} \right) R_{Ti}. \tag{4.22}$$

And,

$$X_{L2} = \omega L_m = \frac{R_i}{\sqrt{\frac{R_i}{R_{Ti}} - 1}}. \tag{4.23}$$

Rearranging the above equations, the inductance L_1 can be given as follows.

$$L_1 = \left(Q_L - \sqrt{\frac{R_i}{R_{Ti}} - 1} \right) \frac{R_{Ti}}{\omega}. \tag{4.24}$$

The magnetizing inductance,

$$L_m = \frac{R_i}{\omega \sqrt{\frac{R_i}{R_{Ti}} - 1}}. \tag{4.25}$$

The external inductance L_{ext},

$$L_{ext} = L_1 - L_{lp}. \tag{4.26}$$

The value for shunt capacitance C_1 for the class E resonant inverter can be determined by its reactance X_{C1} which can be given as,

$$X_{C1} = \frac{1}{\omega C_1} = \frac{\pi(\pi^2 + 4)}{8} R_{Ti}. \tag{4.27}$$

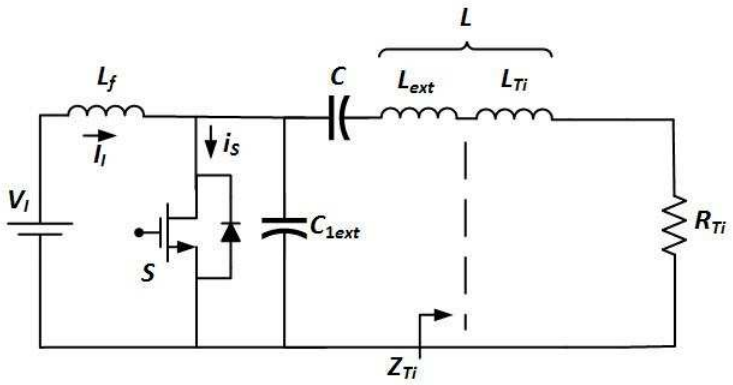

Figure 4.9: Class-E Resonant ZVS Inverter with Coupling-Dependent Resistor R_{Ti} and Resonant Inductor L [20].

The shunt capacitance C_1,

$$C_1 = \frac{8}{\omega\pi(\pi^2+4)R_{Ti}}. \tag{4.28}$$

The shunt capacitance C_1 also incorporates the output capacitance of the MOSFET i.e. C_o. The output capacitance of the MOSFET is simply the difference between the drain to source capacitance C_{ds} and gate to drain capacitance C_{gd} i.e. $C_o = C_{ds} - C_{gd}$. Generally, the design of the Class-E resonant inverter requires the value of the actual shunt capacitance excluding the output capacitance. Therefore, we will define the difference between shunt capacitance C_1 and output capacitance C_o as external shunt capacitance C_{1ext} i.e.

$$C_{1ext} = C_1 - C_o. \tag{4.29}$$

The resonant circuit comprises of series combination of resonant capacitance C and resonant inductance L. The value of the series resonant capacitance can be determined with the help of quality factor Q_L, coupling dependent resistance R_{Ti} and the operating frequency. The series resonant capacitance can be given as follows.

$$C = \frac{1}{\omega X_C} = \frac{1}{\omega\left(Q_L - \frac{\pi(\pi^2-4)}{16}\right)R_{Ti}}. \tag{4.30}$$

Finally, the choke inductance L_f can be determined by following expression,

$$L_f = 2\left(\frac{\pi^2}{4} + 1\right)\frac{R_{Ti}}{4f}. \tag{4.31}$$

4.6 Losses in Class-E Resonant ZVS Inverter

The loss analysis requires real circuit of the Class-E resonant inverter which consists of practical components. The passive components in the inverter circuit such as inductor and capacitor consist of equivalent series resistance (ESR) across them. When the MOSFET is in ON condition, a series on-state resistance originates across the switch. The losses incurred in the resonant inverter are due to these ESR's and on-state resistance, basically known as conduction losses. The inverter loss analysis can be carried out by determination of the values of these ESR's and on-state resistance.

The efficiency of the resonant inverter is nothing but the ratio of output power P_O to the input power P_I. The output power P_O is dependent on the load resistance R_i and the current I_m and is given as follows.[18]

$$P_O = \frac{R_i I_m^2}{2}. \tag{4.32}$$

Generally, the current I_I through choke inductance L_f is nearly constant. The rms value of the inductor current is equal to the current through the choke inductance I_I and can be given as follows.

$$I_{Lfrms} = I_I = \frac{2I_m}{\sqrt{\pi^2 + 4}}. \tag{4.33}$$

The equivalent series resistance (ESR) across the choke inductance L_f can be termed as r_{Lf}. The power loss incurred in the choke inductance is simply the product of square of the rms value of inductor current and the ESR across the choke inductance.

This power loss can be given as follows.

$$P_{rLf} = r_{Lf} I_{Lfrms}^2. \tag{4.34}$$

When the switch is OFF, switch current is zero and the switch voltage increases from zero to maximum value V_{SM} and then again reduces to zero at switch turn ON. When the switch is in ON condition, the switch current flows through the switch and the switch voltage is zero. The rms value of the switch current can be given as follows.

$$I_{Srms} = \frac{I_I\sqrt{\pi^2+28}}{4} = \frac{I_m}{2}\sqrt{\frac{\pi^2+28}{\pi^2+4}}. \tag{4.35}$$

The equivalent series resistance (ESR) across the MOSFET is termed as r_{DS}. The conduction loss occurred due to the switch on-state resistance is the product of square of the rms value of switch current and the ESR across MOSFET. This power loss can be given as follows.

$$P_{rDS} = r_{DS} I_{Srms}^2. \tag{4.36}$$

When the switch is ON, the difference between the DC current through choke inductance I_I and the sinusoidal current i flows through the switch. On the contrary, when the switch is OFF, the difference between current $I_I - i$ flows through the shunt capacitance C_1. The rms value of the current through shunt capacitance C_1 can be given as follows.

$$I_{C1rms} = \frac{I_I\sqrt{\pi^2-4}}{4} = \frac{I_m}{2}\sqrt{\frac{\pi^2-4}{\pi^2+4}}. \tag{4.37}$$

The equivalent series resistance (ESR) across the shunt capacitance can be termed as r_{C1}. The power loss occurred is the product of square of rms value of current through shunt capacitance and ESR of the shunt capacitance. This power loss can be given as follows.

$$P_{rC1} = r_{C1} I_{C1rms}^2. \tag{4.38}$$

The resonance in the Class-E resonant inverter is achieved by the series resonant circuit formed by resonant inductance L and the resonant capacitance C. As we

discussed earlier, every practical component has equivalent series resistance associated with it. The ESR's of the resonant inductance and the resonant capacitance can be termed as r_L and r_C respectively. The power loss across ESR of the resonant inductance r_L can be given as follows.

$$P_{rL} = \frac{r_L I_m^2}{2}. \tag{4.39}$$

And, the power loss across the ESR of the resonant capacitance can be given as follows.

$$P_{rC} = \frac{r_C I_m^2}{2}. \tag{4.40}$$

However, the total power loss associated with the Class-E resonant inverter can be expressed by combining the power loss across individual components. The total power loss across the Class-E resonant inverter is expressed as follows.

$$P_{LS} = P_{rLf} + P_{rDS} + P_{rC1} + P_{rL} + P_{rC}. \tag{4.41}$$

The power loss across all the components assists in calculating the overall efficiency of the Class-E resonant inverter. We know that, efficiency is simply ratio of output power to the input power. However, input power can be described as combination of output power and the total power loss. Therefore, the efficiency of the Class-E resonant inverter can be represented as follows.

$$\eta_I = \frac{P_O}{P_I} = \frac{P_O}{P_O + P_{LS}} = \frac{1}{1 + \frac{P_{LS}}{P_O}}. \tag{4.42}$$

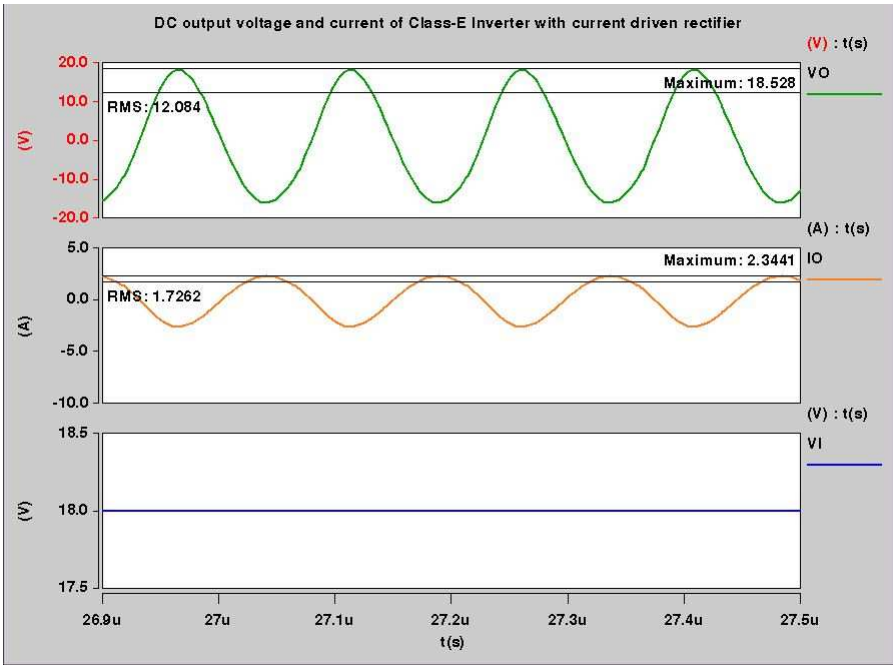

Figure 4.10: Output voltage, current and input voltage of Class-E resonant ZVS inverter coupled with current-driven Class-E ZVS rectifier.

4.7 Results

4.7.1 Class-E Resonant ZVS Inverter coupled with Current-Driven Class-E ZVS Rectifier

The simulation results of the Class-E resonant ZVS inverter coupled with current-driven Class-E ZVS rectifier are shown below. The output voltage and current waveforms for the corresponding input voltage of the Class-E inverter are shown in Fig. 4.10. Observing the above figure, we can say that the output voltage and current are sinusoidal. The maximum and rms value of output voltage obtained is 18.528 V and 12.084 V respectively. The maximum and rms value of the output current obtained is 2.3441 A and 1.7262 A respectively.

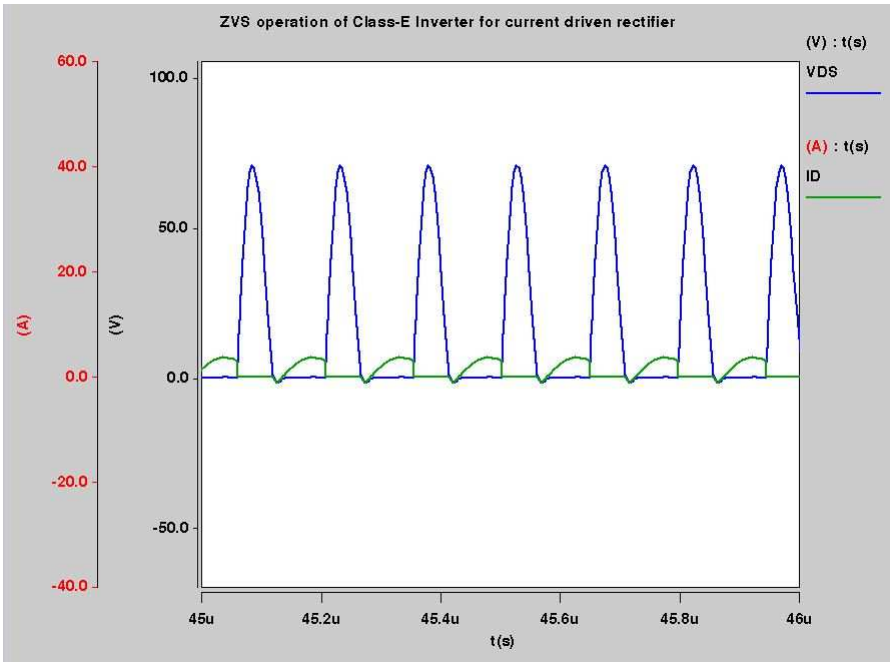

Figure 4.11: ZVS operation of Class-E resonant ZVS inverter coupled with current-driven Class-E ZVS rectifier.

The ZVS operation waveforms of the Class-E inverter coupled with current-driven Class-E ZVS rectifier are shown in Fig. 4.11. The Class-E inverter exhibits the zero voltage switching so as to have higher efficiency. The switching of the MOSFET is determined by the magnitude of the drain to source voltage and the drain current. To achieve proper zero voltage switching (ZVS), it is necessary that the MOSFET turns ON at zero switch voltage and there should not be any overlap of drain current and drain to source voltage waveform. Observing the figure, we can say that, when there is a finite drain current, the MOSFET is turned ON. In the next cycle, when the drain current gradually decreases to zero, the switch voltage or the drain to source voltage increases and MOSFET turns OFF. Since, there is no overlap in drain current and drain to source voltage waveform, the switching losses are minimal.

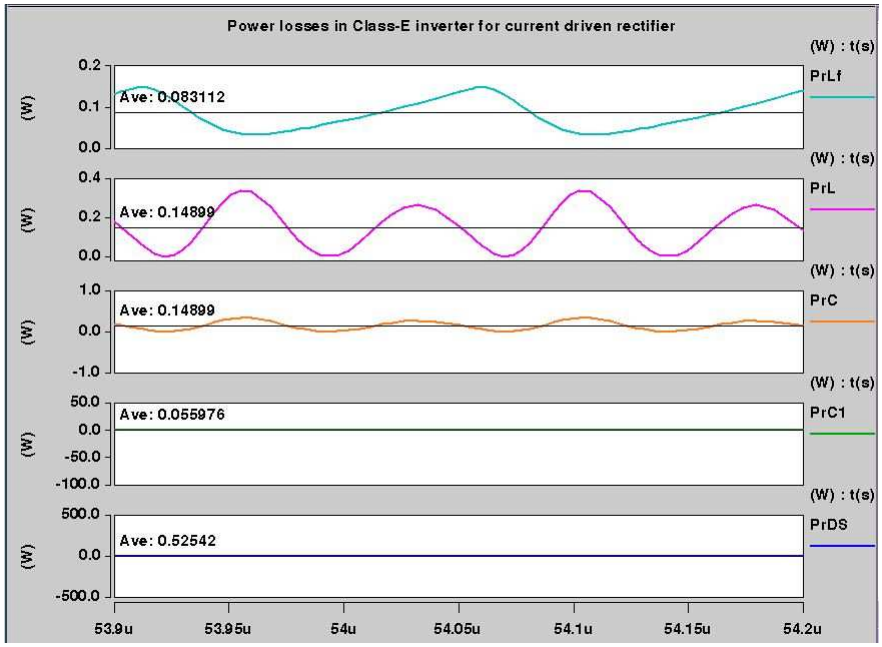

Figure 4.12: Power losses incurred in Class-E resonant ZVS inverter coupled with current-driven Class-E ZVS rectifier.

The power loss waveforms of the Class-E inverter coupled with current-driven Class-E ZVS rectifier are shown in Fig. 4.12. The power loss occurred in each passive component and the MOSFET is calculated to determine the total power loss incurred in the Class-E inverter. The average value of the power loss occurred in the choke inductance P_{rLf}, resonant inductance P_{rL}, resonant capacitance P_{rC}, shunt capacitance P_{rC1} and MOSFET on-resistance P_{rDS} is 0.0831 W, 0.1489 W, 0.1489 W, 0.055 W and 0.5254 W respectively. The ESR's for all the components is equal to 50 mΩ.

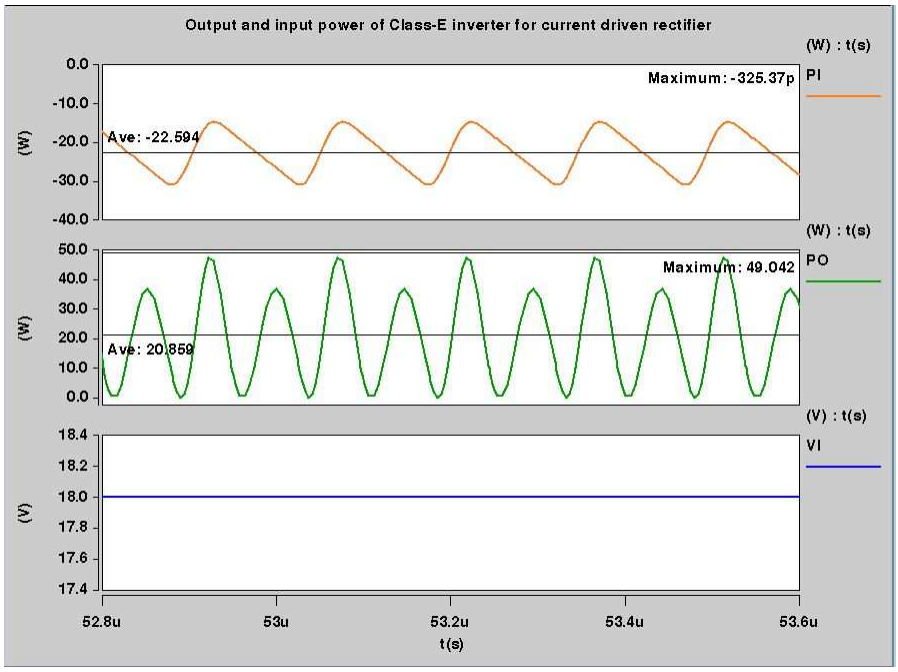

Figure 4.13: Input, output power and the input voltage of Class-E resonant ZVS inverter coupled with current-driven Class-E ZVS rectifier.

The input and output power waveform of the Class-E inverter coupled with current-driven Class-E ZVS rectifier are shown in Fig. 4.13. The efficiency of the Class-E inverter is nothing but the ratio of the average value of the output power to the input power. The maximum and average value of the input power obtained is -325.37p W and -22.594 W respectively. The maximum and average value of the output power obtained is 49.042 W and 20.859 W respectively.

4.7.2 Component Values for Class-E Resonant ZVS Inverter coupled with Current-Driven Class-E ZVS Rectifier

The specifications considered for designing the Class-E resonant ZVS inverter are also dependent upon the configuration of rectifier chosen. The desired DC voltage and power range at the output of Class-E resonant ZVS inverter is 12 V to 15 V and 25 W to 40 W respectively. The operating frequency is equal to 6.78 MHz. The primary and secondary inductance for the current-driven Class-E ZVS rectifier configuration is 45 μH and 30 μH respectively. The component values obtained for the above specifications are as follows.

The load resistance at the output of inverter can be given as product of the equivalent resistance of the current-driven Class-E ZVS rectifier R_{ir} and the square of the turns ratio n^2. The load resistance is denoted by R_i and is obtained as,

$$R_i = n^2 R_{ir} = 4.6712\ \Omega. \tag{4.43}$$

The input voltage of the inverter can be determined with the help of the load resistance and the desired output power. The input voltage is obtained as,

$$V_I = \sqrt{\frac{R_{ir} P_o}{0.5768}} = 18\ \text{V}. \tag{4.44}$$

The equivalent input resistance of the inverter can be determined with the help of load resistance, primary self inductance and the coupling coefficient. The coupling coefficient in this case is equal to $k = 0.5$. The equivalent input resistance is obtained as,

$$R_{Ti} = \frac{\omega^2 L_p^2 k^2 R_i}{R_i^2 + \omega^2 L_p^2 k^2} = 7\ \Omega. \tag{4.45}$$

Similarly, the equivalent input inductance is obtained as,

$$L_{Ti} = \frac{\omega^2 (1-k) k^2 L_p^3 + L_p R_i^2}{R_i^2 + \omega^2 L_p^2 k^2} = 22.501\ \mu\text{H}. \tag{4.46}$$

The magnetizing inductance is obtained as,

$$L_m = \frac{R_i}{\omega \sqrt{\frac{R_i}{R_{Ti}} - 1}} = 22.501\ \mu\text{H}. \tag{4.47}$$

The primary and secondary leakage inductance are obtained as

$$L_{lp} = (1-k)L_p = 22.50\ \mu\text{H}. \tag{4.48}$$

And,

$$L_{ls} = (1-k)L_s = 15\ \mu\text{H}. \tag{4.49}$$

In order to cancel the leakage at the secondary side of the transformer, it is required to add a resonant capacitance. The secondary side resonant capacitance is obtained as,

$$C_s = \frac{n^2}{4\pi^2 f_s^2 (1-k)L_p} = 36.73\ \text{pF}. \tag{4.50}$$

The total resonant inductance is obtained as,

$$L = L_{ext} + L_{Ti} = 1.6447\ \mu\text{H}. \tag{4.51}$$

The resonant capacitance is obtained as,

$$C = \frac{1}{\omega\left(Q_L - \frac{\pi(\pi^2-4)}{16}\right)R_{Ti}} = 0.3786\ \text{nF}. \tag{4.52}$$

The choke inductance is obtained as,

$$L_f = 2\left(\frac{\pi^2}{4}+1\right)\frac{R_{Ti}}{4f} = 1.7916\ \mu\text{H}. \tag{4.53}$$

The shunt capacitance is obtained as,

$$C_1 = \frac{8}{\omega\pi(\pi^2+4)R_{Ti}} = 0.6151\ \text{nF}. \tag{4.54}$$

The total power losses incurred in the Class-E resonant inverter coupled with current-driven Class-E ZVS rectifier can be given as,

$$P_{LS} = P_{rLf} + P_{rDS} + P_{rC1} + P_{rL} + P_{rC} = 0.956\ \text{W}. \tag{4.55}$$

Finally, the efficiency of the inverter can be given as ratio of the average values of the output power to the input power i.e.,

$$\eta = \frac{P_O}{|P_I|} = 92.32\ \%. \tag{4.56}$$

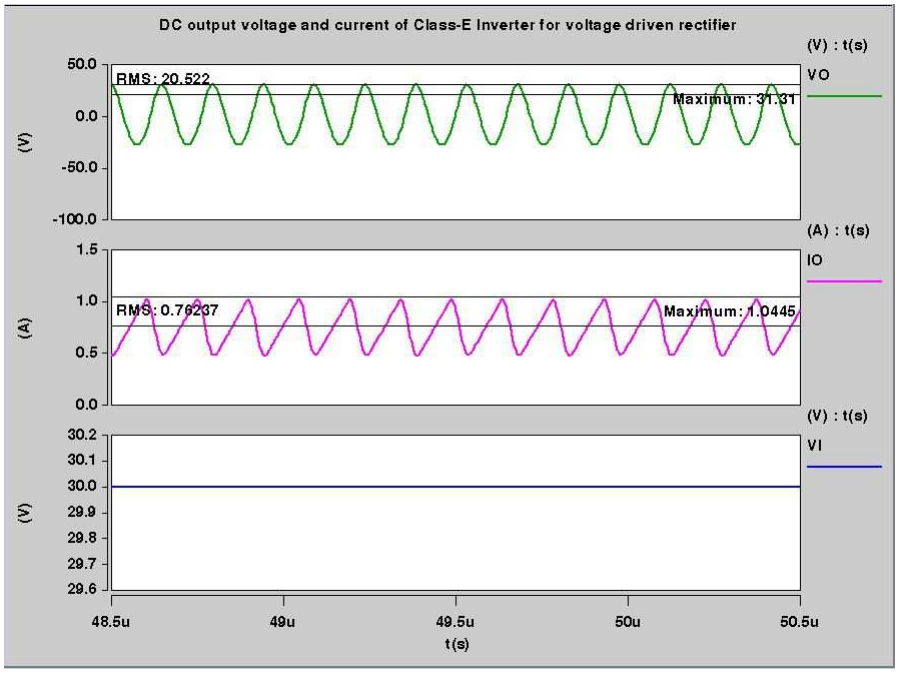

Figure 4.14: Output voltage, current and input voltage of Class-E resonant ZVS inverter coupled with voltage-driven Class-E ZCS rectifier.

4.7.3 Class-E Resonant ZVS Inverter coupled with Voltage-Driven Class-E ZCS Rectifier

The simulation results of the Class-E resonant inverter coupled with voltage-driven Class-E ZCS rectifier are shown below. The output voltage and current waveforms for the corresponding input voltage of the Class-E inverter are shown in Fig. 4.14. The maximum and rms value of output voltage obtained is 31.31 V and 20.522 V respectively. The maximum and rms value of the output current obtained is 1.0445 A and 0.7623 A respectively.

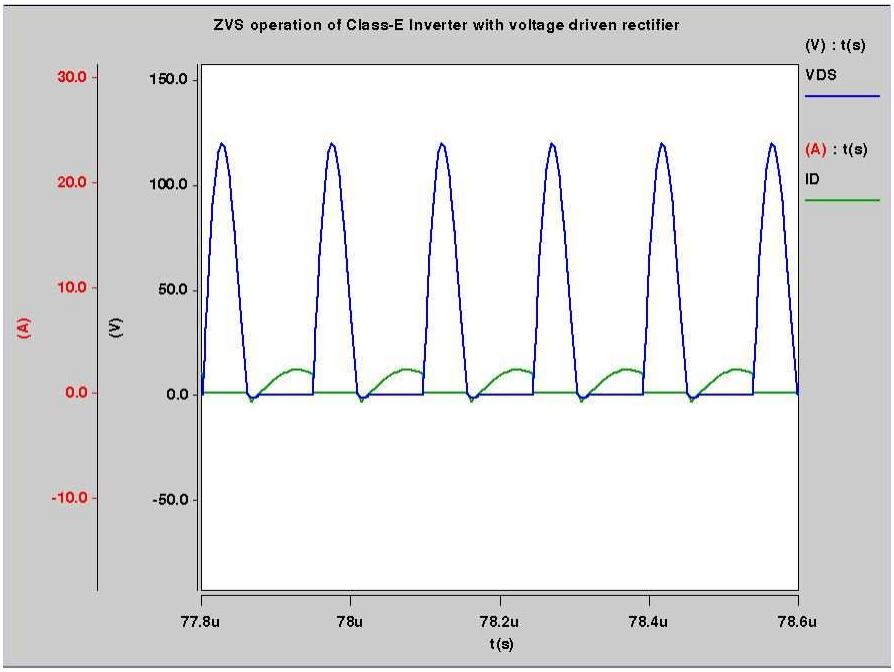

Figure 4.15: ZVS operation of Class-E resonant ZVS inverter coupled with voltage-driven Class-E ZCS rectifier.

The ZVS operation waveforms of the Class-E inverter coupled with voltage-driven Class-E ZCS rectifier are shown in Fig. 4.15. Observing the waveform, we can say that, there is no overlap in drain current and drain to source voltage waveform, the switching losses are minimal which leads to higher efficiency.

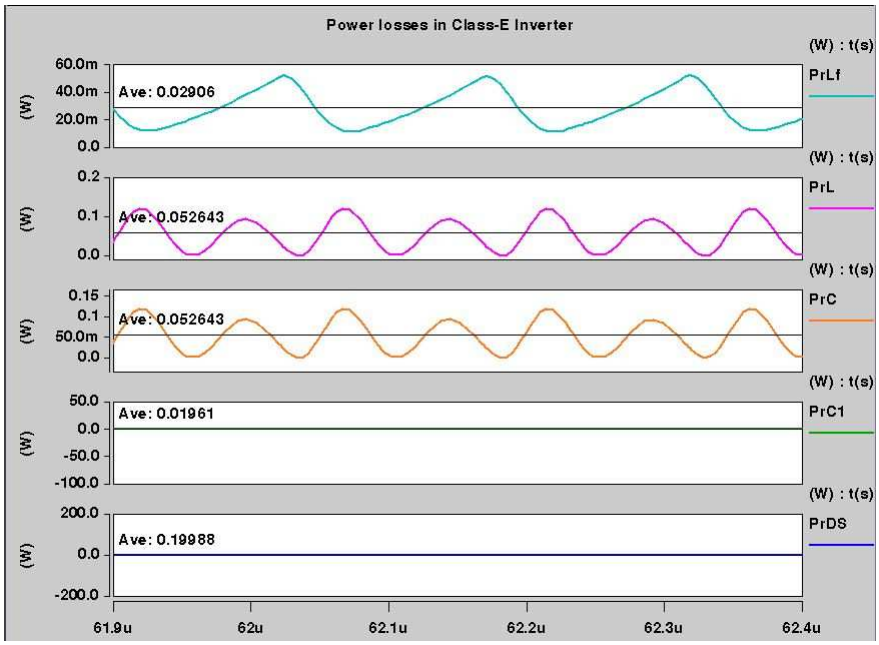

Figure 4.16: Power losses incurred in Class-E resonant ZVS inverter coupled with voltage-driven Class-E ZCS rectifier.

The power loss waveforms of the Class-E inverter coupled with voltage-driven Class-E ZCS rectifier are shown in Fig. 4.16. The power loss occurred in each passive component and the MOSFET is calculated to determine the total power loss incurred in the Class-E inverter. The average value of the power loss occurred in the choke inductance P_{rLf}, resonant inductance P_{rL}, resonant capacitance P_{rC}, shunt capacitance P_{rC1} and MOSFET on-resistance P_{rDS} is 0.0296 W, 0.0526 W, 0.0526 W, 0.0196 W and 0.1998 W respectively. The ESR's for all the components is equal to 50 mΩ.

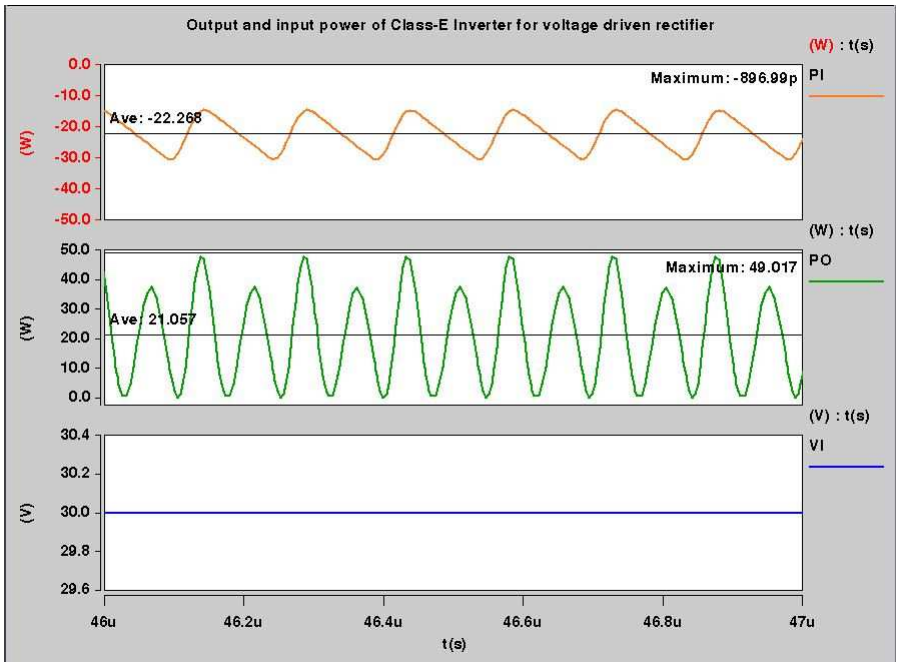

Figure 4.17: Input, output power and the input voltage of Class-E resonant ZVS inverter coupled with voltage-driven Class-E ZCS rectifier.

The input and output power waveform of the Class-E inverter coupled with voltage-driven Class-E ZCS rectifier are shown in Fig. 4.17. The efficiency of the Class-E inverter is nothing but the ratio of the average value of the output power to the input power. The maximum and average value of the input power obtained is -896.99p W and -22.268 W respectively. The maximum and average value of the output power obtained is 49.017 W and 21.057 W respectively.

4.7.4 Component Values for Class-E Resonant ZVS Inverter coupled with Voltage-Driven Class-E ZCS Rectifier

The specifications considered for designing the Class-E resonant ZVS inverter are also dependent upon the configuration of rectifier chosen. The desired DC voltage and power range at the output of Class-E resonant ZVS inverter is 12 V to 15 V and 25 W to 40 W respectively. The operating frequency is equal to 6.78 MHz. The primary and secondary inductance for the voltage-driven Class-E ZCS rectifier configuration

is 150 μH and 100 μH respectively. The component values obtained for the above specifications are as follows.

The load resistance at the output of inverter can be given as product of the equivalent resistance of the voltage-driven Class-E ZCS rectifier R_{ir} and the square of the turns ratio n^2. The load resistance is denoted by R_i and is obtained as,

$$R_i = n^2 R_{ir} = 13.3471\ \Omega. \tag{4.57}$$

The input voltage of the inverter can be determined with the help of the load resistance and the desired output power. The input voltage is obtained as,

$$V_I = \sqrt{\frac{R_{ir} P_o}{0.5768}} = 30\ \text{V}. \tag{4.58}$$

The equivalent input resistance of the inverter can be determined with the help of load resistance, primary self inductance and the coupling coefficient. The coupling coefficient in this case is equal to k=0.5. The equivalent input resistance is obtained as,

$$R_{Ti} = \frac{\omega^2 L_p^2 k^2 R_i}{R_i^2 + \omega^2 L_p^2 k^2} = 20\ \Omega. \tag{4.59}$$

Similarly, the equivalent input inductance is obtained as,

$$L_{Ti} = \frac{\omega^2 (1-k) k^2 L_p^3 + L_p R_i^2}{R_i^2 + \omega^2 L_p^2 k^2} = 75\ \mu\text{H}. \tag{4.60}$$

The magnetizing inductance is obtained as,

$$L_m = \frac{R_i}{\omega \sqrt{\frac{R_i}{R_{Ti}} - 1}} = 112.50\ \mu\text{H}. \tag{4.61}$$

The primary and secondary leakage inductance are obtained as,

$$L_{lp} = (1-k) L_p = 75\ \mu\text{H}. \tag{4.62}$$

And,

$$L_{ls} = (1-k) L_s = 50\ \mu\text{H}. \tag{4.63}$$

In order to cancel the leakage at the secondary side of the transformer, it is required to add a resonant capacitance. The secondary side resonant capacitance is obtained as,

$$C_s = \frac{n^2}{4\pi^2 f_s^2 (1-k) L_p} = 33.062 \text{ pF}. \tag{4.64}$$

The total resonant inductance is obtained as,

$$L = L_{ext} + L_{Ti} = 4.70 \ \mu\text{H}. \tag{4.65}$$

The resonant capacitance is obtained as,

$$C = \frac{1}{\omega\left(Q_L - \frac{\pi(\pi^2-4)}{16}\right) R_{Ti}} = 0.1325 \text{ nF}. \tag{4.66}$$

The choke inductance is obtained as,

$$L_f = 2\left(\frac{\pi^2}{4} + 1\right)\frac{R_{Ti}}{4f} = 5.1194 \ \mu\text{H}. \tag{4.67}$$

The shunt capacitance is obtained as,

$$C_1 = \frac{8}{\omega\pi(\pi^2+4)R_{Ti}} = 0.2152 \text{ nF}. \tag{4.68}$$

The total power losses incurred in the Class-E resonant inverter coupled with voltage-driven Class-E ZCS rectifier can be given as,

$$P_{LS} = P_{rLf} + P_{rDS} + P_{rC1} + P_{rL} + P_{rC} = 0.329 \text{ W}. \tag{4.69}$$

Finally, the efficiency of the inverter can be given as ratio of the average values of the output power to the input power i.e.

$$\eta = \frac{P_O}{|P_I|} = 94.56 \ \%. \tag{4.70}$$

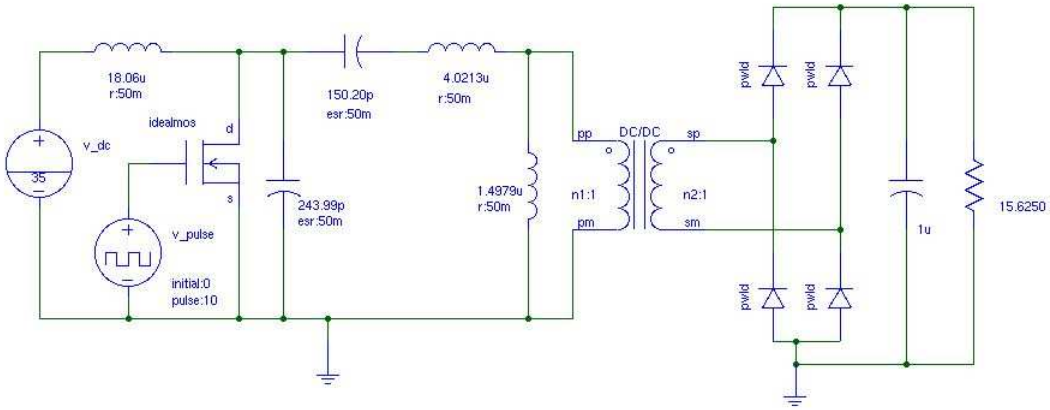

Figure 5.1: High-frequency wireless power transfer system

5 Results

Fig. 5.1 represents the complete circuit of the High-frequency Wireless Power Transfer (WPT) System. The circuit is simulated using Saber (version-4.0, release-2012.12.0.0). The system is designed for providing the output power of 40 W at the output voltage of 25 V. The operating frequency of the system is chosen as per the ISM band as 6.78 MHz. The system is provided with a DC input voltage of 35 V.

5.1 Component values

The high-frequency wireless power transfer system comprises of Class-E resonant ZVS inverter, Transformer and a bridge rectifier. Initially, the parameters of Class-E resonant ZVS inverter are determined. The load resistance of the inverter can be given as,

$$R_i = \frac{8}{(\pi^2+4)}\frac{V_I^2}{P_O} = 17.66\ \Omega \tag{5.1}$$

The inductance L of the inverter can be calculated with the help of inductive reactance. The inductive reactance of the inverter can be given as,

$$X_L = Q_L R_i \ = 176.64 \tag{5.2}$$

where, Q_L is the quality factor. The value of the quality factor is chosen as Q_L=10. The inductance L of the inverter is the ratio of the inductive reactance and the angular operating frequency and can be given as,

$$L = \frac{X_L}{\omega} \ = 4.1466 \ \mu\text{H} \tag{5.3}$$

Similarly, the value of the shunt capacitance C_1 can be calculated with the help of the capacitive reactance. The capacitive reactance can be given as,

$$X_{C1} = \frac{\pi(\pi^2 + 4)}{8} R_i \ = 96.2115 \tag{5.4}$$

The shunt capacitance C_1 of the inverter is the reciprocal of product of the capacitive reactance and the angular operating frequency and can be given as,

$$C_1 = \frac{1}{\omega X_{C1}} \ = 243.99 \text{ pF} \tag{5.5}$$

The reactance of the resonant capacitance X_C can be determined using quality factor and load resistance of the inverter. The reactance of the resonant capacitance can be given as,

$$X_C = Q_L - \frac{\pi(\pi^2 - 4)}{16} R_i \ = 156.2867 \tag{5.6}$$

The resonant capacitance C of the inverter is the reciprocal of the product of the reactance of the resonant capacitance and the angular operating frequency and can be given as,

$$C = \frac{1}{\omega X_C} \ = 150.20 \text{ pF} \tag{5.7}$$

Finally, the choke inductance of the inverter can be given as,

$$L_f = 2\left(\frac{\pi^2}{4} + 1\right)\frac{R_i}{f} \ = 18.06 \ \mu\text{H} \tag{5.8}$$

The system is designed for providing output power of 40 W at the output voltage of 25 V. Therefore, the actual load resistance of the complete circuit can be given as,

$$R_L = \frac{V_O^2}{P_O} \ = 15.625\ \Omega \tag{5.9}$$

The output of the transformer is given to the bridge rectifier. The input resistance of the bridge rectifier is related to the actual load resistance as,

$$R_{ib} = \frac{\pi^2}{8} R_L \ = 19.276\ \Omega \tag{5.10}$$

The primary and secondary inductance of the transformer are assumed to be equal. Hence, the turns ratio n of the transformer is equal to 1. In order to match the resistance of the Class-E inverter, the input resistance of the bridge rectifier should be reflected onto the primary side. The resistance obtained after reflecting is denoted as R_{Lr} and can be given as,

$$R_{Lr} = n^2 R_{ib} \ = 19.276\ \Omega \tag{5.11}$$

since, turns ratio n is equal to 1, R_{ib} and R_{Lr} are equal. The impedance transformation of the Class-E resonant ZVS inverter is carried out using $\pi 2a$ matching circuit. The resonant inductance L is split into two series inductances say L_1 and L_2. Inductance L_1 resonates with resonant capacitance C. The value of the inductance L_1 can be determined with the help of inductive reactance X_{L1}, which can be given as,

$$X_{L1} = \left(Q_L - \sqrt{\frac{R_{Lr}}{R_i} - 1} \right) R_i \ = 171.30 \tag{5.12}$$

Inductance L_1 is the ratio of inductive reactance X_{L1} to the angular operating frequency and can be given as,

$$L_1 = \frac{X_{L1}}{\omega} \ = 4.0213\ \mu\text{H} \tag{5.13}$$

On the other hand, the series connection of inductance L_2 and the input resistance of bridge rectifier R_{ib} is transformed into parallel connection. The inductance L_2 acts

as a magnetizing inductance L_m of the transformer. The inductive reactance X_{L2} can be given as,

$$X_{L2} = \left(\frac{R_{Lr}}{\sqrt{\frac{R_{Lr}}{R_i} - 1}} \right) \ = 63.80 \tag{5.14}$$

Inductance L_2 is the ratio of inductive reactance X_{L2} and the angular operating frequency and can be given as,

$$L_2 = \frac{X_{L2}}{\omega} \ = 1.4979 \ \mu\text{H} \tag{5.15}$$

The value of the smoothing capacitor in the bridge rectifier is chosen as $C_s = 1 \ \mu\text{F}$

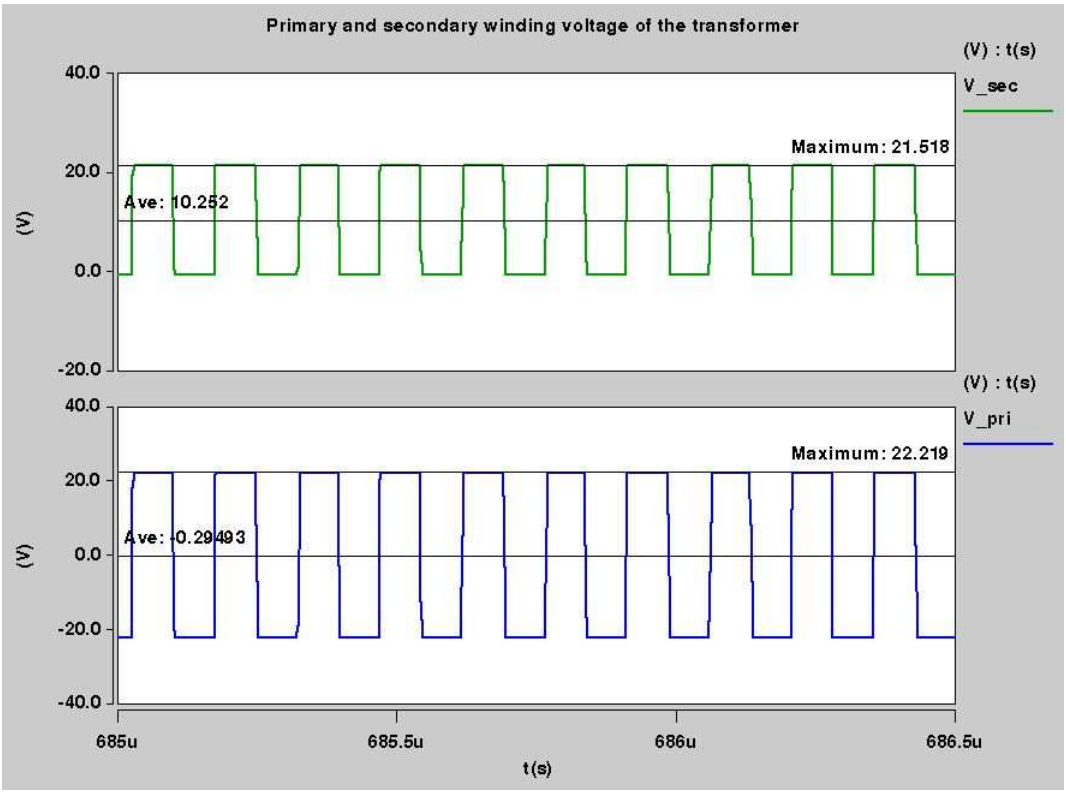

Figure 5.2: Primary and secondary winding voltage of high-frequency wireless power transfer system

5.2 Simulation results

Fig. 5.2 shows the voltage at the primary winding and the secondary winding. The turns ratio between the windings is equal to 1. Therefore, primary and secondary winding voltage is equal. The maximum and average value of voltage across the primary winding is equal to 22.219 V and -0.2949 V respectively. The maximum and average value of the voltage across the secondary winding is equal to 21.518 V and 10.252 V respectively.

Fig. 5.3 shows the response of gate to source voltage, drain to source voltage and drain current at R $<$ R_{opt}. The optimum resistance for the specification is obtained as R_{opt} = 15.6250 Ω. In order to observe the difference between the zero voltage switching and the zero derivative switching operation of the system, the load

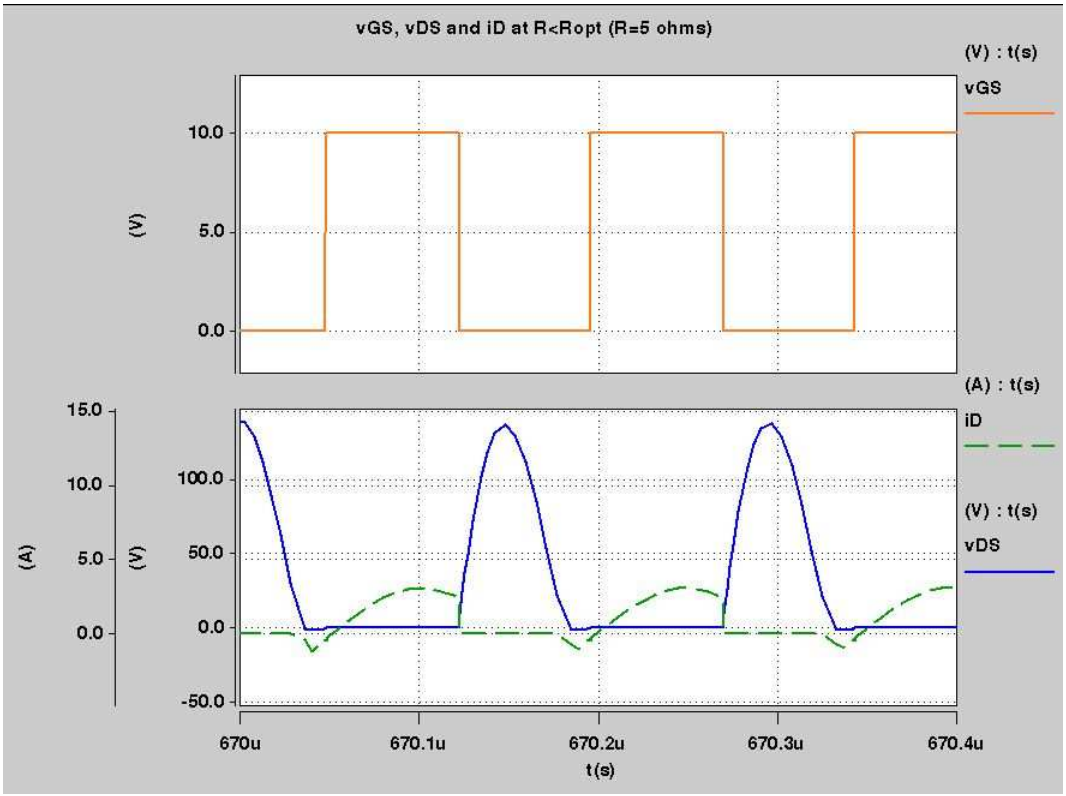

Figure 5.3: Gate to source, drain to source voltage and drain current at R $<$ R_{opt}

resistance is made less than the optimum resistance. The load resistance is set at R $= 5\ \Omega$. When the load resistance is less than the optimum load resistance, the switch voltage reaches to zero but not at the turn ON instance i.e. $\omega t = 2\pi$. Moreover, a negative drain current can be seen in the waveform. As a result, only zero voltage switching (ZVS) operation is obtained for R $<$ R_{opt} range.

Fig. 5.4 shows the response of gate to source voltage, drain to source voltage and drain current at R $= R_{opt}$. The zero derivative switching (ZDS) operation is also known as the optimum operation. The zero derivative switching (ZDS) condition requires the switch voltage to be zero at turn ON of the MOSFET. The ZDS condition satisfies only when the load resistance is tuned to be optimum. The optimum resistance for the specification is obtained as R_{opt}= 15.6250 Ω. When the load resistance is equal to the optimum load resistance, the switch voltage reaches to zero exactly at

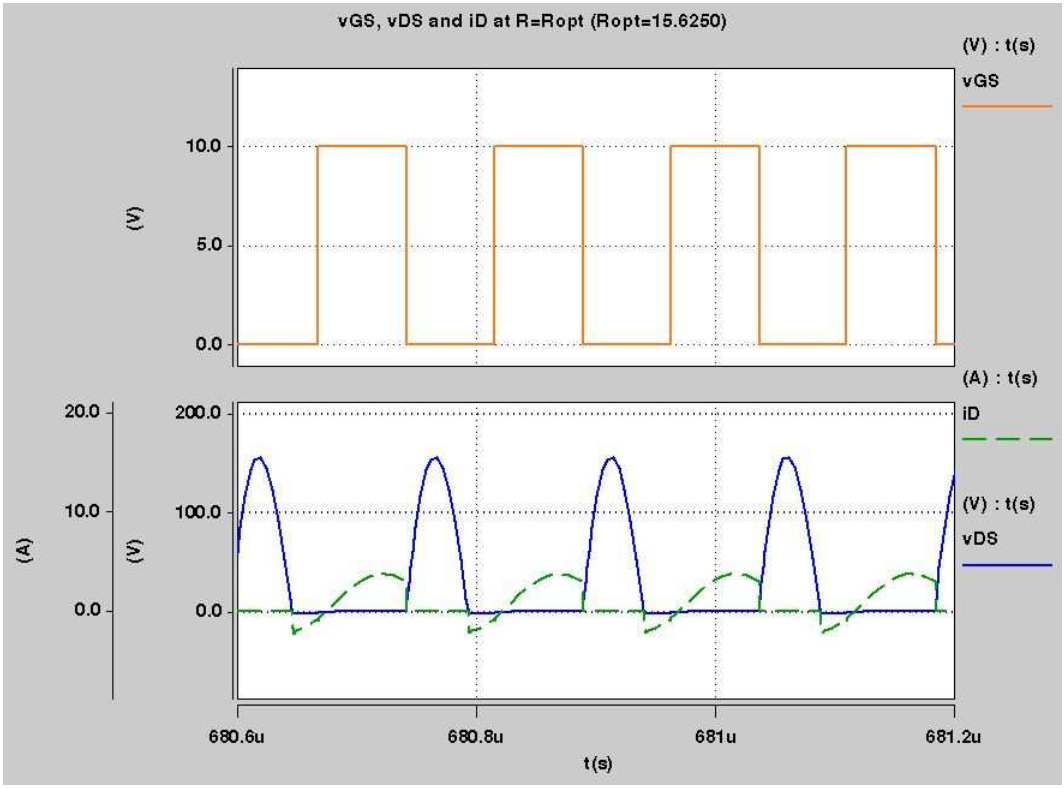

Figure 5.4: Gate to source, drain to source voltage and drain current at R=R_{opt}

the turn ON instance i.e. $\omega t = 2\pi$. Moreover, the magnitude of the drain current is maintained in the positive portion of the waveform. As a result, the zero derivative switching (ZDS) operation is achieved for R = R_{opt}.

Fig. 5.5 shows the response of gate to source voltage, drain to source voltage and drain current at R $>$ R_{opt}. The zero derivative switching (ZDS) condition requires the switch voltage to be zero at turn ON of the MOSFET. The ZDS condition satisfies only when the load resistance is tuned to be optimum. The optimum resistance for the specification is obtained as R_{opt}= 15.6250 Ω. In order to observe the non zero voltage switching of the system, the load resistance is made greater than the optimum resistance. The load resistance is set at R= 40 Ω. When the load resistance is greater than the optimum load resistance, the switch voltage does not reach to zero at the turn ON instance i.e. $\omega t = 2\pi$. Moreover, large spikes of drain current can be seen

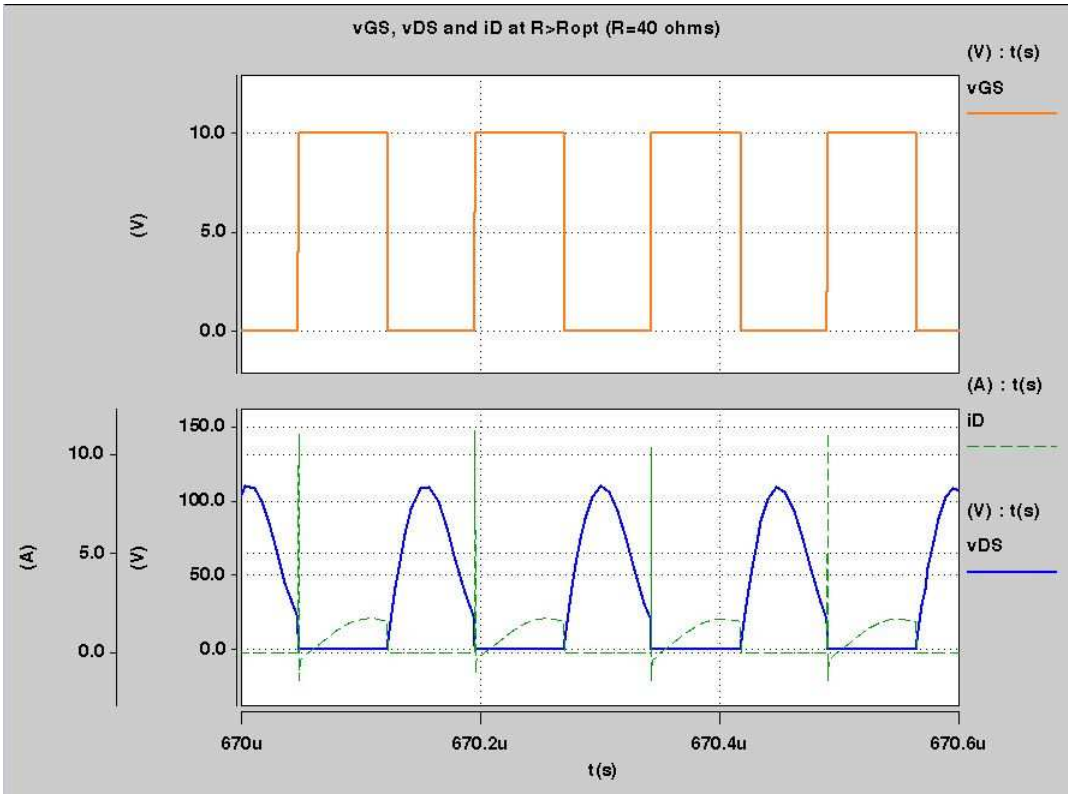

Figure 5.5: Gate to source, drain to source voltage and drain current at R $>$ R_{opt}

in the waveform. As a result, non zero voltage switching (ZVS) operation is achieved for R $>$ R_{opt} range.

Fig. 5.6 shows the waveforms of output voltage, output current and the input voltage of the complete high-frequency wireless power transfer system. The Class-E resonant ZVS inverter is provided with DC input voltage of 35 V. The output of the inverter is provided to the primary winding of the transformer. The output voltage of the transformer is sinusoidal in nature, which is given to the bridge rectifier. Finally, the bridge rectifier converts the sinusoidal voltage to the DC output voltage and the corresponding current. The maximum and average value of the DC output voltage is obtained as 20.836 V and 20.803 V respectively. The maximum and average value of the DC output current is obtained as 1.3335 A and 1.3314 A respectively.

Fig. 5.7 shows the waveforms of output power and input power of the high-

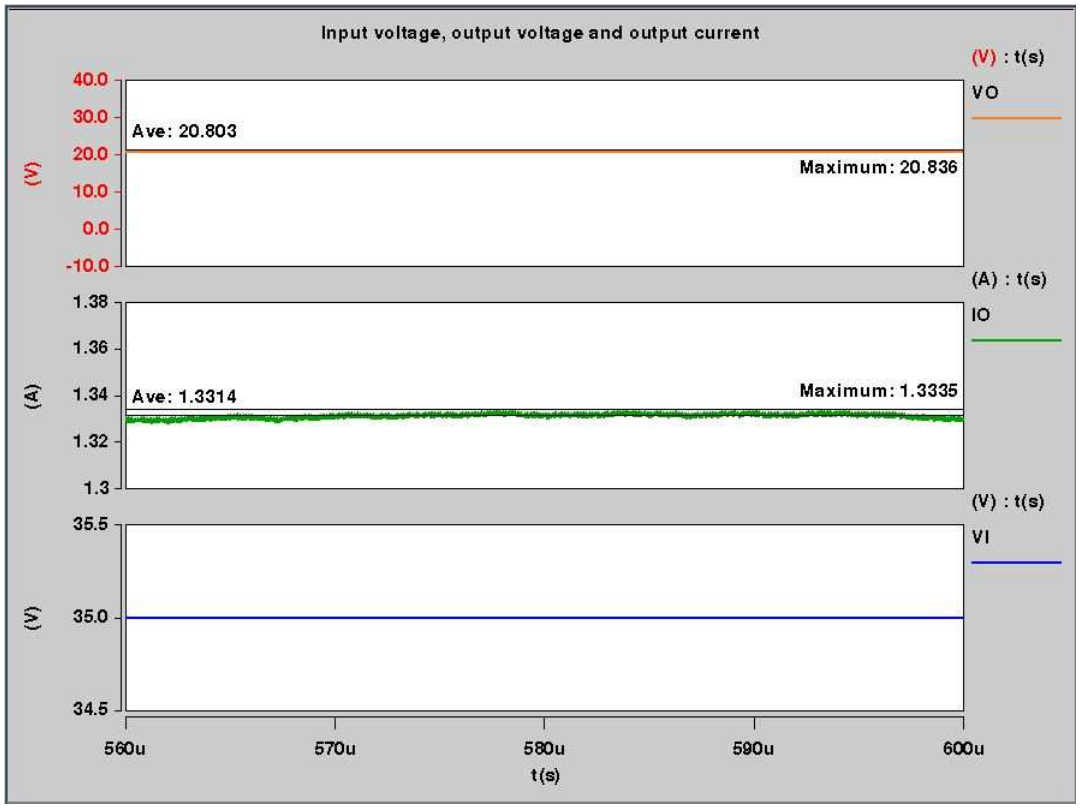

Figure 5.6: Output voltage, output current and input voltage of the high-frequency wireless power transfer system

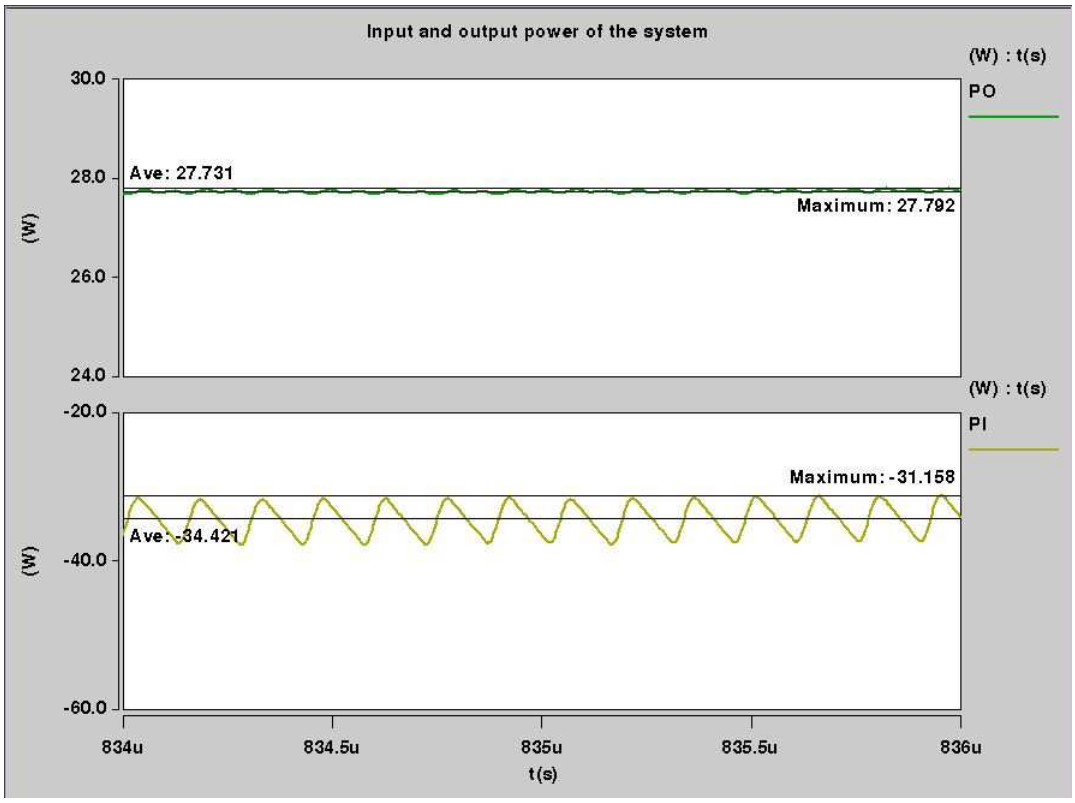

Figure 5.7: Output and input power of the high-frequency wireless power transfer system

frequency wireless power transfer system. In order to obtain the efficiency of the high-frequency wireless power transfer system, the input and output power is measured. The input power is measured across the DC voltage supply provided to the Class-E resonant ZVS inverter and the output power is measured across the load resistance of the system. The maximum and average value of the input power is obtained as -31.158 W and -34.421 W respectively. The maximum and average value of the output power is obtained as 27.792 W and 27.731 W respectively.

The efficiency of the high-frequency wireless power transfer system can be defined as ratio of the average output power to the input power which can be given as,

$$\eta = \frac{P_o}{P_I} = \frac{27.731}{|34.421|} = 80.56\ \% \tag{5.16}$$

Comparison of Existing Trends in WPT and The Work Done in this Thesis

The methods to achieve the wireless power transfer are categorized in two types 1. Magnetic resonance coupling and 2. Inductive coupling [21]. These types have one thing in common and i.e. the magnetic induction principle. In the magnetic resonance coupling method [35], the two coils are brought into resonance by appropriately setting the values of capacitors and inductors. The resonance between the coils has various functions such as achieving maximum transfer efficiency, maximum power transfer, controlling the power transfer by frequency variation, reducing EMI, etc., [22] Also, due to the resonance, the magnetic resonance coupling method provide immunity to the neighboring environment and eliminates the requirement of line of sight transfer of power. The biggest advantage of the magnetic resonance coupling method is that, it can establish power transfer between one transmitter resonator and multiple receiver resonators [31],[32],[33],[34]. The range of power transfer for this method is up to several meters [23]. In 2007, the MIT scientist demonstrated the wireless power transfer based on magnetic resonance including lighting a 60 W bulb placed more than two meters away. The transmission efficiency was reported around 40 % and can be increased to 90 %, when the transmission distance is reduced to one meter. The efficiency of the magnetic resonance coupling method is based on the gain bandwidth of the coils [24],[25]. The inductive coupling method follows the magnetic induction principle but the coils are off resonance. The magnetic induction principle states that the primary coil of the transmitter generates magnetic flux which is spread in all directions by inverse square law and the secondary coil must be in vicinity of the primary and tuned to the operating frequency to capture the maximum amount of magnetic flux. The effective transmission distance for the inductive cou-

pling method is reported as 20 cm [29]. The transmission distance can be increased by implementing the inductively coupled radio frequency identification (RFID) up to tens of centimeters. But inductively coupled radio frequency identification (RFID) technique involves reduction in efficiency up to 1 to 2 % [27],[28]. In summary, the inductive coupling method is easy to implement and provides maximum efficiency in close distance. MIT scientist also introduced a wireless charging technology called MagMIMO, claiming that it can charge the device wirelessly up to 30 cm away. They claimed that MagMIMO projects a beam of energy and can charge the phone even when it is in the pocket of the user [23],[26]. The work done in this thesis related to the wireless power charging based on the principle of inductive coupling. The inductive coupling method is a very old concept and was introduced based on the laws proposed by Faraday and Ampere. The inductive coupling involves appropriately coupling of two coils and then by the induction principle, the current in one coil induces voltage into the other coil and eventually this voltage can be utilized in powering the applications such as batteries of laptops, tablets, smartphones etc., The power required for charging the portable applications is in the range of several watts. Since the work done in this thesis is related to wirelessly charging the devices, there are some important factors which should be considered while designing the individual stages such as distance between the coils, size of the coils, misalignment, directivity, amplification and rectification mechanism, etc., The power required for portable applications such as smartphones, laptops etc., is considered while doing this thesis. The design in this work can deliver the power of 40 W at distance of 3 to 5 cm. The operating frequency of this design is chosen based on the requirement of portable applications, i.e., 6.78 MHz. The overall transmission efficiency of the design is obtained as 80.56 % at coupling coefficient of 0.5. Considering the size of the devices, users nowadays need their devices to be small and compact. Now to manufacture small

and compact devices, there should be less number of components on the board. The biggest advantage of this design is that the compensation is achieved by absorbing the leakage flux into the main resonant tank circuit. The existing wireless charging methods have achieved the absorption technique for $k = 0.77$ [20], but in this thesis, the absorption is achieved at a much lower value of coupling coefficient i.e. $k = 0.5$ which enables larger distance of power transfer. The conventional methods need extra components to cancel the leakage flux such as series compensation capacitor, which increase the size of the board and eventually size of the device. For the transmitter section of this design, Class-E DC-AC zero voltage switching (ZVS) inverter has been employed. This inverter topology is known to be one of the most efficient and easy to implement. The matching resonant circuit i.e., $\pi 2a$, impedance matching enables the transmitter section to tolerate any changes in the receiver section, which means that based on the applications even if the load resistance of the overall design varies, the transmitter section will continue to perform efficiently. Another important parameter is the frequency of operation, most of the existing wireless power charging methods related to the portable applications operate on around 1 MHz frequency [30] but the design in this thesis is for high frequency range i.e. 6.78 MHz. The existing technologies have the designs which can successfully charge a smartphone which requires output power of about 5 W [36],[37], but when it comes to charging laptops, tablets, etc., the design must deliver large output power. Therefore, the circuit in this work is designed considering the output power of 40 W. The employment of the soft switching converters is a key factor, since it has impacted on the overall efficiency of the design reducing the switching losses and electromagnetic interference (EMI).

Relationship of Coupling Coefficient and Distance between The Coils

The coupling coefficient of the coils and the distance between them is a very important important relation as far as the overall performance of the design is concerned.

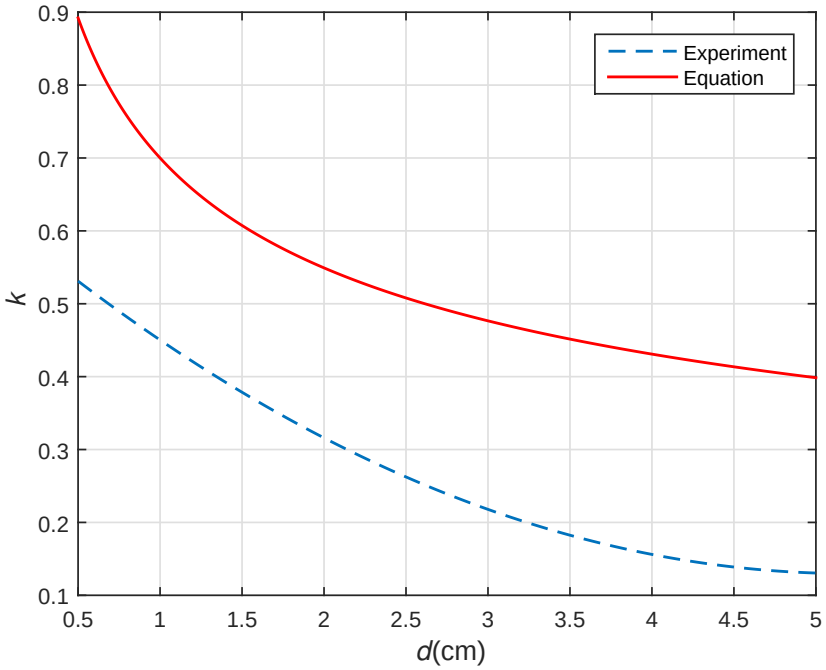

Figure 5.8: Coupling coefficient and distance between the coils

However, in the literature related to the wireless power transfer technology, there is no equation which indicates the direct relation between these two parameters. Hence, the relation is purely established on the basis of the values obtained by the experiments. Fig. 5.8 represents the relation of the distance and the coupling coefficient [43]. By the approximation technique, the equation relating the coupling coefficient and the distance between the coils can be given as follows

$$k \propto \frac{\alpha}{d^{\beta}} \tag{5.17}$$

Also, the relation can also be expressed in terms of polynomial given below.

$$k = a_0 dx^2 + a_1 dx + C \tag{5.18}$$

The red line in the Fig. 5.8 is obtained for the values $a_0 = 0.0181$, $a_1 = -0.1887$ and $C = 0.6209$.

6 Conclusions

6.1 Summary

The key aspects of the High-frequency Wireless Power Transfer (WPT) System studied in this thesis are as follows:

- A detailed and thorough literature study of the overall High-frequency Wireless Power Transfer (WPT) System has been performed.

- The design and operation of the high-frequency and highly efficient Class-E rectifiers have been studied. The complete analysis of the four configurations of the Class-E rectifiers namely current-driven Class-E low dv/dt (ZVS) rectifier, voltage-driven Class-E low dv/dt (ZVS) rectifier, current-driven Class-E low di/dt (ZCS) rectifier and voltage-driven Class-E low di/dt (ZCS) rectifier have been performed.

- The Class-E rectifiers are designed to be operated on standard International, Scientific and Medical (ISM) band frequency of 6.78 MHz, for output power range of 25 W to 40 W at the output voltage range of 12 V to 15 V.

- The zero voltage switching (ZVS) and zero current switching (ZCS) operation of all the above mentioned Class-E rectifiers have been performed and verified. The key parameters such as phase, AC-to-DC voltage transfer function, AC-to-DC current transfer function, loaded quality factor etc. have been determined. In addition, the effect of variation in duty cycle on other parameters is also observed.

- The average and maximum values of voltage and current of each component of the Class-E rectifiers are measured. The efficiencies for all the Class-E rectifiers

have been determined. Furthermore, the effect of change in load resistance on the efficiencies of each rectifier have been observed.

- In order to couple the rectifier with transformer and inverter, two configurations of the rectifier i.e. current-driven Class-E low dv/dt (ZVS) rectifier and voltage-driven Class-E low di/dt (ZCS) rectifier have been chosen. The equivalent models for the two rectifier configurations have been derived.

- The characteristics, design and operation of high-frequency transformer have been studied and performed. The losses associated with the transformer such as hysteresis and eddy current losses have been discussed.

- In order to determine the component values of the transformer, Area Product method has been employed. The specifications chosen for the design of the core are as follows.

  - Type of material - L
  - Type of core - Ferrite core
  - Shape of core - EE
  - Area product - 0.59 cm^4

- The component values for the transformer coupled with current-driven Class-E low dv/dt (ZVS) rectifier and voltage-driven Class-E low di/dt (ZCS) rectifier have been determined. Also, maximum efficiency criterion for the transformer has been elaborated.

- The design and operation of the high-frequency and highly efficient Class-E resonant ZVS inverter have been studied. The sub-optimum and optimum operation of the Class-E resonant ZVS inverter is performed.

- The Class-E resonant ZVS inverter is designed to be operated on standard International, Scientific and Medical (ISM) band frequency of 6.78 MHz, for output power range of 25 W to 40 W at the output voltage range of 12 V to 15 V.

- The Class-E resonant ZVS inverter is coupled with current-driven Class-E low dv/dt (ZVS) rectifier and voltage-driven Class-E low di/dt (ZCS) rectifier and component values associated with each configuration are determined.

- The parameters of Class-E resonant ZVS inverter coupled with Class-E rectifier such as output voltage, output power, power losses in individual components, and efficiency have been determined.

- A complete High-frequency Wireless Power Transfer (WPT) system have been designed for delivering output power in range of 25 W to 40 W, output voltage of 25 V and operating at 6.78 MHz. The system comprises of highly efficient Class-E inverter, transformer and a bridge rectifier.

- The zero voltage switching (ZVS) and zero derivative switching (ZDS) operation have been achieved for the complete system. Furthermore, the boundaries of load resistance at which the system delivers the ZVS, ZDS and non-ZVS operation are also determined.

- The parameters of the complete system such as primary and secondary winding voltage, output voltage, input power, and output power are obtained. Also, the efficiency of the overall system has been determined.

6.2 Conclusions

The main conclusions that can be drawn from this thesis are as follows:

- It has been observed that, while designing the Class-E rectifiers, if p-n junction diodes are used, they exhibit the reverse recovery effect and result in reverse current. In order to overcome the effect of reverse recovery effect, Schottky diodes are used. Schottky diodes have low threshold voltage (0.4 V) as compared to p-n junction diodes (0.7 V). In the design of all the four configurations of Class-E rectifiers, Schottky diode (MBR1060G) has been employed.

- Out of the four configurations of the Class-E rectifiers, current-driven Class-E low dv/dt (ZVS) rectifier is the most efficient with 89.72 % efficiency. On the other hand, current-driven Class-E low di/dt (ZCS) rectifier is the least efficient with 70.44 %.

- In case of current-driven Class-E low dv/dt (ZVS) rectifier, diode power dissipation is kept low with the help of shunt capacitor, the Schottky diodes have ability to turn-ON and turn-OFF at low dv/dt reducing the current through junction capacitance C_j yielding proper ZVS and the highest efficiency.

- In case of current-driven Class-E low di/dt (ZCS) rectifier, the junction capacitance C_j is not included in the topology which results in parasitic resonant circuit including the inductance L and C_j. The parasitic resonant circuit generates oscillations which gives rise to ringing problem. The above mentioned problems hinder the proper ZCS operation and limit the efficiency of the rectifier. This rectifier is driven for duty cycle of 0.75 unlike the other configurations, since the output voltage and output power obtained at $D = 0.5$ were not in the desired range.

- The ZVS and ZCS operations of Class-E rectifiers are the salient features which enables the designer to build high-frequency rectifiers which have multiple applications in field of modern electronics systems. These technologies provide

flexibility in choosing components with lower conduction losses, lower driving currents and higher energy density.

- It has been observed that the design of the high-frequency rectifiers have a major impact on overall efficiency of the wireless power transfer system. Most of the wireless power transfer systems for example, Inductive Power Transfer (IPT) employ Class-E or Class-D inverters as their coil driver. Although, the Class-E and Class-D are the most efficient inverters and also deliver sinusoidal output voltage, it is not necessary that the rectifier in conjunction with inverter will have a sinusoidal input current or sinusoidal input voltage. Therefore, the incompatibility issues may arise in such designs.

- The design of the transformer for such a high frequency was a main challenge. The core material required for operation on 6.78 MHz is C-type material. The C-type material offers maximum usable frequency less than 8 MHz at initial permeability of 900. Since, Area product method is employed, the required of $A_p = 1.314$ cm^4 was not available for the C-type material. Therefore, the material type was compromised and in place, L-type material has been used.

- A ferrite EE shaped core with following specifications was chosen for the transformer coupled with both rectifier configurations.

  - Area product (A_p) = 0.59 cm^4
  - Length of the core (L_e) = 61.9 mm
  - Area of the core (A_e) = 83.2 mm^2
  - Volume of the core (V_e) = 5150 mm^3

  Therefore, the value of the parameters such as magnetic energy (W_m), Window area of core (W_a) and Mean turn length (MTL) for both the rectifier config-

urations are similar. the skin depth value is also similar since, it is frequency dependent.

- The coupling coefficient was set to $k = 0.5$ which introduced the leakages in primary and secondary windings of the transformer. Since, $k = 0.5$, the value of magnetizing inductance L_m and the primary leakage inductance L_{l1} is same.

- At high operating frequencies, it has been observed that the core losses or the magnetic losses increases due to eddy current phenomenon.

- The optimum operation of Class-E resonant ZVS inverter allows the zero voltage switching (ZVS) as well as the zero derivative switching (ZDS) operation which almost eliminates switching losses across the MOSFET. As a result, Class-E resonant ZVS inverter delivers high efficiency.

- The maximum power loss occurred in the Class-E resonant inverter for both the rectifier configurations is across the MOSFET as compared to other passive components.

- The efficiency obtained for the Class-E inverter coupled with current-driven Class-E low dv/dt (ZVS) rectifier is 92.32 % and that coupled with voltage-driven Class-E low di/dt (ZCS) rectifier is 94.56 %.

- Although the Class-E ZVS and ZCS rectifiers have a common feature of reduction in switching losses and achieving high efficiency, they experience various limitations when coupled with other circuits. The Class-E ZVS and ZCS rectifiers have many reactive components which may prove useful when it comes to reduction of losses, but may also prove hinderous when the rectifier is coupled with other circuits.

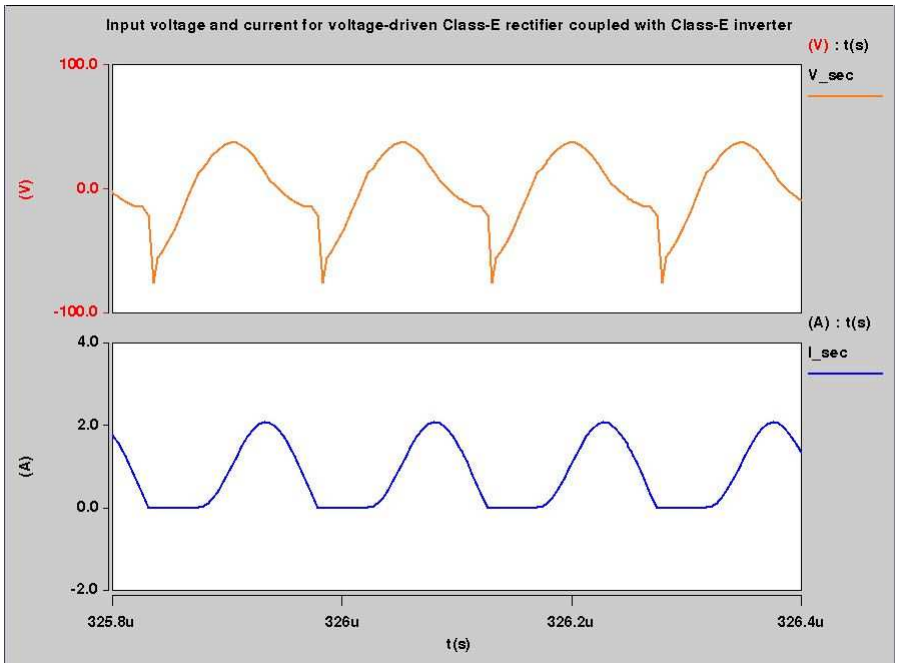

Figure 6.1: Input voltage and current for the voltage-driven Class-E rectifier coupled with Class-E resonant ZVS inverter

- When the voltage-driven Class-E low di/dt (ZCS) rectifier is coupled with the Class-E resonant ZVS inverter, the input of rectifier has non-sinusoidal voltage or current due to the presence of reactive components. As a result, the rectifier is unable to deliver the real output power and output voltage at the load. Observing the Fig. 6.1, it is clear that the voltage provided to the input of the rectifier is non-sinusoidal.

- The solution to this problem is to make use of rectifier with minimum reactive components. The full bridge rectifier is one of the best candidate to employ in this category. When the Class-E resonant ZVS inverter is coupled with the full bridge rectifier via transformer, the complete system delivered output voltage and output power in desired range. Moreover, the zero derivative switching (ZDS) operation has been obtained for the Class-E resonant ZVS inverter.

- The Class-E resonant ZVS inverter is supplied with DC input voltage of 35

V. The primary winding of the transformer acts as an output of the inverter which delivers maximum AC voltage of 22.219 V. The secondary winding of the transformer acts as an input of the full bridge rectifier. The bridge rectifier converts the AC voltage from the inverter to the DC output voltage. The average DC output voltage obtained is 20.803 V. The average DC output power delivered to the load is 27.731 W.

- The overall efficiency obtained for the high frequency wireless power transfer system is 80.56 % at optimum load resistance of 15.6250 Ω.

6.3 Contributions

The main contributions made by this thesis are as follows:

- Comprehensive study and analysis of the inverter, loosely coupled coils and rectifier have been performed.
- This thesis is useful for the design of high efficiency wireless power transfer (WPT) system operating from the high frequency (HF) to very high frequency (VHF) range (i.e., 1 MHz to 10 MHz).
- A detailed analysis and review of the four rectifier topologies is performed.
  - current-driven Class-E low dv/dt (ZVS) rectifier.
  - voltage-driven Class-E low dv/dt (ZVS) rectifier.
  - current-driven Class-E low di/dt (ZCS) rectifier.
  - voltage-driven Class-E low di/dt (ZCS) rectifier.
- Identified the rectifier with highest efficiency out of the four topologies that may be used for the design of the wireless power transfer (WPT) system.

- Identified the challenges in designing the transformer with magnetic core operating at high frequency.
- Designed a Class-E resonant ZVS inverter for operation at 6.78 MHz and also obtained the zero derivative switching (ZDS) operation achieving high efficiency at $k = 0.5$.
- Integrated the stages and investigated the problems in the overall circuit.

7 Bibliography

References

[1] N. Shinohara, "History, Present and Future of WPT," in *Wireless Power Transfer via Radiowaves,"* John Wiley and Sons, Inc., Hoboken, NJ, USA, 2013.

[2] J. Garnica, R. Chinga, and J. Lin, "Wireless Power Transmission: From Far Field to Near Field", *Proceedings of IEEE*, vol. 101, no. 6, pp. 1321-1331, 2013.

[3] Y. Zhang, Z. Zhao, and K. Chen, "Frequency splitting analysis of magnetically-coupled resonant wireless power transfer", *Proceedings of IEEE Energy Conversion Congress and Exposition*, pp. 2227-2232, September, 2013.

[4] A. L. Manez, *Optimization of Inductive Resonant Coupling Links for Low Power and Mid-Range Wireless Power Transfer*, Masters Thesis, Polytechnic University of Madrid, Septemeber 2014.

[5] K. Liu and F. C Lee, "Zero-voltage switching technique in DC/DC converters", *IEEE Transactions on Power Electronics*, vol. 5, no. 3, pp. 293-304, 1990.

[6] M. K. Kazimierczuk and J. Jozwik, "Class-E zero-voltage-switching and zero-current-switching rectifiers", *IEEE Transactions on Circuits and Systems*, vol. 37, no. 3, pp. 436-444, 1990.

[7] M. K. Kazimierczuk and D. Czarkowski, *Resonant power converters*, 2nd. Ed., Hoboken, NJ: Wiley, 2011.

[8] A. Ivascu, M. Kazimierczuk, and S. Birca-Galateanu, "Class E resonant low dv/dt rectifier", *IEEE Transactions on Circuits and Systems I: Fundamental Theory and Applications*, vol. 39, no. 8, pp. 604-613, 1992.

[9] EE33D - Power Electronic Circuits, The University of the West Indies. [Online].

[10] M. Kazimierczuk and J. Jozwik, "Analysis and design of class E zero-current-switching rectifier", *IEEE Transactions on Circuits and Systems*, vol. 37, no. 8, pp. 1000-1009, 1990.,

[11] M. Kazimierczuk and W. Szaraniec, "Analysis of class E low di/dt rectifier with a series inductor", *IEEE Transactions on Aerospace and Electronic Systems*, vol. 29, no. 1, pp. 278-287, 1993.

[12] M. K. Kazimierczuk, *High-Frequency Magnetic Components,* 2nd Ed., Wiley, Chichester, UK. 2012

[13] K. Papastergiou, "A Power Converter with a Rotating Secondary Stage for an Airborne Radar System", Ph.D Dissertation, The University of Edinburgh, 2005.

[14] G. S. Ramanamurthy and V. Ramanarayan, "A modified area product method for the design of inductors and transformers", *Journal of Indian Institute of Science,* vol. 80, pp. 429-435, October 2000.

[15] M. K. Kazimierczuk and H. Sekiya, "Design of AC resonant inductors using area product method", *Proceedings of IEEE Energy Conversion Congress and Exposition*, September 2009.

[16] W. Hurley and W. Woolfle, "Transformers and Inductors for Power Electronics", Chichester, Wiley, pp. 56-91, 2014.

[17] B. Guru and H. Hiziroglu, "Electric Machinery and Transformers", 3rd ed.,pp. 202-277, Oxford University Press, New Delhi, India, 2007.

[18] M. K. Kazimierczuk and D. Czarkowski, *Resonant power converters*, Second. Hoboken, NJ: Wiley, 2011.

[19] M. Uddin, G. Ramasamy, S. Mekhilef, K. Ramar and Y. Lau, "A review on high frequency resonant inverter technologies for wireless power transfer using magnetic resonance coupling", *IEEE Conference on Energy Conversion (CENCON)*, 2014.

[20] F. Corti, F. Grasso, A. Reatti, A. Ayachit, D. Saini and M. Kazimierczuk, "Design of class-E ZVS inverter with loosely-coupled transformer at fixed coupling coefficient", *Proceedings of IEEE Industrial Electronics Society*, pp. 5627-5632, Florence, Italy, October 2016.

[21] https://www.wirelesspowerconsortium.com/technology/magnetic-resonance-and-magnetic-induction-making-the-right-choice-for-your-application.html

[22] Fariborz Musavi, Wilson Eberle, "Overview of wireless power transfer technologies for electric vehicle battery charging", *IET Power Electron*, Vol. 7, Iss. 1, pp.60âĂŞ66, 2014.

[23] Xiao Lu, Ping Wang, Dusit Niyato, Dong In Kim, and Zhu Han, "Wireless Charging Technologies: Fundamentals, Standards, and Network Applications", *IEEE Communications Surveys and Tutorials*, pp. 1-40, November 2015.

[24] A. Kurs, A. Karalis, R. Moffatt, J. D. Joannopoulos, P. Fisher, and M. Soljacic, "Wireless Power Transfer via Strongly Coupled Magnetic Resonances", *Science*,vol. 317, no. 5834, pp. 83-86, June 2007.

[25] http://witricity.com/

[26] Jouya Jadidian, Dina Katabi, "Magnetic MIMO: How To Charge Your Phone in Your Pocket", pp. 495-506

[27] S. Ahson and M. Ilyas, "RFID Handbook: Applications, Technology, Security, and Privacy", *CRC Press*, Boca Raton, Florida, 2008.

[28] L. Roselli, F. Alimenti, G. Orecchini, C. Mariotti, P. P. Mezzanotte, and M. Virili, "WPT, RFID and Energy Harvesting: Concurrent Technologies for the Future Networked Society", *Proceedings of Asia-Pacific Microwave Conference (APMC)*, Seoul, South Korea, Nov.2013.

[29] X. Wei, Z. Wang, and H. Dai, "A Critical Review of Wireless Power Transfer via Strongly Coupled Magnetic Resonances", *Energies*, vol. 7, no. 7, pp. 4316-4341, July 2014.

[30] Jacek J. Jozwik and Marian K. Kazimierczuk. "Analysis and Design of Class-E2 dc/dc Converter", *IEEE Transactions on Industrial Electronics*, VOL 37, NO 2. pp. 173-183, April 1990.

[31] J. Choi, Y. H. Ryu, D. Kim, N. Y. Kim, C. Yoon, Y.-K. Park, S. Kwon, and Y. Yang, "Design of High Efficiency Wireless Charging Pad Based on Magnetic Resonance Coupling" *Proceedings of European Radar Conference (EuRAD)*, Amsterdam, Netherlands,Nov. 2012.

[32] D. Z. Kim, K. Y. Kim, N. Y. Kim, Y.-K. Park, W.-S. Lee, J.-W. Yu, and S. Kwon, "One-to-N Wireless Power Transmission System Based on Multiple Access One-way in-band Communication", *Proceedings of Asia Pacific Signal and Information Processing Association Annual Summit and Conference (APSIPA ASC)*, Hollywood, CA,Dec. 2012.

[33] A. Kurs, R. Moffatt, and M. Soljacic, "Simultaneous Mid-range Power Transfer to Multiple Devices", *Appl. Phys. Lett.*, vol. 96, pp. 044102- 1044102-3,Jan. 2010.

[34] S. Rajagopal, and F. Khan, "Multiple Receiver Support for Resonance Coupling Based Wireless Charging", *Proceedings of IEEE International Conference on Communications Workshops (ICC)*, Kyoto, Japan,June 2011.

[35] M. Galizzi, M. Caldara, V. Re, and A. Vitali, "A Novel Qi-standard Compliant Full-bridge Wireless Power Charger for Low Power Devices" *Proceedings of IEEE Wireless Power Transfer Conference (WPTC)*, Perugia, Italy,May 2013.

[36] P. H. V. Quang, T. Tien Ha, and J. Lee, "A Fully Integrated Multimode Wireless Power Charger IC With Adaptive Supply Control and Built-In Resistance Compensation" *IEEE Transactions on Industrial Electronics*, vol. 62, no. 2, pp. 1251-1261, Feb. 2015.

[37] A. Karalis, J. Joannopoulos, and M. Soljacic, "Efficient Wireless Nonradiative Mid-range Energy Transfer" *Ann. Phys.*, vol. 323, no. 1, pp. 34-48, 2008.

[38] Mohamed M. El Rayes, Gihan Nagib, Wahied G. Ali Abdelaal, "A Review on Wireless Power Transfer", *International Journal of Engineering Trends and Technology (IJETT)*, Volume 40, No.5, pp. 272-280, October 2016.

[39] Grant Anthony Covic and John Talbot Boys, "Modern Trends in Inductive Power Transfer for Transportation Applications" *IEEE Journal of Emerging and Selected Topics in Power Electronics*, Vol. 1, No. 1, pp. 28-41, March 2013.

[40] Md. Saifuddin, Tushar Saha, Monirul Islam, Md. Mujammel Hossain Akhand, "Wireless Power Transmission Compare and Contrast with the Form of Resonance Frequency, Mutual Inductance and Solar Energy" *International Journal of Engineering Research and Applications*, Vol. 4, Issue 10 (Version 6), pp.66-96, October 2014.

[41] Mohammad Bani Shamseh, Atsuo Kawamura, Itsuo Yuzurihara, Atsushi Takayanagi, "A Wireless Power Transfer System Optimized for High Efficiency and High Power Applications" *International Power Electronics Conference*, pp-2794-2801, 2014.

[42] B. Cannon, J. Hoburg, D. Stancil, and S. Goldstein, "Magnetic Resonant Coupling as a Potential Means for Wireless Power Transfer to Multiple Small Receivers" *IEEE Trans. Power Electron.*, vol. 24, no. 7, pp. 1819- 1825, ,July 2009.

[43] Agasthya Ayachit, Dalvir Saini, Marian K. Kazimierczuk, Tadashi Suetsugu, "Three-Coil Wireless Power Transfer System Using Class E 2 Resonant DC-DC Converter" *Telecommunications Energy Conference (INTELEC)*, pp. 1-4, 2015.